EXPERIMENTAL STUDY OF CRACK INITIATION ANGLE IN PMMA AND PS PLATES UNDER MIXED-MODE LOADING

by

A. Cenk Işık

BS. in M.E., Istanbul Technical University, 2001

Submitted to the Institute for Graduate Studies in
Science and Engineering in partial fulfillment of
the requirements for the degree of
Master of Science

Graduate Program in Mechanical Engineering

Boğaziçi University

2006

ACKNOWLEDGEMENTS

I wish to thank to Prof. Günay Anlaş, my thesis supervisor, for his invaluable help and patience and, also to Assoc. Prof. Vahan Kalenderoğlu for his suggestions and interest during this study.

I also wish to thank to Çiğdem Sürücüoğlu, Alpay Oral, İlhan Polat, Ergin Özgen and Hakan Çopur for their guidance and help in this work.

Besides, I am grateful to my family for their understanding and support during this work.

ABSTRACT

EXPERIMENTAL STUDY OF CRACK INITIATION ANGLE IN PMMA AND PS PLATES UNDER MIXED-MODE LOADING

The purpose of this study is to determine crack initiation angles, the effect of critical radius and T-stress on crack initiation angles using experimental and analytical techniques. The results obtained using the maximum tangential stress (MTS-criterion), the generalized maximum tangential stress (GMTS-criterion), the minimum strain energy density (S-criterion) and the maximum triaxial stress (M-criterion) criteria are compared to experimental results of PMMA and PS specimens with an inclined center crack, under mixed-mode loading.

ÖZET

KARIŞIK TİP YÜKLEME ALTINDA PMMA VE PS LEVHALARINDA ÇATLAK İLERLEME AÇILARININ DENEYSEL ÇALIŞMASI

Bu tezde, çatlak ilerleme açılarının, kritik yarıçap ve T stresin çatlak ilerleme açılarının üzerindeki etkilerinin deneysel ve analitik teknikler kullanılarak belirlenmesi amaçlanmıştır. MTS, GMTS, S ve M kriterleri kullanılarak, elde edilen analitik sonuçlar ile karışık tip yükleme altında ve merkezi çatlaklı PMMA ve PS plakalardan elde edilen deneysel sonuçlar karşılaştırılmıştır.

TABLE OF CONTENTS

LIST OF FIGURES

LIST OF TABLES

LIST OF SYMBOLS/ABBREVIATIONS

a	Crack length
B	Biaxiality ratio
a_{11}, a_{12}, a_{22}	Arbitrary constants
E	Modulus of elasticity
F_1	Boundary correction factor
G_s	Modulus of rigidity
I, II	Subscripts denoting mode of loading
K	Stress intensity factor
K_{eff}	Effective stress intensity factor
K_{Ic}, K_{IIc}	Critical fracture toughness
L	Height of plate
M	Stress triaxiality ratio
M^e	Mode mixity parameter
N	Arbitrary constant
r, θ	Polar co-ordinate system
r_c	Critical radius
S	Stress energy density factor
T	T-stress
t	Thickness of the plate
x, y	Cartesian co-ordinate at the crack tip
W	Width of the plate
α	Ratio of critical radius of the crack length
β	Crack inclination angle
ε_B	Elongation at break
μ	Ratio of stress intensity factors
ν	Poisson's ratio
σ	Uniform stress applied on the upper boundary of the plate

σ_Y	Yield strength
σ_M	Ultimate strength
σ_B	Stress at break
σ_{xx}	Normal stress along x-direction
σ_{yy}	Normal stress along y-direction
σ_{zz}	Normal stress along z-direction
σ_{xy}	Shear stress on x-plane along y-direction
σ_{rr}	Normal stress along radial direction
$\sigma_{\theta\theta}$	Normal stress along tangential direction
$\sigma_{r\theta}$	Shear stress on r-plane along θ direction
σ_H	Hydrostatic stress
σ_{eq}	Equivalent stress
θ_c	Crack initiation angle
$(\theta_c)_{avg.}$	Average value of crack initiation angel

1. INTRODUCTION

1.1. Objective

Crack propagation requires the knowledge of the angle of crack initiation. With recent advances in computational tools, simulation of crack initiation is easier. For crack growth under mixed-mode, a number of criteria have been proposed to predict crack initiation angles. The criteria available in literature can be grouped under three main heading: stress-based criteria, energy-based criteria, and strain-based criteria. The maximum tangential stress (MTS-criterion), the generalized maximum tangential stress (GMTS-criterion) the minimum strain energy density, (S-criterion), and the maximum triaxial stress (M-criterion) criteria are the most common ones for the prediction of the crack initiation angle for ideally brittle isotropic material.

In this experimental study, polymethylmethacrylate (PMMA) and polystyrene (PS) plates under mixed-mode loading are used to investigate crack initiation angles in brittle materials. The study addresses the problem of brittle fracture under mixed-mode loading in PMMA and PS materials. PMMA and PS are relatively homogeneous isotropic materials showing brittle fracture behavior at room temperature. In this study, they are used because of ease to introduce a natural sharp crack into the specimens by using a razor blade.

PMMA and PS plate specimens containing a central crack inclined at different crack inclination angles β are tested using Zwick/Roell Z010 Tensile Testing Machine. Crack initiation angles θ_c are measured. The maximum tangential stress (MTS-criterion), the generalized maximum tangential stress (GMTS criterion), the strain energy density (S-criterion) and the maximum triaxial stress (M-criterion) criteria are used to obtain θ_c numerically and these criteria are discussed.

Another purpose of this study is to determine crack initiation angles, the effect of critical radius r_c and T-stress on crack initiation angles using experimental and analytical

techniques. The specimen used is shown in Fig 1.1. The plate is under uniaxial uniform tension σ with a central crack of length 2a. The crack is inclined at an angle, β (crack inclination angle), which is measured clockwise to the direction of the load. The crack initiation is assumed to occur at an angle θ_c, measured clockwise from crack line.

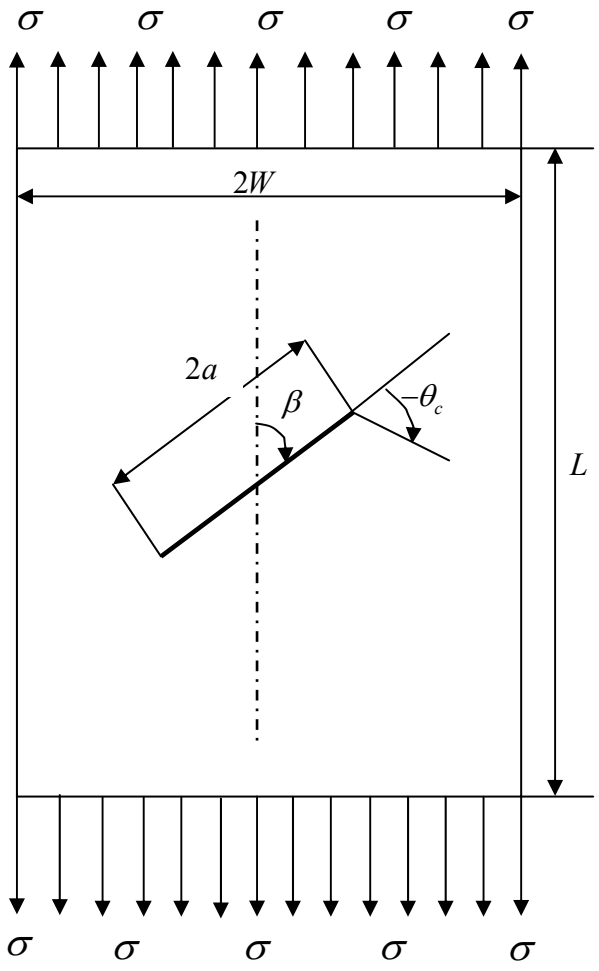

Figure 1.1. Uniaxial loading

1.2. Asymptotic Stress Field at the Crack Tip

For the general case of a solid body containing a crack subjected to loading, the overall stress field in the vicinity of the crack tip can be separated into three basic modes, namely mode I (opening), mode II (sliding), and mode III (tearing).

All criteria that will be used in this study depend on stress field around the crack tip just before the onset of crack propagation. Stress field in Cartesian co-ordinate and polar co-ordinate systems are shown in Figure 1.2(a) and 1.2(b).

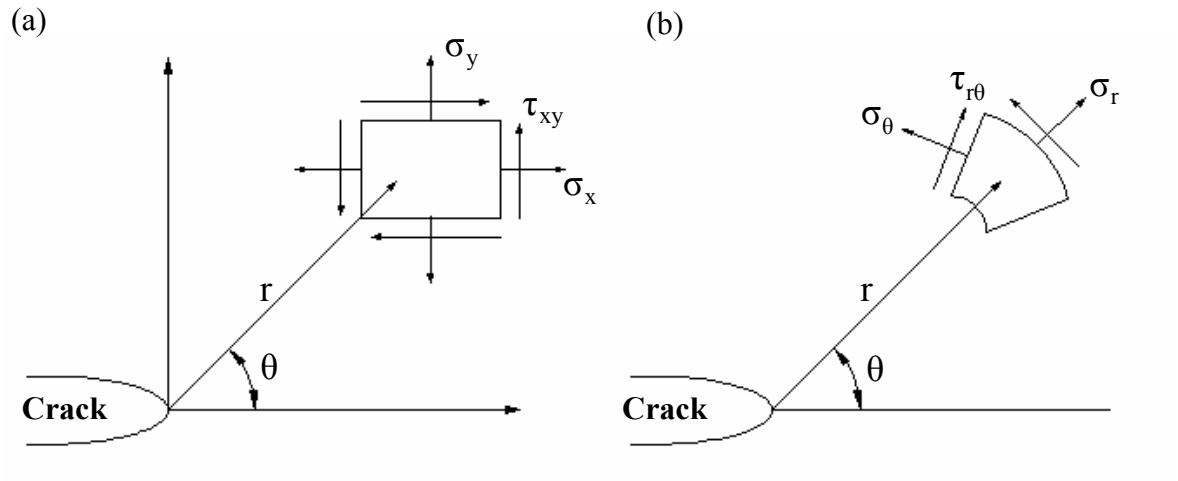

Figure 1.2. Stress field in (a) Cartesian co-ordinate system, (b) Polar co-ordinate system

For a two dimensional elastic stress field in crack problems, Westergard [1] and Williams [2] proposed a set of asymptotic solutions for stresses that would satisfy equilibrium and compatibility conditions near the crack tip. The stress field in any linear elastic cracked body is defined as follows;

$$\sigma_{ij} = \frac{K}{\sqrt{2\pi r}} f_{ij}(\theta) + other\ terms, \tag{1.1}$$

where σ_{ij} is the stress tensor, θ and r are shown in Figure 1.2, K is a constant (stress intensity factor) and f_{ij} are functions of θ as shown with a subscript to denote the mode of loading; *i.e.*, Mode-I, Mode-II [3].

The stress field at the crack tip in Cartesian co-ordinates is defined as:

$$\sigma_{xx} = \frac{1}{\sqrt{2\pi r}}\left[\left\{K_I \cos\frac{\theta}{2}\left(1 - \sin\frac{\theta}{2}\sin\frac{3\theta}{2}\right)\right\} - \left\{K_{II} \sin\frac{\theta}{2}\left(2 + \cos\frac{\theta}{2}\cos\frac{\theta}{2}\right)\right\}\right] + T + O(r), \tag{1.2}$$

$$\sigma_{yy} = \frac{1}{\sqrt{2\pi r}}\left[\left\{K_I \cos\frac{\theta}{2}\left(1+\sin\frac{\theta}{2}\sin\frac{3\theta}{2}\right)\right\}+\left\{K_{II}\sin\frac{\theta}{2}\cos\frac{\theta}{2}\cos\frac{3\theta}{2}\right\}\right]+O(r), \qquad (1.3)$$

$$\tau_{xy} = \frac{1}{\sqrt{2\pi r}}\left[\left\{K_I \cos\frac{\theta}{2}\sin\frac{\theta}{2}\cos\frac{3\theta}{2}\right\}+\left\{K_{II}\cos\frac{\theta}{2}\left(1-\sin\frac{\theta}{2}\sin\frac{3\theta}{2}\right)\right\}\right]+O(r) \qquad (1.4)$$

$$\sigma_{zz} = v(\sigma_x + \sigma_y) \quad \textit{for plane strain}, \qquad (1.5)$$

$$\sigma_{zz} = 0 \quad \textit{for plane stress}. \qquad (1.6)$$

In polar co-ordinates:

$$\sigma_{\theta\theta} = \frac{1}{\sqrt{2\pi r}}\left[\left\{\frac{K_I}{2}\cos\frac{\theta}{2}(1+\cos\theta)\right\}-\left\{\frac{3K_{II}}{2}\sin\frac{\theta}{2}(1+\cos\theta\right\}\right]+T\sin^2\theta+O(r), \qquad (1.7)$$

$$\sigma_{rr} = \frac{1}{\sqrt{2\pi r}}\left[\left\{\frac{K_I}{2}\cos\frac{\theta}{2}(3-\cos\theta)\right\}-\left\{\frac{K_{II}}{2}\sin\frac{\theta}{2}(1-3\cos\theta\right\}\right]+T\cos^2\theta+O(r), \qquad (1.8)$$

$$\tau_{r\theta} = \frac{1}{\sqrt{2\pi r}}\left[\left\{\frac{K_I}{2}\sin\frac{\theta}{2}(1+\cos\theta)\right\}-\left\{\frac{K_{II}}{2}\cos\frac{\theta}{2}(1-3\cos\theta\right\}\right]+T\sin\theta\cos\theta+O(r). \qquad (1.9)$$

The equations above represent singular elastic stress field and assume a global elastic behavior with a small scale yielding represented by a small plastic zone at the crack tip. Terms multiplying $1/\sqrt{r}$ are singular parts of the elastic stress field. T is the constant non-singular part of the elastic stress field. $O(r)$ are the higher order terms which are negligible at the crack tip. Stresses far from the crack tip can not be defined by Equations 1.2-1.9. A region called K-dominant region is considered as the region where the equations above can be used to describe the stress field accurately.

1.3. Loading Under Mixed-Mode

To calculate crack initiation angles, intensity factors are defined for the angled crack problem for different loading conditions. General forms of stress intensity factors are given by [4]

$$K_I = \sigma_n \sqrt{\pi a}, \tag{1.10}$$

$$K_{II} = \tau_n \sqrt{\pi a} \tag{1.11}$$

For a crack embedded in an infinite medium, σ_n and τ_n are the normal and the tangential stresses to the crack plane respectively, as shown Figure 1.3. To get the definitions for σ_n and τ_n for the slant crack problem, the most general loading case is considered as the following:

$$\sigma_n = \sigma_{x'} \cos^2 \beta + \sigma_{y'} \sin^2 \beta - \tau_{x'y'} \sin 2\beta, \tag{1.12}$$

$$\tau_n = \frac{\left(\sigma_{y'} - \sigma_{x'}\right)}{2} \sin 2\beta - \tau_{x'y'} \cos 2\beta. \tag{1.13}$$

Equations 1.10 to 1.13 are used to get the stress intensity factors for various loading conditions as illustrated in Figure 1.3.

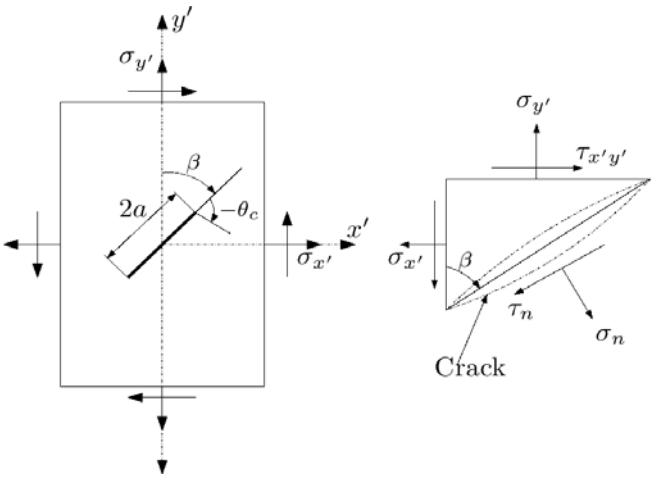

Figure 1.3. General loading conditions for angled crack problem [4]

For the case of a central crack in a large plate loaded by a remote uniaxial tensile stress, we assume:

$$\sigma_{x'} = 0,$$

$$\sigma_{y'} = \sigma, \tag{1.14}$$

$$\tau_{x'y'} = 0$$

and the stress intensity factors can be given by

$$K_I = \sigma \sin^2 \beta \sqrt{\pi a}, \tag{1.15}$$

$$K_{II} = \sigma \sin \beta \cos \beta \sqrt{\pi a} \tag{1.16}$$

where a is a half length of the crack. By rearranging Equations 1.15 and 1.16, the ratio of K_I and K_{II} can be related to β by:

$$\frac{K_I}{K_{II}} = \tan \beta \tag{1.17}$$

and it is obvious that the factor $\tan \beta$ provides a convenient measure of the mode-I and mode-II ratio regardless of the testing configuration employed.

$$\beta_{eq} = \tan^{-1}\left(\frac{K_I}{K_{II}}\right) \tag{1.18}$$

where β_{eq} is the equivalent crack angle.

1.4. Fracture Toughness

The stresses in the vicinity of a crack tip can be defined in terms of the stress intensity factor. A critical value of K can be computed to specify the conditions for brittle fracture, and this critical value is called "the fracture toughness K_c", defined by:

$$K_c = Y(a/w)\sigma_c\sqrt{\pi a} \tag{1.19}$$

Here, σ_c is the critical stress for crack propagation, and Y is represented as a function of both crack length a and the component width W and tabulated for almost all conceivable shapes and sizes of specimens [5].

By definition, fracture toughness is a property that is a measure of a material's resistance to brittle fracture when a crack is present. Its unit is the same as for the stress intensity factor (*i.e.* $\text{MPa}\sqrt{\text{m}}$ or $\text{psi}\sqrt{\text{in.}}$).

For relatively thin specimens, the value of K_c will depend on and decrease with increasing specimen thickness B, as given Figure 1.4 at which the plane strain is said to exist. The constant K_c value for thicker specimens is known as the plane strain fracture toughness K_{Ic}, which is also defined by

$$K_{Ic} = Y\sigma\sqrt{\pi a} \tag{1.20}$$

The *I* subscript for K_{Ic} denotes that this critical value of *K* is for mode-I condition. Brittle materials, for which appreciable plastic deformation is not possible in front of an advancing crack, have low K_{Ic} values and are vulnerable to catastrophic failure. On the other hand, K_{Ic} values are relatively large for ductile materials. Fracture mechanics is especially useful in predicting catastrophic failure in materials having intermediate ductility.

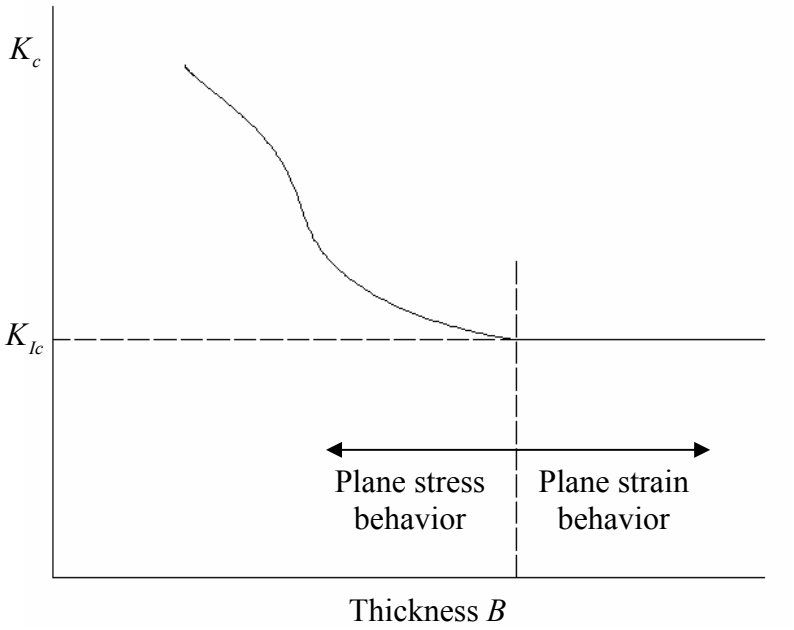

Figure 1.4. Schematic representation showing the effect of plate thickness on fracture toughness [5]

A material may be subjected to varying levels of different types of stress, however, there is a specific stress level at which the material plastically deforms that is, the yield strength. Likewise, a variety of K's are possible, whereas K_{Ic} is unique for a particular material, and indicates the conditions of flaw size and stress necessary for brittle fracture.

The plane strain fracture toughness K_{Ic} is a fundamental material property that depends on many factors, the most influential of which are temperature, strain rate, and microstructure. Cracked structures are subjected mixed-mode loading, thus in general the stress intensity factors K_I and K_{II} are both nonzero, yet we usually measure only mode-I fracture toughness K_{Ic}. Thus, so far the only fracture propagation criterion we have is for mode-I. In other words, the stress intensity factor is the main tool to determine the stress field. K is a measure of all stresses and strains. Crack extension will occur when the stresses and strains at the crack tip reach a critical value. This means that the fracture must be expected to occur when K_I reaches a critical value K_{Ic}. The critical value K_{Ic} is expected to be material parameter.

1.5. Literature Survey

Irwin is one of the very early researchers who studied the local stress field around the crack tip by applying the Griffith's concept to solve fracture problems. He proposed three modes of crack extension which are identified by stress intensity factors k_1, k_2 and k_3 [4].

For mixed-mode loading, there are several criteria for predicting fracture. Using stress as a parameter, the angled crack problem presents an example of mixed-mode fracture in two-dimensional stress field. It was first examined by Erdogan and Sih [6], who proposed the maximum tangential stress criterion (MTS-criterion). It was the first criterion to predict the crack initiation angle under mixed-mode loading. According to MTS-criterion, a crack initiates in a direction corresponding to the direction of maximum tangential stress along a constant radius around the crack tip. The MTS-criterion is based on the assumption that the material behaves ideally brittle. Erdogan and Sih also performed uniaxial tensile experiments to support their theory. They used polymethylmethacrylate (PMMA) specimens, which are considered as a good homogeneous, isotropic, and linearly elastic brittle material. The results show a good agreement between the theoretical and the experimental results.

Some of the first experiments to explore the application of a brittle fracture criterion for mixed-mode loading were investigated by Williams and Ewing [7]. They used polymethylmethacrylate (PMMA) specimens in their experiments. The experimental results from the test on PMMA specimens containing an angled crack were in a band, which was wider for cracks subjected to large amounts of shear (small crack angles relative to the tensile loading direction). Williams and Ewing showed that there was an important difference between mixed-mode behavior predicted by the MTS-criterion and their experiments, which the largest errors occur at small loading angles. They stated that one reason for this difference was the presence of the T-stress, where the T-stress is a constant stress parallel to the crack. Williams and Ewing added a non-singular term to the elastic stress field and applied the MTS-criterion to predict crack initiation angle. Later, Ueda *et*

al. [8] and Theocaris [9] carried out their experiments using PMMA specimens. They observed the same effects with those illustrated by Williams and Ewing.

Vallejo [10] performed mixed mode fracture experiments under uniaxial compression, for both brittle and ductile states. Vallejo used kaolinite clay specimens in his experiments, and stated that a sample with water content less than 20% behaves in brittle manner. Vallejo showed strong agreement between the theoretical predictions by MTS-criterion and the experimental data for brittle material under uniaxial compression [11].

In 1973, Sih [12] proposed the minimum strain energy density criterion (S-criterion). This criterion states that the crack initiation will start in a radial direction along which the strain energy density is a minimum. The importance of this criterion which makes it different from the other approaches is that S-criterion is the only one that shows dependence of crack initiation on the material elastic properties represented by the Possion's ratio v and the state of the stress. A limited amount of experimental data was presented in support of this criterion. It shows good agreement with the experimental data for PMMA for $v = 1/3$.

Williams and Ewing [7] illustrated a special case for the influence of the T-stress on brittle fracture in their experiments where they used a plate containing an angled crack. In this work, the generalized MTS-criterion was presented to investigate mixed-mode fracture for linear elastic and brittle materials where the size of the plastic zone around the crack tip is negligible relative to the size of the crack and the process zone. The generalized MTS-criterion takes into account the effects of both the singular terms and T term in tangential stress around the crack tip. The generalized MTS-criterion is then used to validate earlier experimental results of Williams and Ewing and Ueda et al. [8]. They showed that brittle failure can be associated with the singular stress, T-stress or a combination of two [13]

The Maximum triaxial stress (M-criterion) was proposed by Kong [14]. This criterion states that the crack starts to grow from where the triaxiality ration is maximum. In his experiments, steel FeE 550 specimens were used. At room temperature, the fracture of the steel shows ductility. Therefore, the experiments for the steel FeE 550 were conducted at a temperature of -140^{o} C.

Under these considerations, Crack initiation fracture for PMMA and PS materials under mixed-mode loading condition is analyzed in this work following an experimental work. The results are then compared with those obtained by the means of MTS-criterion, GMTS criterion, S-criterion, and M-criterion. The difference among these predictions for the central angled crack problem under uniaxial tensile loading is shown.

2. DESCRIPTION OF CRACK GROWTH CRITERIA USED IN THIS STUDY

The maximum tangential stress (MTS-criterion), the generalized maximum tangential stress (GMTS-criterion), the minimum strain energy density (S-criterion) and the maximum triaxial stress (M-criterion) criteria will be briefly explained in this section

2.1. MTS-criterion

This criterion was proposed by Erdogan and Sih [6]. The maximum tangential stress criterion is the first criterion which predicts the crack initiation angle. MTS-criterion states that crack extension starts at the crack tip in radial direction. This extension is in that radial direction perpendicular to the direction of the greatest tension. Crack extension begins when this tension reaches a certain critical value at a certain distance from the crack tip. In other words, it can be stated that the crack will start to grow from the tip in the direction along which the tangential stress $\sigma_{\theta\theta}$ is maximum and shear stress $\tau_{r\theta}$, is zero.

For two dimensional elastic crack problems, the stress field in any linear elastic cracked body in K-dominant region is defined as the following,

$$\sigma_{ij} = \frac{K}{\sqrt{2\pi r}} f_{ij}(\theta) + other\ terms \tag{2.1}$$

Including only the singular term of this equation, the tangential stress $\sigma_{\theta\theta}$ near the crack tip in polar co-ordinate system is defined as ;

$$\sigma_{\theta\theta} = \frac{1}{\sqrt{2\pi r}} \cos\frac{\theta}{2}\left(K_I \cos^2\frac{\theta}{2} - \frac{3}{2} K_{II} \sin\theta \right) \tag{2.2}$$

where K_I and K_{II} are the mode-I and mode-II stress intensity factors respectively. The maximum tangential stress criterion can be stated as;

$$\frac{\partial \sigma_{\theta\theta}}{\partial \theta} = 0 \text{ and } \frac{\partial \sigma^2{}_{\theta\theta}}{\partial \theta^2} < 0 \tag{2.3}$$

Therefore, we obtain the following form:

$$\left(\cos\frac{\theta_c}{2}\right)\left(K_I \sin\theta_c + K_{II}\left(3\cos\theta_c - 1\right)\right) = 0 \tag{2.4}$$

and,

$$\frac{3}{8}\left(1-3\cos\theta_c\right)\left(K_I \cos\frac{\theta_c}{2} - K_{II}\sin\frac{\theta_c}{2}\right) + \frac{9}{4}K_{II}\left(1+\cos\theta_c\right)\sin\frac{\theta_c}{2} < 0 \tag{2.5}$$

where θ_c is the crack propagation angle.

Equation 2.4 has two solutions:

First one is the trivial solution;

$$\theta_c = \pm\pi \ \ for \ \cos\frac{\theta_c}{2} = 0 \tag{2.6}$$

The second one is non-trivial solution which is known as a classical Erdogan and Sih equation:

$$K_I \sin\theta_c + K_{II}\left(3\cos\theta_c - 1\right) = 0 \tag{2.7}$$

For pure mode-I, $K_{II} = 0$ and Equation 2.7 becomes:

$$K_I \sin\theta_c = 0 \Rightarrow \theta_c = 0 \tag{2.8}$$

For pure mode-II, $K_I = 0$ and Equation 2.7 becomes:

$$K_{II}\left(3\cos\theta_c - 1\right) = 0 \Rightarrow \theta_c = \pm 70,53^0 \tag{2.9}$$

For mixed-mode which is a combination of mode-I and mode-II, Equation 2.7 can be rewritten as following:

$$K_I \sin\theta_c + K_{II}\left(3\cos\theta_c - 1\right) = 0$$

$$2\left(\tan\frac{\theta_c}{2}\right)^2 - \mu\left(\tan\frac{\theta_c}{2}\right) - 1 = 0, \text{ where } \mu = \frac{K_I}{K_{II}} \tag{2.10}$$

Therefore, the crack initiation angle θ_c can be written as a function of μ as seen in Equation 2.11:

$$\theta_c = 2\arctan\left(\frac{\mu}{4} - \frac{1}{4}\sqrt{(\mu^2 + 8)}\right) \tag{2.11}$$

The value of M^e is 1 for pure mode-I and zero for pure mode-II. For mixed-mode, the parameter takes values between 0 and 1. The value of M^e is can be stated in following equation.

$$M^e = \frac{2}{\pi}\tan^{-1}\left(\frac{K_I}{K_{II}}\right) \tag{2.12}$$

In the case of plane strain or generalized plane stress where material contains a straight crack, Erdogan and Sih [6] states that the stress state in the neighborhood of the crack tip can be written as Equation 2.1. In this equation, K_I and K_{II} are symmetric and skew-symmetric components of the stress intensity factors, and are functions of the external loads. For the case of a central crack in a large plate loaded by remote uniaxial

tensile stress, σ oriented at an angle, β with respect to the axis of the crack, K_I and K_{II} are given by:

$$K_I = \sigma a^{1/2} \sin^2 \beta, \tag{2.13}$$

$$K_{II} = \sigma a^{1/2} \sin \beta \cos \beta. \tag{2.14}$$

where a is a half the length of the crack. When we rearrange Equation 2.12, the value of M^e can be rewritten as following equation:

$$M^e = \frac{2}{\pi} \tan^{-1}\left(\frac{K_I}{K_{II}}\right) \Rightarrow \frac{2}{\pi} \tan^{-1}\left(\frac{\sigma a^{1/2} \sin^2 \beta}{\sigma a^{1/2} \sin \beta \cos \beta}\right)$$

$$M^e = \frac{2}{\pi} \tan^{-1}\left(\tan \beta\right) \Rightarrow \frac{2}{\pi} \beta \tag{2.15}$$

It is apparent that $M_e = 1$ for pure mode-I and $M_e = 0$ for pure mode-II.

Also, the fracture surface is determined for each criterion. Fracture surface is a loci of points in K_I-K_{II} space where the combined action K_I and K_{II} reaches to a particular material dependent value. Experimental results show that this surface has an elliptical form and it can be written in the following form [15],

$$\left(\frac{K_I}{K_{IC}}\right)^2 + \left(\frac{K_{II}}{K_{IIC}}\right)^2 = 1 \tag{2.16}$$

where K_{IC} and K_{IIC} are fracture toughness values for mode-I and mode-II .

Erdogan and Sih [6] performed uniaxial tensile experiments to check their results. They used PMMA specimens with inclined central crack. The results are in agreement with the theoretical predictions and the experimental results. They obtained eight different crack initiation angles, θ_c for each crack inclination angle β. The experimental data for four sets of test are given in Table 2.1.

Table 2.1. Measured values of the fracture angle [12].

β		30	40	50	60	70	80
θ_c at right	1	-64	-55.5	-50	-40	-29	-17
	2	-60	-52	-50	-43.5	-30.5	-18
	3	-63	-57	-53	-44.5	-	-15.5
	4	-	-57	-52	-43.5	-	-
θ_c at left	1	-65	-58	-50.5	-44	-31.5	-18.5
	2	-	-53	-52	-40	-31	-17.5
	3	-60	-55	-51.5	-46	-31.5	-17
	4	-	-57	-50	-43	-	-
$(\theta_c)_{avg.}$		-62.4	-55.6	-51.1	-43.1	-30.7	-17.3

The theoretical calculation for the maximum tangential stress criterion (MTS-criterion) and experiment results can be seen in Table 2.2.

Table 2.2. Measured and calculated values of the fracture angle [6, 12]

Crack Inclination Angle, β	0	30	40	50	60	70	80
Mode Mixitiy Parameter, M^e	0	0.33	0.44	0.55	0.66	0.77	0.88
Experimental Results, $-\theta_c$	-70	-62.4	-55.6	-51.1	-43.1	-30.7	-17.3
Theoretical Results, $-\theta_c$	-70.53	-60.2	-55.7	-50.2	-43.2	-33.2	-19.3

The validity of these predictions can be checked with results of a series of experiments performed on Plexiglas specimens in Figure 2.1.

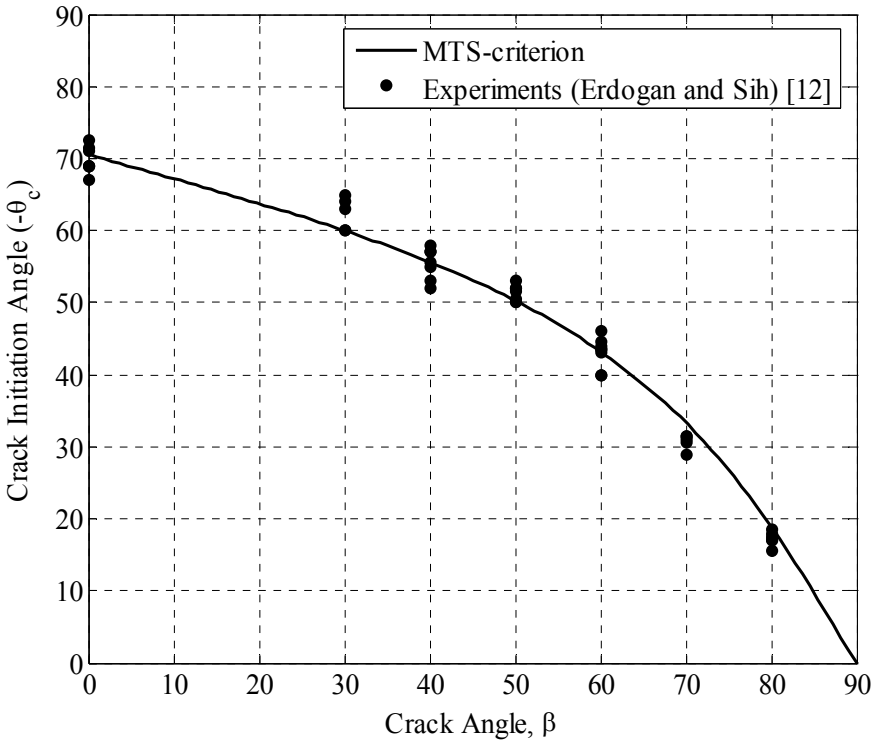

Figure 2.1. Crack angle vs crack initiation angle in a cracked plate under uniform tension

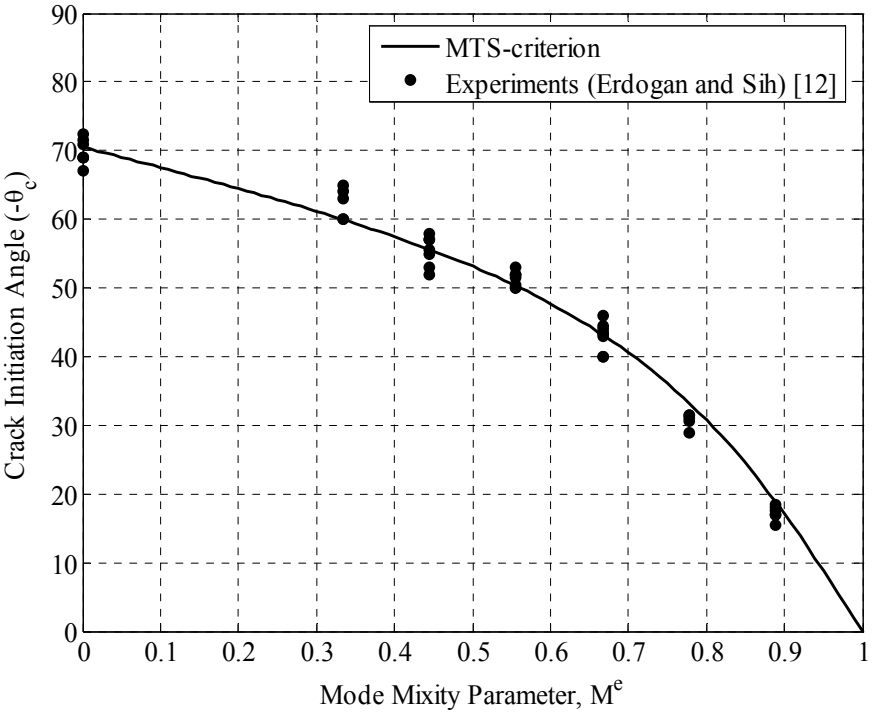

Figure 2.2. Crack initiation angle vs mode mixity parameter M^e based on the MTS criterion

Figure 2.2 shows the solution of Equation 2.11 and all experimental results in graphical form. From Figure 1.5, it can be shown that for pure mode-II conditions ($\beta = 0$) the initiation angle is predicted to be 70.5^{o}. The limited amount of experiments showed good agreement with the predictions of the MTS-criterion presented by Erdogan and Sih .

Williams and Ewing [7] conducted a more detailed experimental investigation of the same problem using PMMA plates under uniaxial uniform tension and confirmed the previous results in the same range of β used by Erdogan and Sih [6]. However, they found in the range of $\beta < 15^{0}$ there was a considerable deviation from prediction of the MTS-criterion and the initiation angle tented more towards 90° than towards 70.5° as approaching pure mode-II conditions. They were also able to show that a better correlation with experiments. William and Ewing present graphically a large number of values of θ_c for various values of β. The precise values for each data point were obtained by zooming into the original Williams and Ewing plot, and then determining the coordinates. The experimental results for crack initiation angles presented by Williams and Ewing are shown in Figure 2.3.

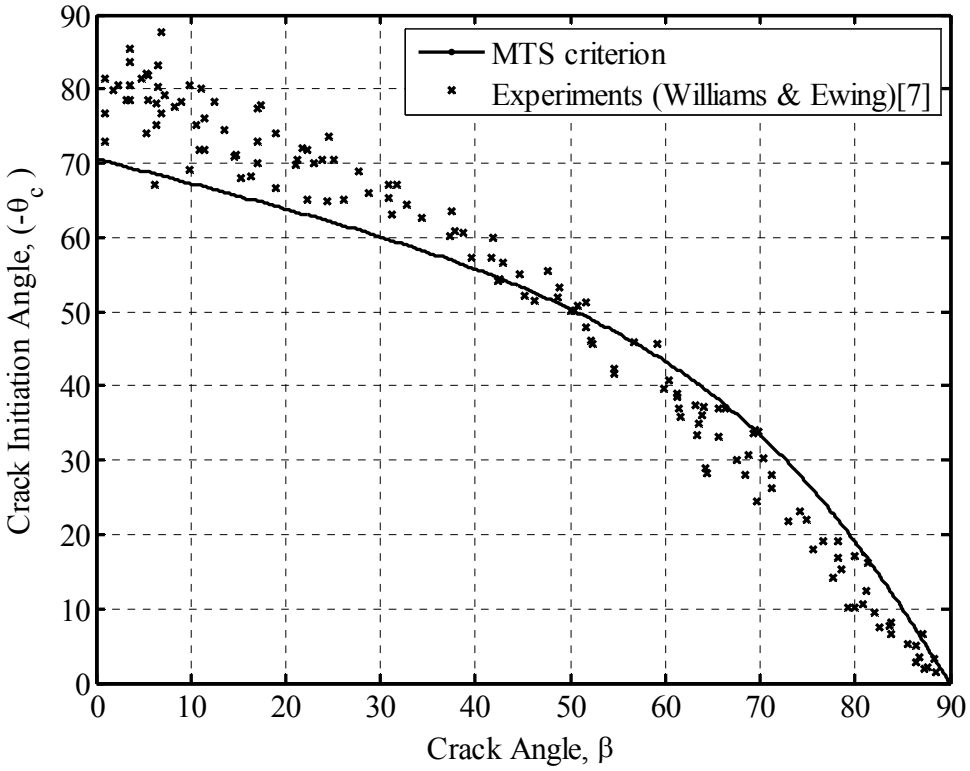

Figure 2.3. Experimental results for crack initiation angle

The experimental results about the crack initiation angles under mixed-mode loading for PMMA plates also were presented by Ueda at al [8]. The predictions from the MTS-criterion and the experimental results are shown in Figure 2.4.

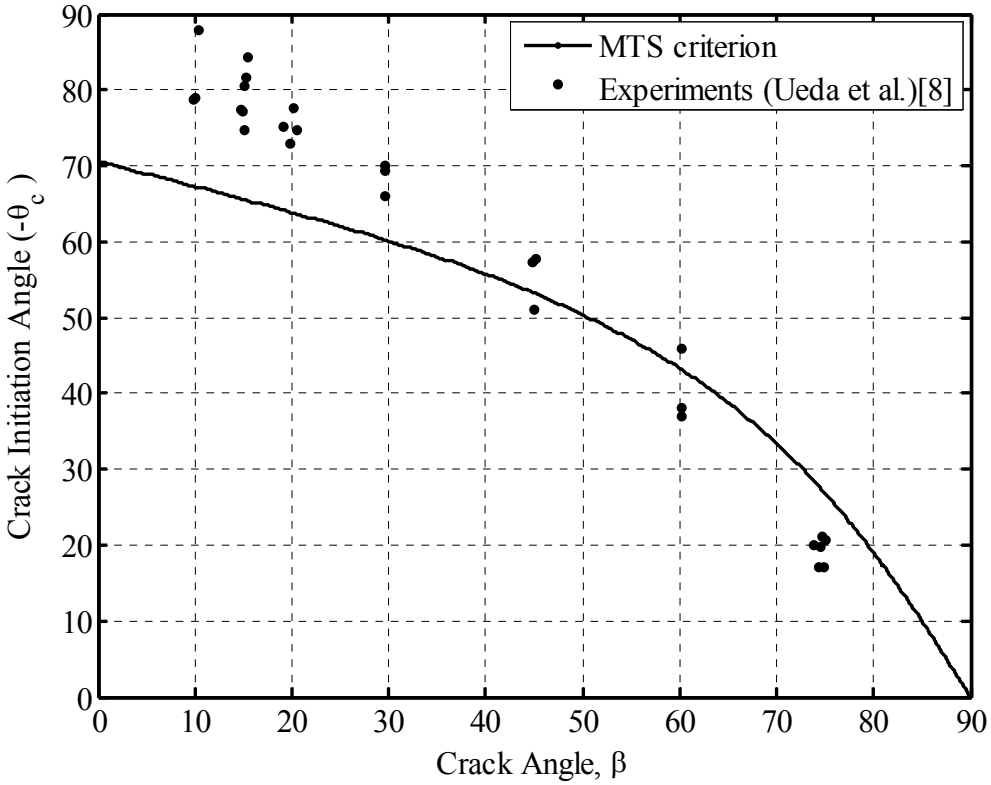

Figure 2.4. Experimental results for crack initiation angle

Both of the experimental results shown in Figures 2.3 and 2.4, show that the T-stress has an influence on mixed-mode loading. In using a plate containing an angled crack, Williams and Ewing illustrated a special case of the influence of the T-stress on brittle fracture. The generalized MTS-criterion is then used to reevaluate earlier experimental results of Williams and Ewing [7], and Ueda et al.[8] Their experimental results show that brittle failure can be associated with the singular stress, T-stress or a combination of both.

2.2. The Generalized MTS-Criterion

Several fracture criteria have been developed to describe brittle failure in linear elastic materials, when subjected to combination of tensile and shear loading conditions. Erdogan and Sih [6] proposed the maximum tensile stress criterion (MTS-criterion), and the minimum strain energy criterion (S-criterion) was developed by Sih [12]. These mixed-mode criteria show same results for the pure mode-I loading conditions and separate from each other for cracks under mixed-mode loading condition.

Some of the first experiments to find the applications of brittle fracture criterion for mixed-mode loading were performed by Williams and Ewing [7] using PMMA. Williams and Ewing showed that there was a difference between mixed-mode fracture based on MTS-criterion proposed by Erdogan and Sih [6] and their experimental results, with the largest errors occurring at small loading angles. One reason for the difference was the presence of the T-stress, where T-stress is a constant stress parallel to the crack.

In later work, Uead et al. [8] illustrated similar effects and their tests were also carried out by using PMMA. The experimental work by Williams and Ewing [7] and Ueda et al. [8] demonstrated that non-singular terms in the series expansion of the stresses ahead of the crack have an important effect on brittle fracture in linear elastic materials subjected to mixed-mode loading condition.

The generalized MTS-criterion takes into account the effects of both the singular terms and the T-term in the tangential stress around the crack tip. Using this criterion, the direction and the crack initiation angle can be predicted for any combination of the crack tip parameters K_I, K_{II} and T. It is shown that positive T reduces the fracture toughness in mixed-mode loading and negative T increases it. The generalized MTS-criterion is used to reevaluate earlier experimental results of Williams and Ewing [7] and Ueda et al. [8].

The tangential stress, in polar co-ordinates, can be written as following form for any homogenous and isotropic body:

$$\sigma_{\theta\theta} = \frac{1}{\sqrt{2\pi r}} \cos\frac{\theta}{2}\left(K_I \cos^2\frac{\theta}{2} - \frac{3}{2} K_{II} \sin\theta \right) + T\sin^2\theta + O(r) \qquad (2.17)$$

The higher order term $O(r)$ can be considered negligible near the crack tip. The crack tip parameters K_I, K_{II} and T depend on the geometry and loading conditions and vary considerably for different specimens.

For brittle crack initiation in linear elastic materials, it is assumed that the crack growth in mode-I condition initiates when the tangential stress $\sigma_{\theta\theta}$ at a critical radius r_c in front of the crack tip, reaches a critical value $(\sigma_{\theta\theta})_c$. The parameter r_c and $(\sigma_{\theta\theta})_c$ are the specific material properties and are assumed to be independent of the geometry of specimen and the loading conditions. This concept can also be used for MTS-criterion in mixed mode loading to investigate the direction of the crack initiation angle at the critical radius r_c from the crack tip [13].

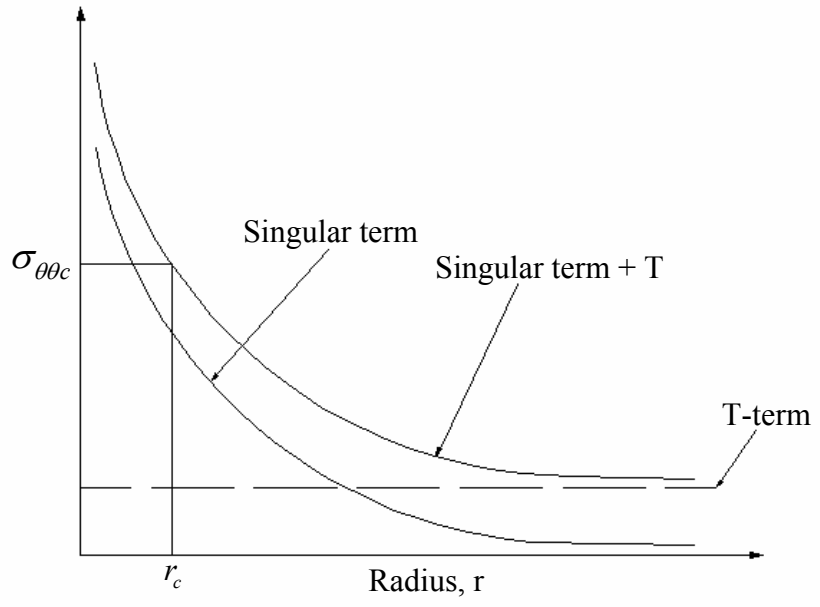

Figure 2.5. Elastic tangential stress along the direction of fracture initiation, θ_c [13]

At the critical distance, r_c where the contribution of the higher order terms $O(r)$ in Equation 2.17 can be ignored, the singular term is finite and T-stress can be a significant

fraction of the tangential stress which is seen in Figure 2.5. For pure mode-I condition, the T-term vanishes in the expansion for the tangential stress in front of the crack tip along the crack line$(\theta = 0)$. Consequently, if it is assumed that the brittle fracture occurs on the crack line, then the T-stress has no effect. In mixed-mode conditions, the crack growth is not in the same plane as the initial crack. For this case, the T-stress contributes to the tangential stress [13].

For the sake of clarity, it is proper to normalize the effect of T-stress, relative to the stress intensity factor in mode-I. First, a dimensionless parameter called the biaxiality ratio *B* was proposed by Leevers and Radon [16].

$$B = \frac{T\sqrt{(\pi a)}}{K_I} \tag{2.18}$$

where a is the crack length and Equation 2.18 can be extended to mixed-mode with K_I replaced by K_{eff}, so that:

$$B = \frac{T\sqrt{(\pi a)}}{K_{eff}} \tag{2.19}$$

where the effective stress intensity factor K_{eff} is defined as:

$$K_{eff} = \sqrt{\left((K_I)^2 + (K_{II})^2\right)} \tag{2.20}$$

The maximum tangential criterion (MTS-criterion) proposed by Erdogan and Sih [6] states that the crack will start to grow from the tip in the direction along which the tangential stress $\sigma_{\theta\theta}$ is maximum and shear stress $\tau_{r\theta}$, is zero. The generalized maximum tangential stress criteria can be stated as;

$$\frac{\partial \sigma_{\theta\theta}}{\partial \theta} = 0 \text{ and } \frac{\partial \sigma^2{}_{\theta\theta}}{\partial \theta^2} < 0 \Rightarrow \theta = \theta_c \tag{2.21}$$

If we rearrange Equation 2.17 and 2.21 for mixed-mode loading, we obtain following equation:

$$K_I \sin\theta_c + K_{II}\left(3\cos\theta_c - 1\right) - \frac{16}{3} T\sqrt{\left(2\pi r_c\right)} \frac{\sin\theta_c}{2} \cos\theta_c = 0 \tag{2.22}$$

where r_c is a critical radius and θ_c is the crack propagation angle.

As we seen that, for T= 0 and r_c = 0, Equation 2.22 turns into the equation obtained from classical MTS-criterion proposed by Erdogan and Sih [6].

$$K_I \sin\theta_c + K_{II}\left(3\cos\theta_c - 1\right) = 0 \tag{2.23}$$

If the critical radius r_c from the crack tip is presented in the dimensionless form as following:

$$\alpha = \sqrt{\frac{2r_c}{a}} \tag{2.24}$$

Substituting Equation 2.24 into Equation 2.22, we obtain:

$$K_I \sin\theta_c + K_{II}\left(3\cos\theta_c - 1\right) - \frac{16}{3}\left(K_{eff} B\alpha\right) \frac{\sin\theta_c}{2} \cos\theta_c = 0 \tag{2.25}$$

Therefore, crack initiation angle θ_c is found from Equation 2.26.

$$\sqrt{2\pi r_c}\left(\sigma_{\theta\theta}\right)_c = \cos\frac{\theta_c}{2}\left(K_I \cos^2\frac{\theta_c}{2} - \frac{3}{2} K_{II} \sin\theta_c\right) + T\sqrt{2\pi r_c}\sin^2\theta_c \tag{2.26}$$

where $(\sigma_{\theta\theta})_c$ is the critical value of tangential stress at the critical radius r_c. For pure mode-I when K_{II}, T and θ_c are equal to zero. And if we replace K_I with the mode-I fracture toughness K_{Ic}, Equation 2.26 reduces to

$$\sqrt{2\pi r_c}\,(\sigma_{\theta\theta})_c = K_{Ic} \tag{2.27}$$

Plugging Equation 2.27 into Equation 2.26, we obtain following equations:

$$K_{Ic} = \cos\frac{\theta_c}{2}\left(K_I\cos^2\frac{\theta_c}{2} - \frac{3}{2}K_{II}\sin\theta_c\right) + T\sqrt{2\pi r_c}\sin^2\theta_c, \tag{2.28}$$

$$K_{Ic} = \cos\frac{\theta_c}{2}\left(K_I\cos^2\frac{\theta_c}{2} - \frac{3}{2}K_{II}\sin\theta_c\right) + B\alpha K_{eff}\sin^2\theta_c \tag{2.29}$$

Dividing Equation 2.29 by K_{II}, we obtain the normalized mode-II fracture toughness,

$$\frac{K_{II}}{K_{Ic}} = \frac{1}{\left[\cos\frac{\theta_c}{2}\left(\mu\cos^2\frac{\theta_c}{2} - \frac{3}{2}\sin\theta_c\right) + B\alpha\sqrt{\left(1+\mu^2\right)}\sin^2\theta_c\right]} \tag{2.30}$$

where $\mu = \dfrac{K_I}{K_{II}}$

And multiplying $\dfrac{K_{II}}{K_{Ic}}$ by μ, we can write $\dfrac{K_I}{K_{Ic}}$ as the following:

$$\frac{K_I}{K_{Ic}} = \frac{\mu}{\left[\cos\frac{\theta_c}{2}\left(\mu\cos^2\frac{\theta_c}{2} - \frac{3}{2}\sin\theta_c\right) + B\alpha\sqrt{\left(1+\mu^2\right)}\sin^2\theta_c\right]} \tag{2.31}$$

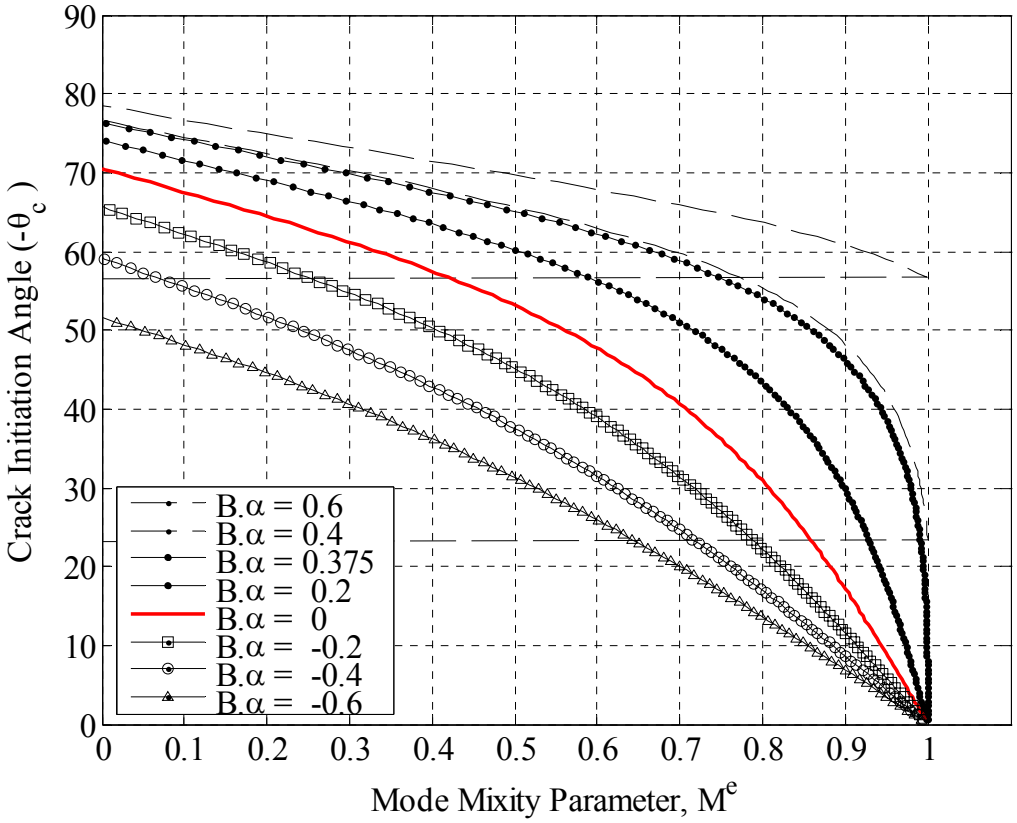

Figure 2.6. The effect of the T-stress and r_c on the crack initiation angle in mixed-mode condition [15]

Equations 2.25, 2.28 and 2.29 describe the generalized MTS-criterion. The solution of these equations is not as same as those presented by Erdogan and Sih [6] for the conventional MTS-criterion. For range $-0.6 < B\alpha < 0.6$, a closed form solution is used to solve equation. The solutions are shown in Figure 2.6. T-stress is represented by dimensionless parameter $B\alpha$. Figure 2.6 shows the effect of $B\alpha$, in the range $-0.6 < B\alpha < 0.375$ on the crack initiation angle. It is most noticeable that for linearly elastic material subjected to pure mode-I, T-stress has no effect on the crack initiation angle when $B\alpha$ is between -0.6 and 0.375. However for mixed-mode, T-stress has a large effect on the crack initiation angle. In addition, for pure mode-I condition and $B\alpha$ greater than 0.375, the figure shows that the crack initiation angle is different from 0^o [13].

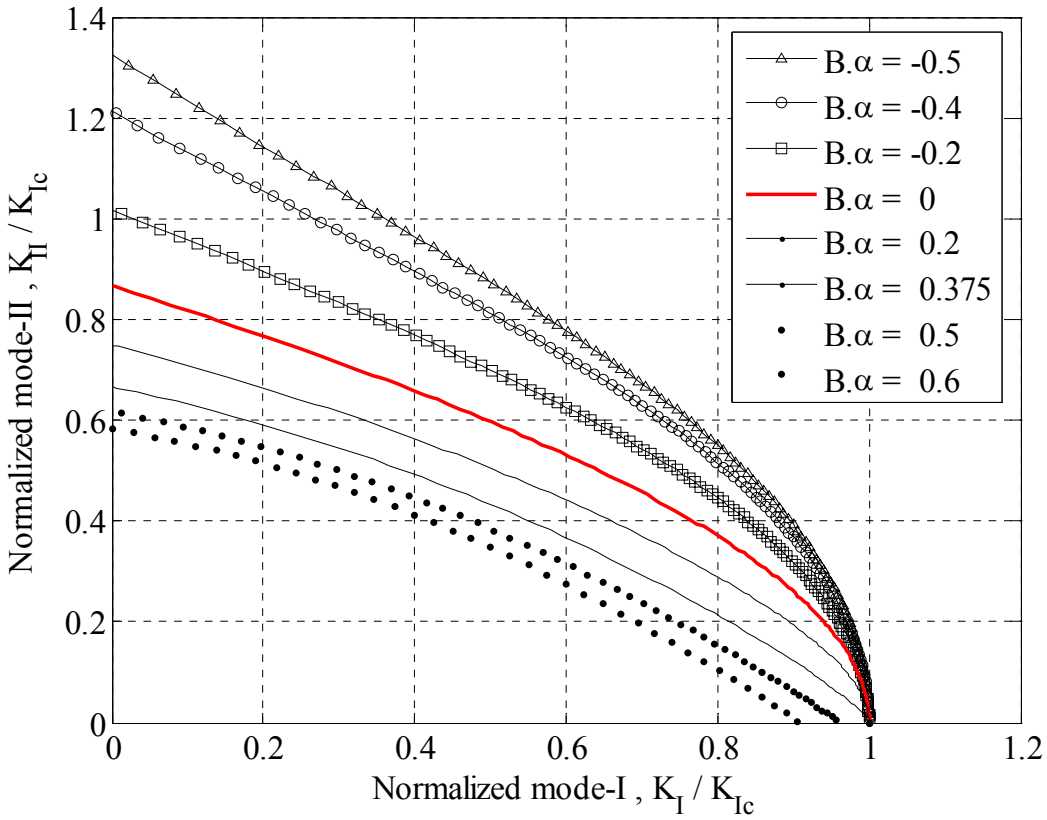

Figure 2.7. Mixed-mode fracture locus based on the generalized MTS-criterion [15]

Mixed-mode fracture locus based on the generalized MTS-criterion for different values of $B\alpha$ is given in Figure 2.7. This figure shows that the results for $B\alpha$ equals to zero are same with those given in MTS-criterion proposed by Erdogan and Sih [6]. And it is observed that the negative values of $B\alpha$ increase the mixed-mode fracture toughness and positive values of $B\alpha$ decrease the mixed-mode fracture toughness. Moreover, in mode-II the T-stress has a significant effect on mode-II fracture toughness.

The generalized MTS-criterion takes into account the effect of the T-stress. This criterion can be used for any mixed-mode geometry and loading conditions. To use the fracture diagrams shown in these figures, first parameters K_I, K_{II} and T need to be determined for given specimen. These parameters are required to calculate the biaxiality ratio B and the mixity parameter M^e. These stress intensity factors can be obtained from the handbooks for simple geometric shapes or can be determined from finite element analysis for more complicated problems.

The parameter $\alpha = \sqrt{2r_c/a}$ is determined from the crack length a and the critical distance r_c which is a material property. Using the calculated values of $B\alpha$ and M^e, the crack initiation angle θ_c is predicted by using Figure 2.7 for the given specimen.

For an infinite plate with inclined crack subjected to uniaxial tensile loading, Stress intensity factors, T-stress term and biaxiality ratio are defined following forms:

$$K_I = \sigma\sqrt{\pi a}\sin^2\beta, \tag{2.32}$$

$$K_{II} = \sigma\sqrt{\pi a}\cos\beta\sin\beta, \tag{2.33}$$

$$T = \sigma\cos 2\beta, \tag{2.34}$$

$$B = \frac{\cos 2\beta}{\sin\beta} \tag{2.35}$$

If we rewrite the generalized MTS-criterion by combining it with Equations 2.32 to 2.35 for the plate with an inclined crack under uniaxial loading, we get:

$$\sin^2\beta\sin\theta_c + \sin\beta\cos\beta(3\cos\theta_c - 1) - \frac{16}{3}(\cos 2\beta)(\alpha)\left(\frac{\sin\theta_c}{2}\cos\theta_c\right) = 0 \tag{2.36}$$

where $\alpha = \sqrt{\frac{2r_c}{a}}$

From Equation 2.36, the crack initiation angle, θ_c is seen as a function of the crack angle, β, and the dimensionless form of critical radius with respect to the crack length, α. Figure 2.8 shows the crack initiation angles as a function of β for different values of α.

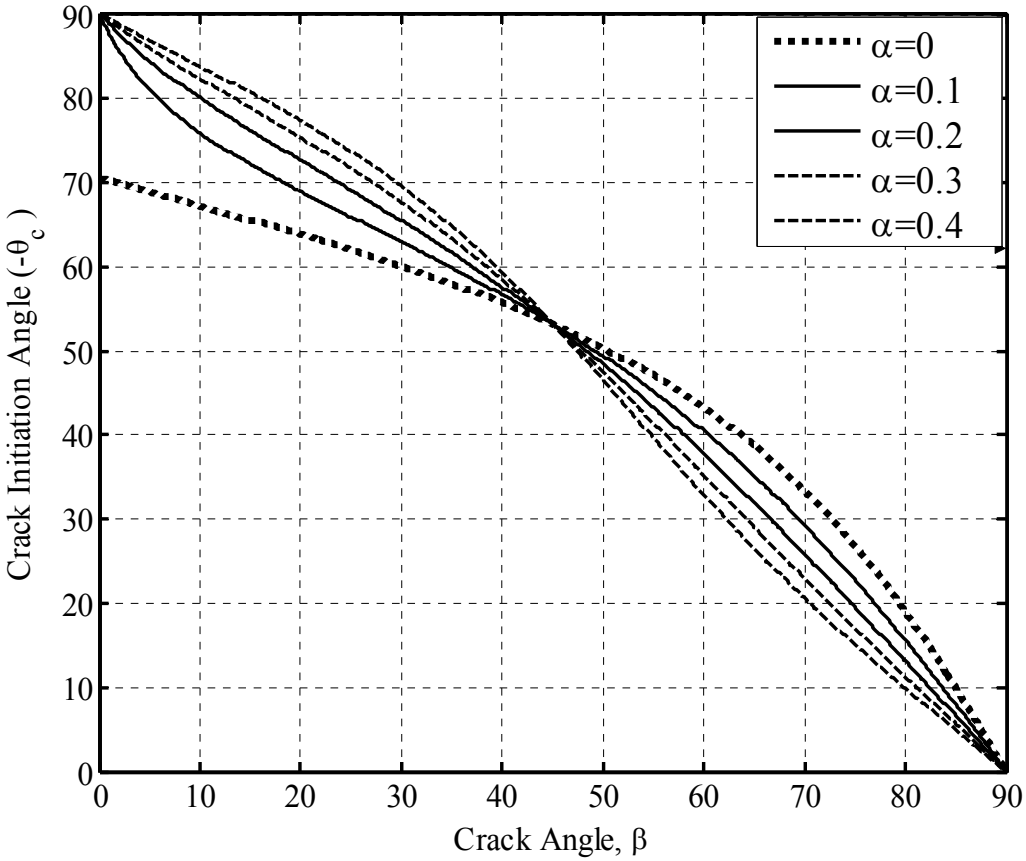

Figure 2.8. Crack initiation angle for the inclined center crack specimen subjected to uniaxial loading, for different α

From Figure 2.8, it can be seen that in the first part where $0^\circ \le \beta \le 45^\circ$, and $T > 0$, the magnitude of the crack initiation angle is higher than that predicted by the conventional MTS-criterion. Secondly, as r_c increases, the crack initiation angle predicted by the generalized MTS-criterion increases. In other part where $45^\circ \le \beta \le 90^\circ$, and $T < 0$, the magnitude of the crack initiation angle is less than that predicted by the conventional MTS-criterion and as r_c increases, the crack initiation angle predicted by the generalized MTS-criterion decreases. The effect of T-stress is also seen clearly.

2.3. S-Criterion

The strain energy density (S-criterion) was proposed by Sih [12]. This criterion states that the crack initiation will start in a radial direction along which the strain energy density is minimum. The feature of this criterion which makes it different from the others is that, S-criterion is the first criterion which shows dependence of crack initiation angle by the Poisson's ratio and the state of the stress (plane stress and plane strain).

The strain energy density factor S is defined in terms of K_I and K_{II} as following form:

$$S = \left(a_{11} K_I^{\,2} + 2a_{12} K_I K_{II} + a_{22} K_{II}^{\,2} \right) \tag{2.37}$$

where a_{11}, a_{12} and a_{22} are function of θ and are defined according to the conditions of plane stress and plane strain, in terms of Poisson's ratio.

$$\begin{aligned} a_{11} &= \frac{1}{16\pi G_s}\left(1+\cos\theta\right)\left(\kappa-\cos\theta\right), \\ a_{12} &= \frac{1}{16\pi G_s}\left(\sin\theta\right)\left[2\cos\theta-\left(\kappa-1\right)\right], \\ a_{22} &= \frac{1}{16\pi G_s}\left[\left(\kappa+1\right)\left(1-\cos\theta\right)+\left(\kappa+1\right)\left(1-\cos\theta\right)\right]. \end{aligned} \tag{2.38}$$

where G_s is the modulus of rigidity, and κ, a constant depending upon stress state.

$$G_s = \frac{E}{2(1+v)}, \tag{2.39}$$

$$\kappa = 3 - 4v \text{ for plane strain}, \tag{2.40}$$

$$\kappa = \frac{3-v}{1+v} \text{ for plane stress}. \tag{2.41}$$

S-criterion states that the direction of crack initiation coincides with the direction of minimum strain energy density around the crack tip. In mathematical form, S-criterion can be stated as:

$$\frac{\partial S}{\partial \theta} = 0 \text{ and } \frac{\partial^2 S}{\partial \theta^2} > 0 \Rightarrow \theta = \theta_c \tag{2.42}$$

When we use Equations 2.37-2.42 for plane stress and plane strain conditions, the crack initiation angles can be obtained for mode-I, mode-II, and mixed-mode. For pure mode-I loading $K_{II} = 0$ and we get:

$$\left[(2\cos\theta_c - \kappa + 1)\sin\theta_c\right] K_I^{\,2} = 0, \tag{2.43}$$

$$\left[2\cos 2\theta_c - (\kappa - 1)\cos\theta_c\right] K_I^{\,2} > 0 \tag{2.44}$$

From Equation 2.43, we get two solutions for θ_c :

$$\theta_c = 0 \text{ and } \theta_c = \cos^{-1}\left(\frac{\kappa - 1}{2}\right) \tag{2.45}$$

On the other hand, Equation 2.44 is only satisfied by $\theta_c = 0$ for plane stress and plane strain conditions. So, for under pure mode-I loading condition, the crack initiation angle θ_c does not depend on the material property *v*.

For pure mode-II loading $K_I = 0$ and we get:

$$\left[\left(-6\cos\theta_c+\kappa-1\right)\sin\theta_c\right]K_{II}{}^2=0, \tag{2.46}$$

$$\left[-6\cos 2\theta_c+\left(\kappa-1\right)\cos\theta_c\right]K_{II}{}^2>0 \tag{2.47}$$

From Equation 2.46, it can be got two solutions for θ_c :

$$\theta_c=0 \text{ and } \theta_c=\cos^{-1}\left(\frac{\kappa-1}{6}\right) \tag{2.48}$$

But for Mode-II loading, Equation 2.47 is satisfied by $\theta_c=\cos^{-1}\left(\frac{\kappa-1}{6}\right)$.

Crack initiation angles under pure mode-II loading depend on the material property Poisson's ratio *v*. For pure mode-II loading, θ_c takes different values for different values of *v* for both plane stress and plane strain conditions. Theoretical results of crack initiation angles under pure mode-II loading for different *v* values are shown in Table 2.2.

Table 2.2. Crack initiation angles under pure mode-II loading

For pure mode-II loading , $\beta=0$						
plane-stress condition						
v	0	0.1	0.2	0.3	0.4	0.5
θ_c	-70.5	-74.2	-77.2	-79.7	-81.8	-83.6
plane-strain condition						
v	0	0.1	0.2	0.3	0.4	0.5
θ_c	-70.5	-74.5	-78.5	-82.3	-86.2	-90

From Table 2.2, it can be seen that the crack initiation angles under pure mode-II loading increase as *v* increases for both plane stress and plane strain conditions. On the other hand, the influence of Poisson's ratio *v* for plane strain is more than the influence for the plane stress.

For the mixed-mode loading, the crack initiation angles can be shown in Figures 2.9, 2.10, and 2.11 for plane stress and plane strain conditions respectively.

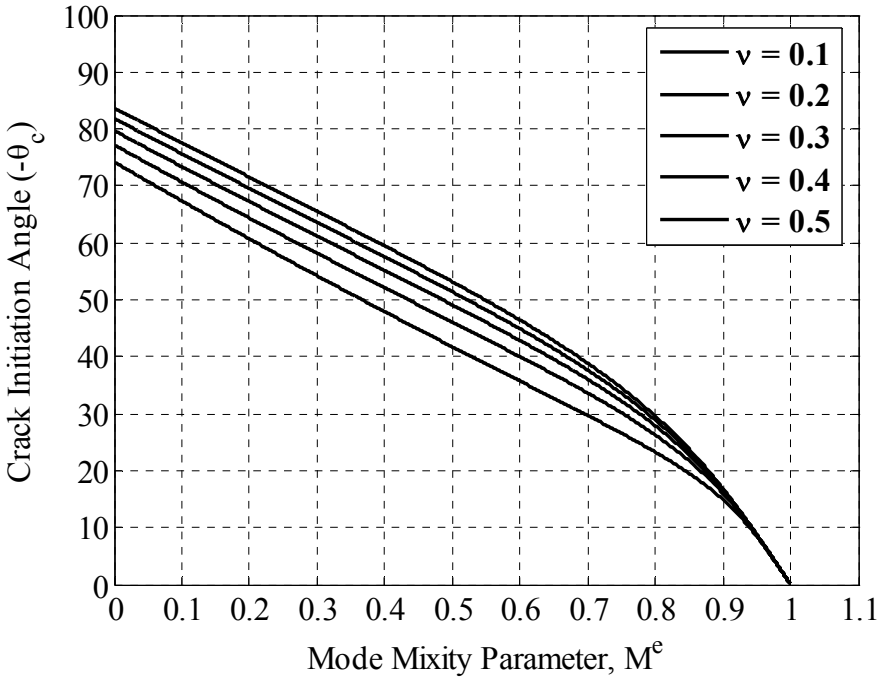

Figure 2.9. The mode mixity parameter M^e vs Crack initiation angle based on S-criterion for plane stress condition

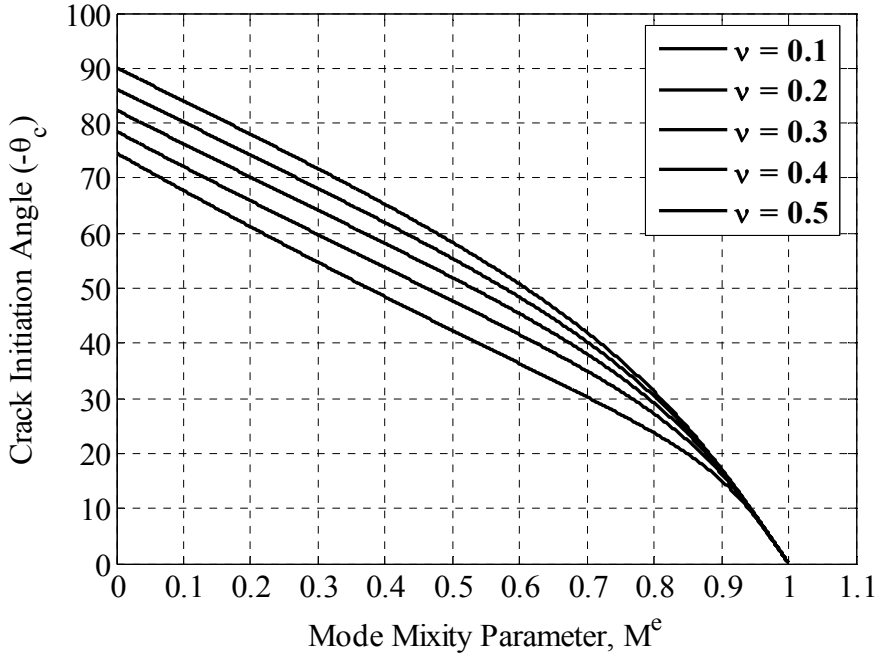

Figure 2.10. The mode mixity parameter M^e vs Crack initiation angle based on S-criterion for plane strain condition

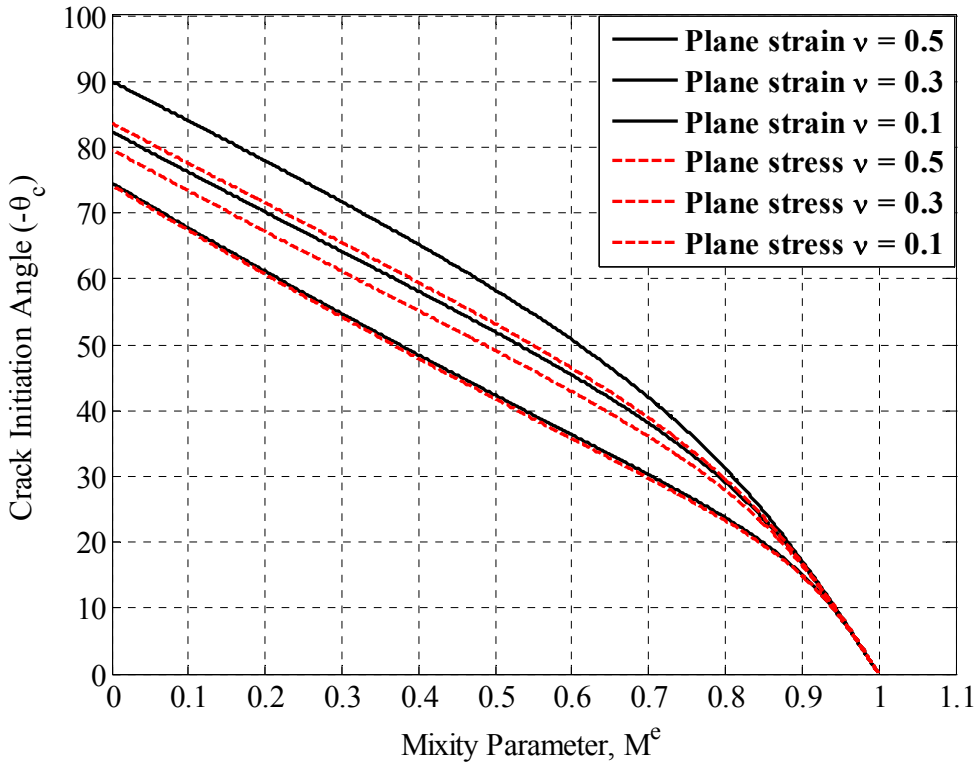

Figure 2.11. The mode mixity parameter M^e vs Crack initiation angle based on S-criterion for plane stress and plane strain in mixed-mode conditions

The experimental data obtained from the experiments performed by Sih [12] are given in Table 2.3. The last two rows give the theoretical calculations for the maximum stress criterion (MTS-criterion) and the strain energy density criterion (S-criterion) with ν=0.3 for plane strain condition. From Figure 2.12, the experimental data is for brittle material under mixed-mode loading, Figure 2.12 shows the results for uniaxial tension. The experimental results for PMMA performed by Sih are also plotted for comparison. It shows good agreement with both MTS-criteria and S-criteria (plane strain) for crack initiation angles greater than 30^o.

Table 2.3. Experimental results and theoretical result for mixed-mode loading

Crack Inclination Angle, β	0	30	40	50	60	70	80	90
Mode Mixitiy Parameter, M^e	0	0.33	0.44	0.55	0.66	0.77	0.88	1
Experimental Results, $-\theta_c$	-70.5	-62.4	-55.6	-51.1	-43.1	-30.7	-17.3	0
MTS-criterion, $-\theta_c$	-70.53	-60.2	-55.7	-50.2	-43.2	-33.2	-19.3	0
S-criterion, $-\theta_c$ for ν=0.3	-81.5	-63.5	-56.7	-49.5	-41.5	-31.8	-18.5	0

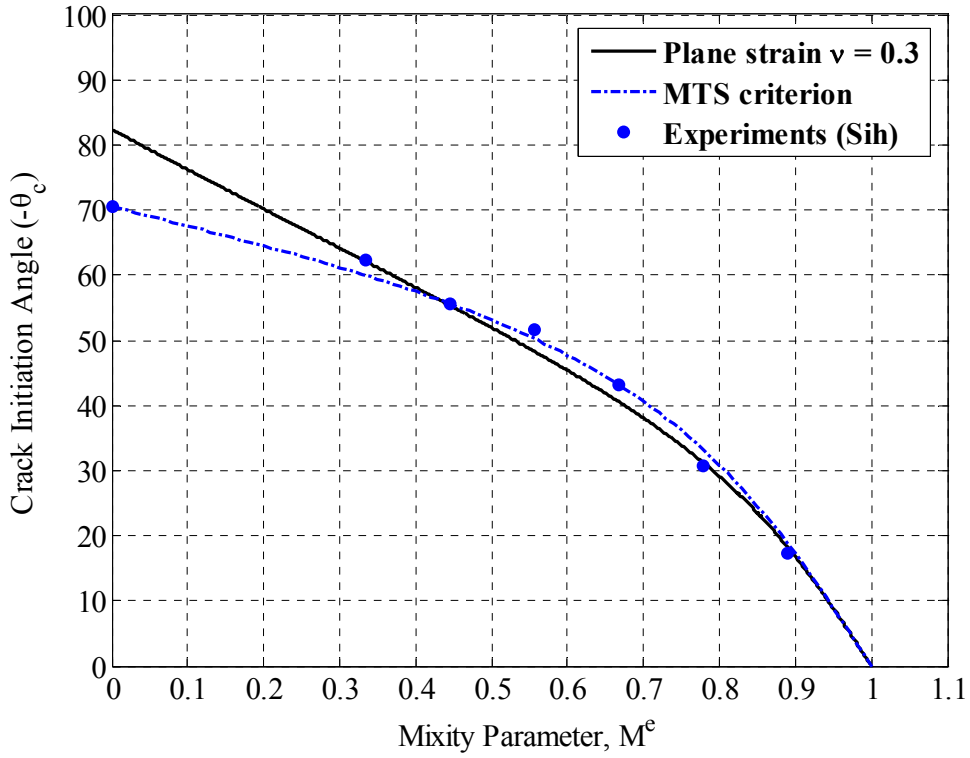

Figure 2.12. Experimental results for crack initiation angle for S-Criterion and MTS-criterion

2.4. M-Criterion

The maximum triaxial stress (M-criterion) criterion is a stress based criterion and presented by Kong [14]. This criterion states that the stress triaxiality ratio determines the crack initiation angle and the crack starts to grow from where the triaxiality ratio is maximum. The stress triaxiality ratio is defined as following

$$M = \frac{\sigma_H}{\sigma_{eq}} \tag{2.49}$$

M-criterion is defined as mathematically as following form

$$\frac{\partial M}{\partial \theta} = 0 \text{ and } \frac{\partial^2 M}{\partial \theta^2} < 0 \tag{2.50}$$

where σ_H is the hydrostatic stress and σ_{eq} is the equivalent stress. Hydrostatic stress components can be shown in Figure 2.13.

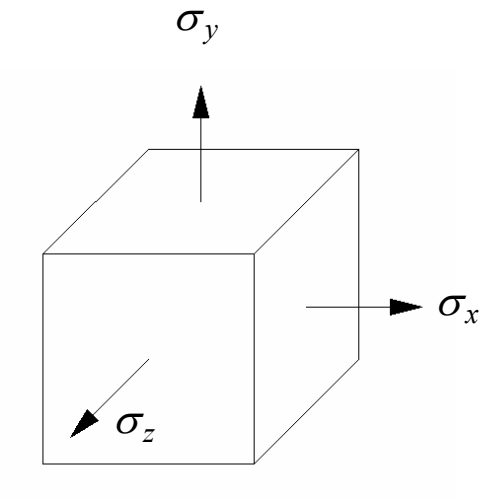

Figure 2.13. Hydrostatic Stress Components

The hydrostatic stress, σ_H can be written as

$$\sigma_H = \frac{\sigma_x + \sigma_y + \sigma_z}{3} \tag{2.51}$$

and the equivalent stress, σ_{eq} is

$$\sigma_{eq} = \left[\frac{(\sigma_x - \sigma_y)^2 + (\sigma_y - \sigma_z)^2 + (\sigma_z - \sigma_x)^2 + 6\tau^2_{xy}}{2} \right]^{1/2} \tag{2.52}$$

Using stress field Equation 1.2 and 1.3, the hydrostatic stress, σ_H for plane stress can be written as

$$\sigma_H = \frac{1}{\sqrt{2\pi r}} \left[K_I \cos(\frac{\theta}{2}) - K_{II} \sin(\frac{\theta}{2}) \right] \tag{2.53}$$

Where, $\sigma_z = 0$ for plane stress condition

The equivalent stress, σ_{eq} based on Von Mises formulation, for plane stress at the crack tip is defined as

$$\sigma_{eq} = \frac{1}{\sqrt{2\pi r}}\left[\left(\frac{2}{3}K_I^2 - \frac{9}{2}K_{II}^2\right)\sin^2\theta + \left(2K_I^2 + 6K_{II}^2\right)\cos^2\frac{\theta}{2}\right.$$

$$\left. + 8K_{II}^2\sin^2\frac{\theta}{2} + K_I K_{II}(3\sin 2\theta - 2\sin\theta)\right]^{1/2} \qquad (2.54)$$

Combining Equations 2.49 -2.54, we obtain the following equation:

$$N^4 - 3\mu N^3 - (1-2\mu^2)N^2 + \frac{1}{2}(1-\mu^2)\mu N - \frac{1}{2}(1+\mu^2) = 0 \qquad (2.55)$$

$$[2(\mu^2+5)]\sin\frac{\theta}{2} + [27(\mu^2+1)]\sin\frac{3\theta}{2} + [5(5\mu^2-3)]\sin\frac{5\theta}{2}$$

$$-[(2(\mu^2+5)]\cos\frac{\theta}{2}[9(\mu^2+1)\mu]\cos\frac{3\theta}{2} - [5(\mu^2-7)\mu]\cos\frac{5\theta}{2} < 0 \qquad (2.56)$$

where $N = \tan\left(\theta/2\right)$ and $\mu = K_I/K_{II}$

The maximum triaxial stress (M-criterion) criterion was proposed first by Kong [14]. In order to check the theoretical predictions from M-criterion, in his experiments, steel FeE 550 specimens were used. At room temperature, the fracture of the steel shows ductility. Therefore, the experiments for the steel FeE 550 were conducted at a temperature of -140^o C. The results of experiments are given as function of the mode mixity parameter in Table 2.4.

Table 2.4. Crack initiation angles from experiments and M-criterion [14]

Me	0.077	0.183	0.372	0.694	1
M-criterion	-92.8	-84.5	-69.8	-42.6	0
Experiments	-91.7	-79.9	-65.4	-46.4	0

By solving Equation 2.55 for $0 < M_e < 1$, the crack initiation angles are obtained. In Figure 2.14, the mode mixity parameter versus the crack initiation angles experimental results is illustrated.

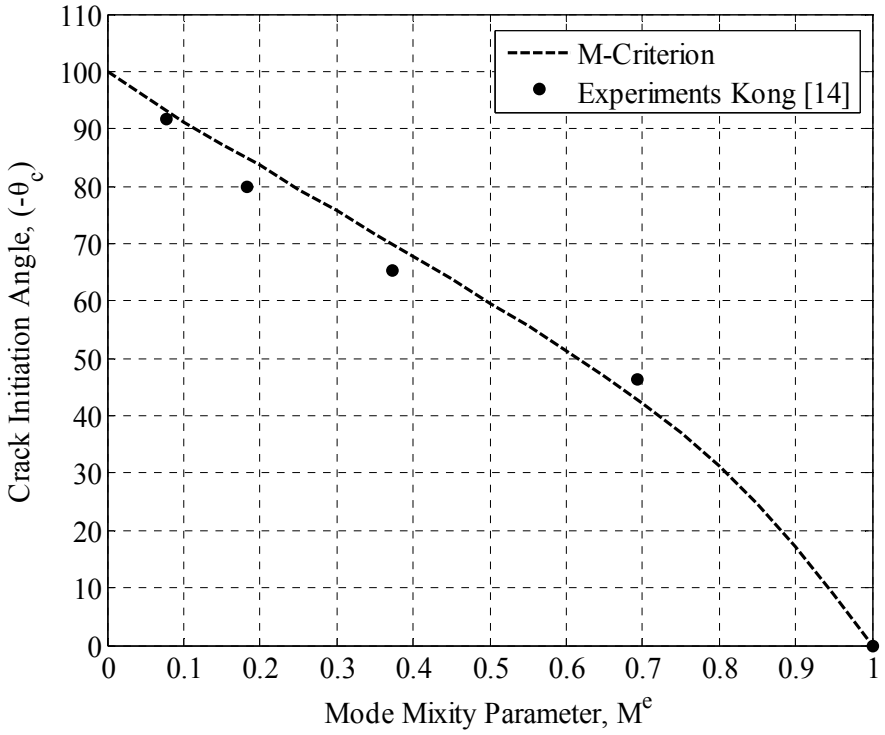

Figure 2.14. Crack initiation angle vs mode mixity parameter based on M-criterion

As we mentioned in section 2.1, the value of M^e is 1 for pure mode-I and zero for pure mode-II. For mixed –mode, the parameter takes values between 0 and 1. M^e is defined as following form

$$M^e = \frac{2}{\pi}\tan^{-1}\left(\frac{K_I}{K_{II}}\right) \tag{2.54}$$

The experimental results on FeE 550 specimens obtained by Kong [14] give a good agreement with theoretical results from M-criterion.

2.5. The Modified M-Criterion

The maximum triaxial stress (M-criterion) criterion was proposed by Kong [14]. M-criterion states that the crack starts to grow from where the triaxiality ratio is maximum around the crack tip. The triaxiality ratio is defined as following;

$$M = \frac{\sigma_H}{\sigma_{eq}} \tag{2.56}$$

where σ_H is hydrostatic stress and σ_{eq} is equivalent stress.

The hydrostatic stress, σ_H can be written as

$$\sigma_H = \frac{\sigma_x + \sigma_y + \sigma_z}{3} \tag{2.57}$$

and the equivalent stress, σ_{eq} is

$$\sigma_{eq} = \left[\frac{(\sigma_x - \sigma_y)^2 + (\sigma_y - \sigma_z)^2 + (\sigma_z - \sigma_x)^2 + 6\tau^2{}_{xy}}{2} \right]^{1/2} \tag{2.58}$$

In conventional M-criterion, the effect of T-stress is not included in the stress field Equations 1.1-1.4. In this study, we inserted T-stress term into stress field equations and modify the M-criterion.

Inserting T-stress term into the stress field equations, the hydrostaticstress, σ_H becomes

$$\sigma_H = \frac{1}{2\sqrt{2\pi r}} \left[2K_I \cos\frac{\theta}{2} - 2K_{II} \sin\frac{\theta}{2} + T\sqrt{2\pi r} \right] \tag{2.59}$$

The equivalent stress, σ_{eq} becomes

$$\sigma_{eq} = \frac{1}{\sqrt{2\pi r}}\left[K_I^2\left(4\cos^2\frac{\theta}{2}3\cos^4\frac{\theta}{2}\right) + K_{II}^2\left(9\cos^4\frac{\theta}{2} - 10\cos^2\frac{\theta}{2} + 4\right)\right.$$

$$+K_I K_{II}\left(12\sin\frac{\theta}{2}\cos^3\frac{\theta}{2} - 8\sin\frac{\theta}{2}\cos\frac{\theta}{2}\right)$$

$$+T\sqrt{2\pi r}\left(K_I\left(4\cos\frac{\theta}{2} + 12\cos^5\frac{\theta}{2} - 15\cos^3\frac{\theta}{2}\right)\right.$$

$$\left.\left.+K_{II}\left(-12\cos^4\frac{\theta}{2} + 9\sin\frac{\theta}{2}\cos^2\frac{\theta}{2}\right)\right) + \left(T\sqrt{2\pi r}\right)^2\right]^{1/2} \tag{2.60}$$

In mathematical form, M-criterion is described as following form

$$\frac{\partial M}{\partial \theta} = 0 \text{ and } \frac{\partial^2 M}{\partial \theta^2} < 0 \tag{2.61}$$

In order to understand the effect of T-stress term and critical radius, r_c in modified M-criterion, these terms are normalized. A dimensionless parameter called the biaxiality ratio, B for T-stress is given by

$$B = \frac{T\sqrt{2(\pi a)}}{K_{eff}} \tag{2.62}$$

where a is the crack length and K_{eff} is the effective stress intensity factor which is given by:

$$K_{eff} = \sqrt{\left(K_I^2 + K_{II}^2\right)} \tag{2.63}$$

The critical radius r_c is represented in the following dimensionless form

$$\alpha = \sqrt{\frac{2r_c}{a}} \tag{2.64}$$

Inserting the dimensionless forms of T-stress and r_c in Equation 2.56 and taking the first derivative of the triaxiality ratio, M with respect to θ, we get

$$\frac{\partial M}{\partial \theta} = \frac{\frac{3}{4}\cos\frac{\theta_c}{2}\left[\left(\mu^2+1\right)\left(M_1\mu+M_2\right)\left(B\alpha\right)^2+\left(\sqrt{\mu^2+1}\right)\left(M_3\mu^2+M_4\mu+M_5\right)\left(B\alpha\right)\right]}{\left[\left(\mu^2+1\right)\left(B\alpha\right)^2+\left(\sqrt{\mu^2+1}\right)\left(M_{10}\mu+M_{11}\right)\left(B\alpha\right)+\left(M_{12}\mu^2+M_{13}\mu+M_{14}\right)\right]^{3/2}} +$$

$$\frac{\frac{3}{4}\cos\frac{\theta_c}{2}\left[M_6\mu^3+M_7\mu^2+M_8\mu+M_9\right]}{\left[\left(\mu^2+1\right)\left(B\alpha\right)^2+\left(\sqrt{\mu^2+1}\right)\left(M_{10}\mu+M_{11}\right)\left(B\alpha\right)+\left(M_{12}\mu^2+M_{13}\mu+M_{14}\right)\right]^{3/2}} = 0 \tag{2.65}$$

where $\mu = \frac{K_I}{K_{II}}$ and $M_1, M_2, M_3, M_4, M_5, M_6, M_7, M_8, M_9, M_{10}, M_{11}, M_{12}, M_{13}$ and M_{14} are given in following form;

$$M_1 = \left(-\frac{15}{2}\sin\frac{\theta_c}{2}\cos\frac{\theta_c}{2}+10\sin\frac{\theta_c}{2}\cos^3\frac{\theta_c}{2}\right), \tag{2.66}$$

$$M_2 = \left(10\cos^4\frac{\theta_c}{2}-\frac{25}{2}\cos^2\frac{\theta_c}{2}+3\right), \tag{2.67}$$

$$M_3 = \left(-7\sin\frac{\theta_c}{2}\cos^2\frac{\theta_c}{2}+12\sin\frac{\theta_c}{2}\cos^4\frac{\theta_c}{2}\right), \tag{2.68}$$

$$M_4 = \left(-44\cos^3\frac{\theta_c}{2}+24\cos^5\frac{\theta_c}{2}+21\cos\frac{\theta_c}{2}\right), \tag{2.69}$$

$$M_5 = \left(-8\sin\frac{\theta_c}{2} + 25\sin\frac{\theta_c}{2}\cos^2\frac{\theta_c}{2} - 12\sin\frac{\theta_c}{2}\cos^4\frac{\theta_c}{2} \right), \tag{2.70}$$

$$M_6 = \left(-2\sin\frac{\theta_c}{2}\cos^3\frac{\theta_c}{2} \right), \tag{2.71}$$

$$M_7 = \left(-10\cos^4\frac{\theta_c}{2} + 8\cos^2\frac{\theta_c}{2} \right), \tag{2.72}$$

$$M_8 = \left(14\sin\frac{\theta_c}{2}\cos^3\frac{\theta_c}{2} - 12\sin\frac{\theta_c}{2}\cos\frac{\theta_c}{2} \right), \tag{2.73}$$

$$M_9 = \left(6\cos^4\frac{\theta_c}{2} + 4 - 12\cos^2\frac{\theta_c}{2} \right), \tag{2.74}$$

$$M_{10} = \left(4\cos\frac{\theta_c}{2} + 12\cos^5\frac{\theta_c}{2} - 15\cos^3\frac{\theta_c}{2} \right), \tag{2.75}$$

$$M_{11} = \left(-12\sin\frac{\theta_c}{2}\cos^4\frac{\theta_c}{2} + 9\sin\frac{\theta_c}{2}\cos^2\frac{\theta_c}{2} - 4\sin\frac{\theta_c}{2} \right), \tag{2.76}$$

$$M_{12} = \left(4\cos^2\frac{\theta_c}{2} - 3\cos^4\frac{\theta_c}{2} \right), \tag{2.77}$$

$$M_{13} = \left(12\sin\frac{\theta_c}{2}\cos^3\frac{\theta_c}{2} - 8\sin\frac{\theta_c}{2}\cos\frac{\theta_c}{2} \right), \tag{2.78}$$

$$M_{14} = \left(-10\cos^2\frac{\theta_c}{2} + 9\cos^4\frac{\theta_c}{2} + 4 \right) \tag{2.79}$$

For an infinite plate with an inclined crack, β subjected to uniaxial loading;

$$K_I = \sigma\sqrt{\pi a}\sin^2\beta, \tag{2.80}$$

$$K_{II} = \sigma\sqrt{\pi a}\cos\beta\sin\beta, \tag{2.81}$$

$$T = \sigma \cos 2\beta, \tag{2.82}$$

$$B = \frac{\cos 2\beta}{\sin \beta} \tag{2.83}$$

Introducing Equations 2.80-2.83 into Equation 2.65, we get the first derivative of the triaxiality ratio, M with respect to θ, depending on the dimensionless form of the critical radius r_c given in following form

$$\alpha = \sqrt{\frac{2r_c}{a}} \tag{2.84}$$

Figure 3.15 shows the solution of Equation 2.65 for crack initiation angels θ_c as a function of crack angle β for different values of α .

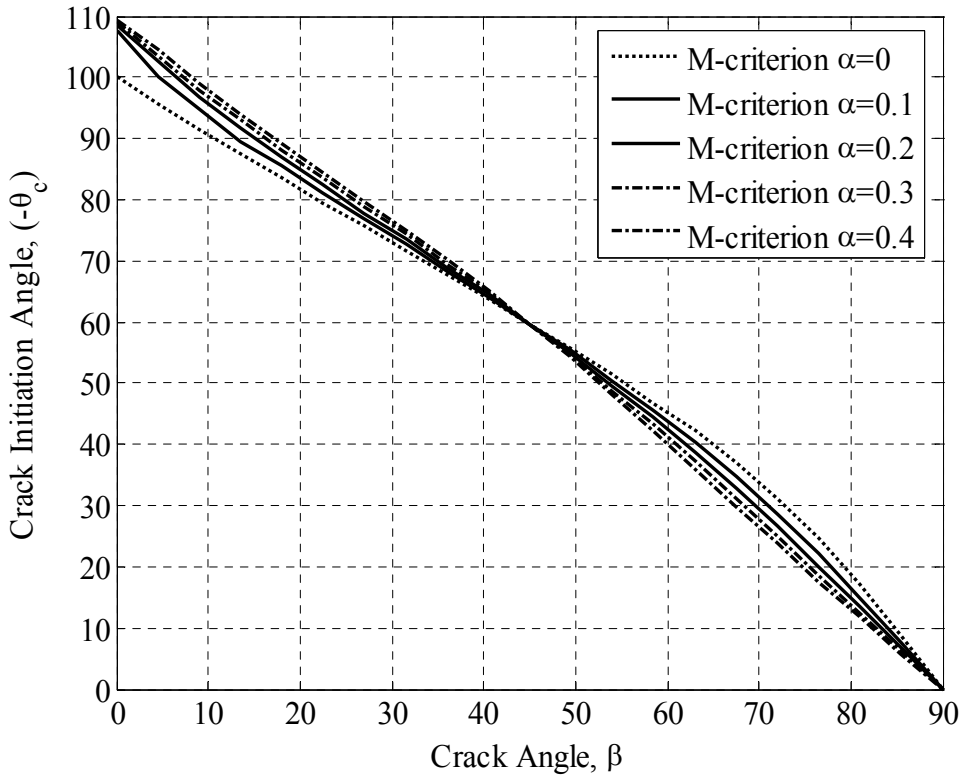

Figure 2.15. Crack initiation angle for the inclined center crack specimen subjected to uniaxial loading, for different α based on the M-criterion

We can analyze Figure 2.15 in two different parts. In the first part where $0^\circ \le \beta \le 45^\circ$, and $T > 0$, we concluded that the magnitude of the crack initiation angle is higher than that predicted by the conventional M-criterion where $\alpha = 0$. Secondly, as r_c increases the crack initiation angle predicted by the modified M-criterion increases. In the other part where $45^\circ \le \beta \le 90^\circ$ and so $T < 0$, the magnitude of the crack initiation angle is less than that predicted by the conventional M-criterion and as r_c increases the crack initiation angle, predicted by the modified M-criterion, decreases. The influence of the T-stress is also seen in Figure 2.15.

3. EXPERIMENTAL MEASUREMENT OF CRACK INITIATION ANGLES

3.1. Mechanical Properties of PMMA and PS

Many of the classical studies on fracture behavior of polymers have been concerned with the fracture of glassy thermoplastics, the most important work ones being polymethylmethacrylate (PMMA) and polystyrene (PS). Thermoplastics are very simple materials from a structural viewpoint, compared to either thermosets which have a complex three-dimensional molecular structure or semicrystalline polymers with a great variety of morphological forms. An advantage of Glassy thermoplastics is that they are transparent.

3.1.1. Polymethylmethacrylate (PMMA)

Polymethylmethacrylate (PMMA) is one the earliest polymers and is well known around the world by a variety of trade names, such as Lucite, Oroglas, Perspex and Plexiglas. The original PMMA was seen as a replacement for glass in a variety of applications and is currently used extensively in glazing applications. The material is one of the hardest polymers, and also is a rigid, glass-clear material with glossy finish and good weather resistance [17].

PMMA is relatively homogeneous and isotropic exhibiting brittle fracture behavior at room temperature. It is relatively easy to introduce a natural crack into this material by pressing a razor blade into the bottom of a notch. Therefore, as a first approximation, it seems reasonable to suppose that the linear elastic field equation of Irwin [18] and of Williams [19] provide good descriptions for stresses and strains near the tip of a sharp crack in PMMA. Using the linear elastic field to describe the situation simplifies as much as possible any analysis of experimental results. This factor, coupled with the relative ease

of working with this material, has prompted a number of experimental studies on mixed-mode fracture behavior of PMMA [20].

Polymethylmethacrylate (PMMA) and polystyrene (PS) used in this study were supplied by BİRNUR CAM Ayna San. Tic. Ltd. Şti. which is the representative of BAYER POLYMERS Sheet Europe Gmbh.

Five specimens of both PMMA and PS which are not machined were tested using Zwick / Roell Z010 tensile testing machine to obtain mechanical properties of the specimens. The extensometer was set to 45 mm. The stress-strain diagram of PMMA specimens is given in Figure 3.1. Modulus of elasticity, Yield strength, Ultimate stress, Stress at break and elongation at break were obtained for PMMA specimens and the test results of these specimens are given in Table 3.1. The mechanical properties of PMMA are illustrated in Table 3.2.

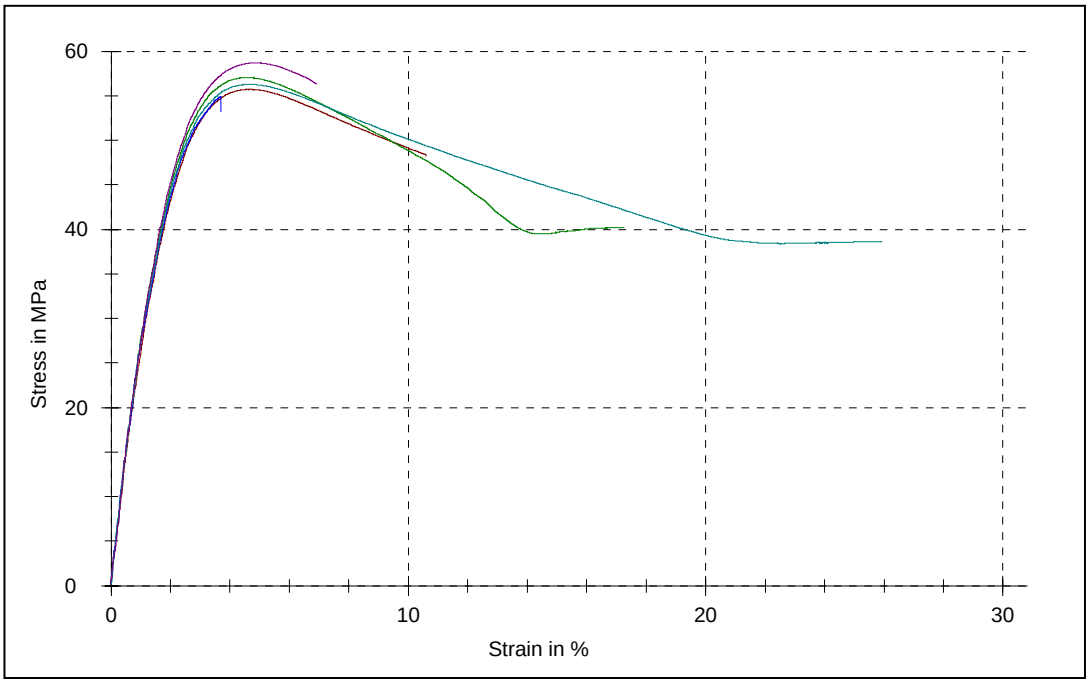

Figure 3.1.The stress-strain diagram of PMMA specimens

Table 3.1. The test results of PMMA specimens

Specimen Number	Modulus of Elasticity $E\,(MPa)$	Yield Strength $\sigma_Y\,(MPa)$	Ultimate Stress $\sigma_M\,(MPa)$	Stress at Break $\sigma_B\,(MPa)$	Elongation at Break $\varepsilon_B\,(\%)$
1	2638.71	55.71	55.71	48.22	10.60
2	2804.46	57.04	57.04	40.20	17.26
3	2745.10	-	54.93	53.14	3.69
4	3183.66	56.27	56.27	38.56	25.62
5	2490.03	58.68	58.68	56.31	6.92
Average	2772.39	56.93	56.53	47.29	12.82

Table 3.2. Average mechanical properties of PMMA

Elongation at break (%)	12.82
Hardness-Rockwell	M92-100 [17]
Poisson's ratio	0.37 [17]
Density	1.19 [17]
Modulus of elasticity (MPa)	2772.39
Yield Strength (MPa)	56.93
Ultimate Strength (MPa)	56.53
Stress at Break (MPa)	47.29

As seen in Table 3.2, for PMMA, the yield strength and ultimate strength are the almost same.

3.1.2. Polystyrene (PS)

Polystyrene is a polymer made from the monomer styrene, a liquid hydrocarbon that is commercially manufactured from petroleum. At room temperature, polystyrene is normally a solid thermoplastic, but can be melted at higher temperature for molding or extrusion, then resolidified. Styrene is an aromatic monomer, and polystyrene is an aromatic polymer. Pure solid polystyrene is a colorless, hard plastic with limited flexibility. It can be cast into molds with fine detail. Polystyrene can be transparent or can be made to take various colors. As with PMMA, it is a transparent glass at room temperature [21].

The stress-strain diagram of five specimen of Polystyrene (PS) which is not machined is given in Figure 3.2 and the test results can be seen in Table 3.3. The mechanical properties of PS are illustrated in Table3.4.

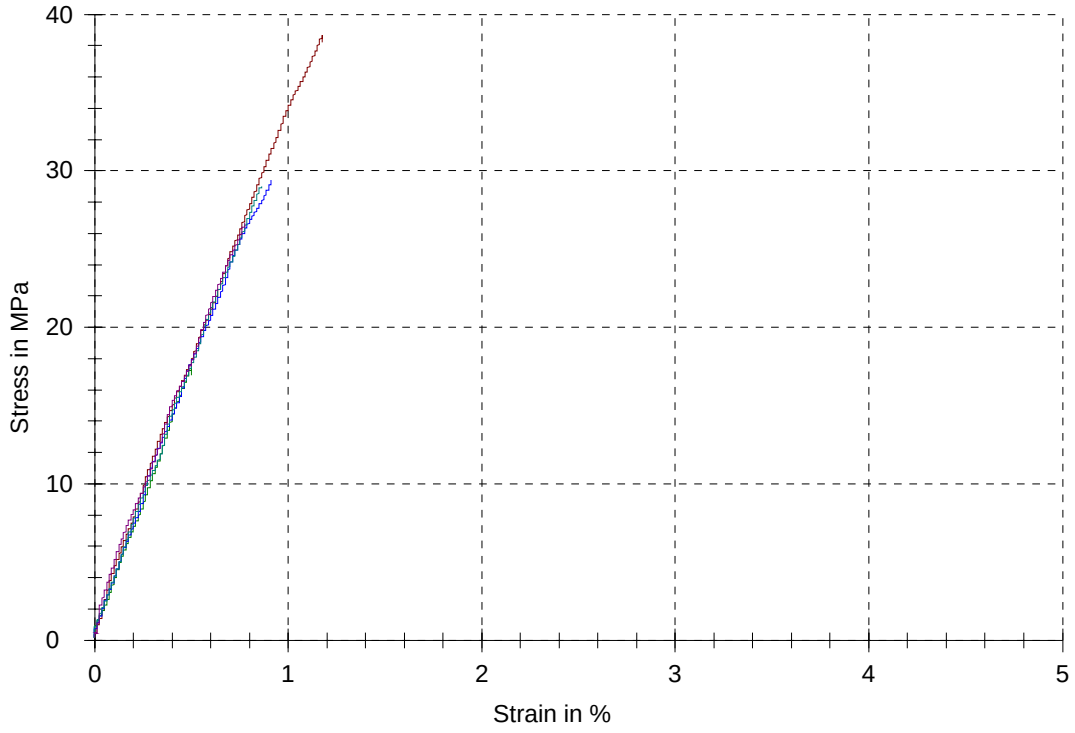

Figure 3.2. The stress-strain diagram of PS specimens

Table 3.3. The test results of PS specimens

Specimen Number	Modulus of Elasticity $E\,(MPa)$	Yield Strength $\sigma_Y\,(MPa)$	Ultimate Stress $\sigma_M\,(MPa)$	Stress at Break $\sigma_B\,(MPa)$	Elongation at Break $\varepsilon_B\,(\%)$
1	3442.25	-	38.68	38.24	1.17
2	3311.03	-	17.58	16.91	0.50
3	3341.82	-	29.42	29.42	0.91
4	3602.76	-	29	29.00	0.86
5	3373.51	-	26.67	26.67	0.78
Average	3415.07	-	28.27	28.05	0.84

Table 3.4. Average mechanical properties of PS

Elongation at break (%)	0.84
Hardeness-Rockwell	M70-74 [21]
Poisson's ratio	0.33 [21]
Density	1.07 [21]
Modulus of elasticity (MPa)	3415.07
Yield Strength (MPa)	-
Ultimate Strength (MPa)	28.27
Stress at Break (MPa)	28.05

3.2. Specimens and Experimental Set-Up

The measurements were performed using PMMA and PS sheet specimens of 3 mm nominal thickness. The specimens are 160 mm long and 50 mm wide. Figure 3.3 shows the geometry of PMMA and PS specimens used. Both plates contain cracks of length $2a = 5$ mm.

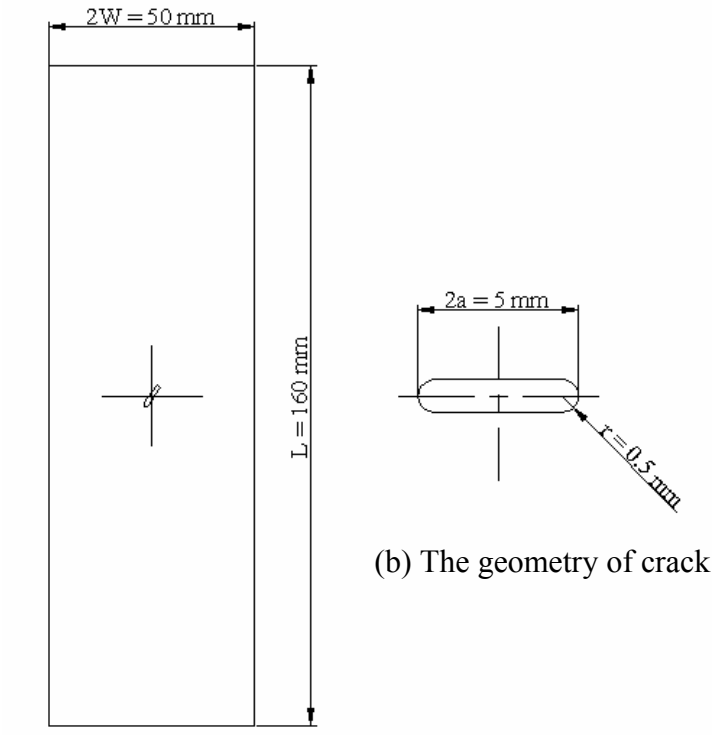

(b) The geometry of crack

(a) The geometry of specimens

Figure 3.3. The geometry of PMMA and PS specimens tested

The plate contains an inclined internal crack of length $2a$, as shown in Figure 3.4. The crack makes an angle β with the vertical direction. By changing β, different combination of modes I and II can be achieved. The plate is subjected to a uniform far-field stresses, σ in the vertical direction.

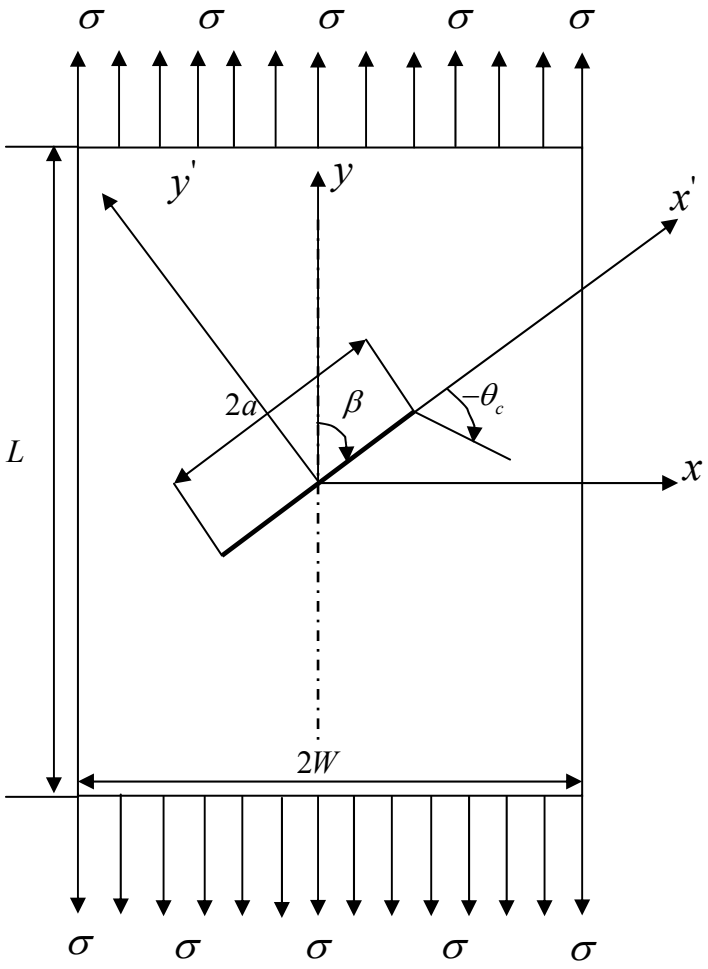

Figure 3.4. Uniaxial loading

Where,

2a is the crack length

L is total length of the specimen

2W is the width of the specimen

In both materials, specimens are prepared using milling machine with 1 mm diameter drill bit. After milling operation, the special tool is used to obtain a V shape at crack tips. The geometry of this special tool is given Figure 3.5. In all cases the end of the cracks were formed by forcing a razor blade into the end of the slits.

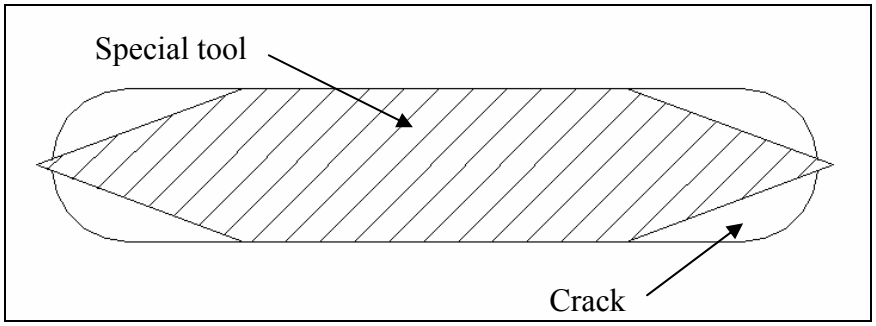

(a)

(b)

Figure 3.5. (a) The cross-sectional view of the special tool, (b) the view of the special tool

All testing under mixed-mode loading is performed using a Zwick/Roell Z010 tensile testing machine at room temperature. Figures 3.6 and 3.7 show the Zwick/Roell Z010 tensile testing machine, grips and the extensometer.

Figure 3.6. Zwick / Roell Z010 tensile testing machine

Figure 3.7. Grips and the extensometer

To study crack propagation direction, PMMA and PS plates with central angled crack were loaded under tension. PMMA and PS specimens with various crack angles, β 90°, 80°, 75°, 70°, 60°, 50°, 45°, 40°, 30° and 15° with $a/W = 0.1$. 10 specimens with same geometry are tested.

Under pure mode-I loading, the cross-head speed of each crack angle group and the rate of increase of K_I are equivalent, but for mixed-mode loading they are not. The rate of cross-head speed ranging from 0.05 mm/min to 500 mm/min doesn't change the value of the critical fracture toughness [22]. Therefore, for PMMA specimens, a constant cross-head speed of 5 mm/min is used to compare directly the present results with test results of William and Ewing [7]. For PS specimens, the cross-head speed of 0.5 mm/min is also used [23].

3.3. Measurement of Fracture Toughness

One can take a plate with a crack of known size and pull this plate to fracture using a tensile testing machine. From experimental results, the ultimate stress, σ_c can be obtained. Then, it follows that the critical value of the stress intensity factor at the moment of failure is given by:

$$K_{Ic} = \sigma_c \sqrt{\pi a} \tag{3.1}$$

In reality the solution is slightly more complicated. First of all, the used expression for the stress intensity factor is valid only for an infinite plate where there is no effect of a nearby boundary. For a plate of finite size the following equation replaces Equation 3.1.

$$K_I = \sigma \sqrt{\pi a} f\left(a/W\right) \tag{3.2}$$

where W is the plate width.

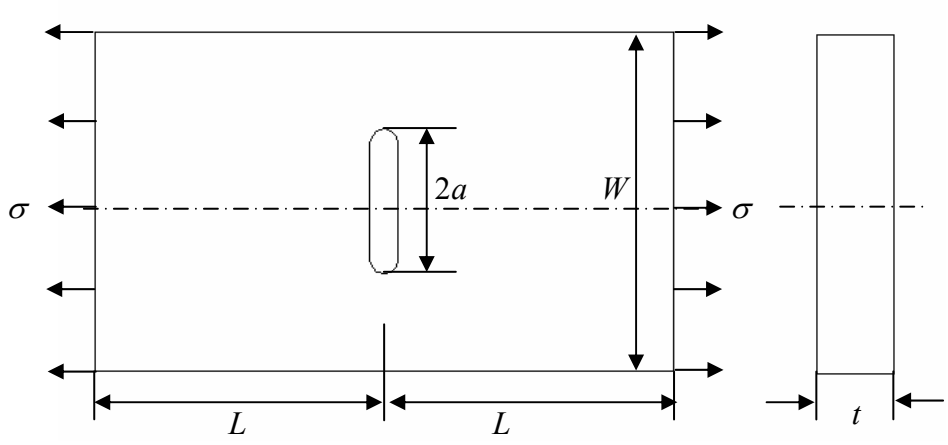

Figure 3.8. Central cracked rectangular plate under uniform tension [24].

The function $f(a/W)$ has to be known before K_{Ic} can be determined. Of course $f(a/W)$ approaches unity for small values of a/W . For a central cracked rectangular plate under uniform tension shown in Figure 3.8, the function $f(a/W)$ can be obtained by expansions of complex stress potentials combined with a boundary collocation method [23].

$$K_I = \sigma\sqrt{\pi a}.F_I(\alpha,\beta) \tag{3.3}$$

Where,

$$\alpha = \frac{2a}{W} \text{ and } \beta = \frac{2L}{W} \tag{3.4}$$

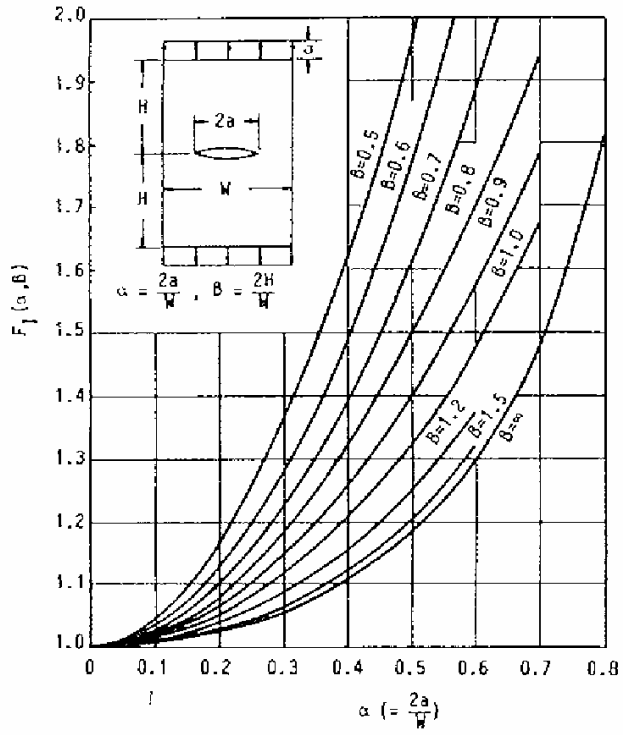

Figure 3.9. Boundary correction factors, $F_1(\alpha,\beta)$ [24]

Table 3.5. Boundary correction factors, $F_1(\alpha,\beta)$, for the case of uniform tension [24]

α \ β	0.4	0.5	0.6	0.7	0.8	0.9	1	1.2	1.5	1.8	∞
0	1.000	1.000	1.000	1.000	1.000	1.000	1.000	1.000	1.000	1.000	1.000
0.1	1.069	1.046	1.033	1.026	1.021	1.017	1.014	1.010	1.007	1.006	1.006
0.2	1.256	1.175	1.130	1.103	1.083	1.067	1.055	1.039	1.029	1.025	1.025
0.3	1.520	1.371	1.285	1.228	1.184	1.150	1.123	1.088	1.066	1.060	1.058
0.4	1.843	1.629	1.497	1.400	1.323	1.262	1.216	1.158	1.122	1.112	1.109
0.5	2.247	1.967	1.773	1.619	1.496	1.403	1.334	1.251	1.203	1.190	1.187
0.6	2.806	2.424	2.123	1.883	1.702	1.572	1.481	1.38	1.32	1.31	1.303
0.7	3.67	3.04	2.55	2.19	1.94	1.78	1.68				1.488

To calculate the critical fracture toughness in this study, the experiments were performed using PMMA and PS sheet specimens of 3 mm nominal thickness. The specimen's length 2L is 160 mm and width's W is 50 mm wide. Figure 3.10 shows the geometry of PMMA and PS specimens. Both plates contain a crack of length $2a = 5$ mm.

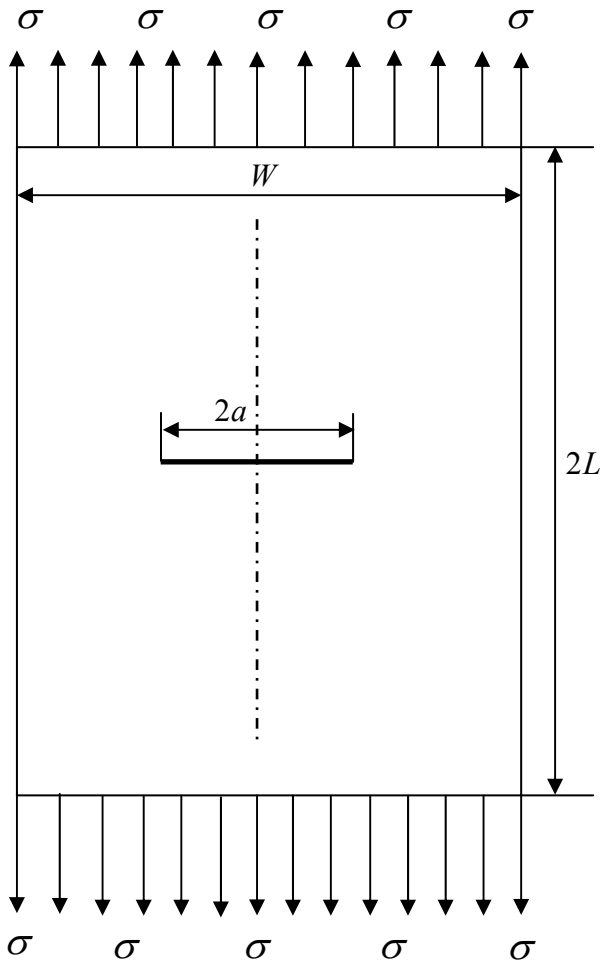

Figure 3.10. Geometry of PMMA and PS specimens under pure mode-I loading

Using equation 3.3 and 3.4, we get, $\alpha = 0.1$ and $\beta = 3.2$. In Table 3.5, the value of $F_I(\alpha, \beta)$ is given as 1.006 for $\alpha = 0.1$ and $\beta = 3.2$. Therefore, the critical stress intensity factor K_{Ic} becomes;

$$K_{Ic} = 1.006\sigma_c\sqrt{\pi a} \tag{3.5}$$

To find the values of ultimate strength for PMMA and PS materials, the tensile test results of both plates with a crack angle, β of 90^o are used.

The stress-strain diagram of PMMA and PS plates for pure mode-I loading and tensile test results are given Figures 3.11-3.12 and Tables 3.6-3-7 respectively.

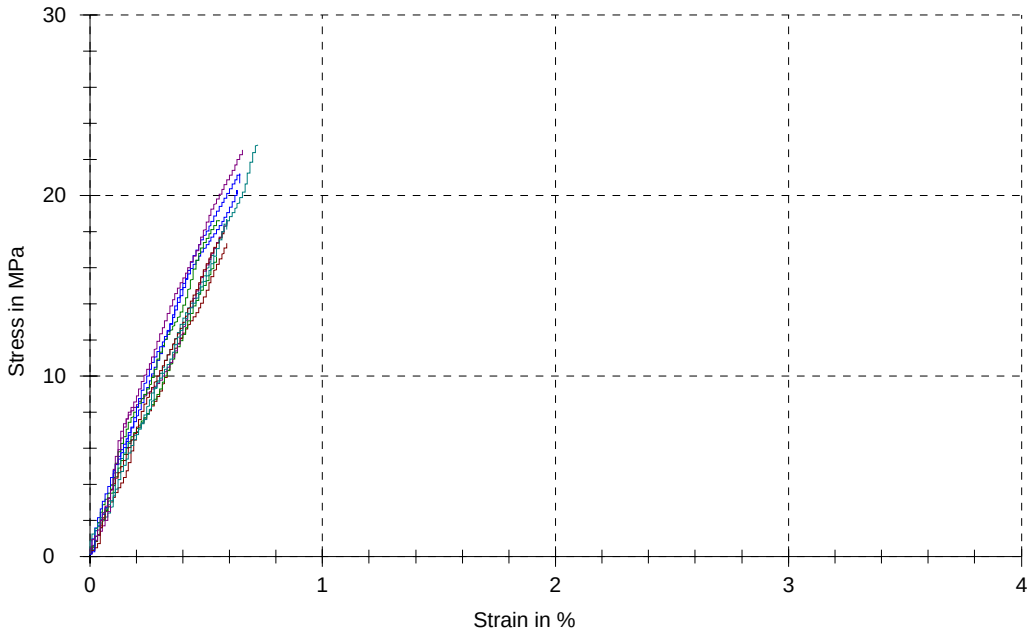

Figure 3.11. The stress-strain diagram of PMMA for β=90 (Mode-I) and a/w=0.1

Table 3.6. Results for PMMA at β=90 (Mode-I) and a/w=0.1

Specimen Number	Modulus of Elasticity $E\,(MPa)$	Yield Strength $\sigma_Y\,(MPa)$	Ultimate Stress $\sigma_M\,(MPa)$	Stress at Break $\sigma_B\,(MPa)$	Elongation at Break $\varepsilon_B\,(\%)$
1	3192.26	-	17.32	17.32	0.59
2	3344.33	-	16.6	16.6	0.54
3	3623.72	-	20.27	20.04	0.63
4	3329.13	-	22.78	22.78	0.72
5	4635.98	-	18.58	18.38	0.59
6	3430.92	-	18.01	18.01	0.58
7	3694.37	-	18.62	18.62	0.56
8	3601.18	-	21.2	20.68	0.64
9	3177.22	-	18.68	18.09	0.59
10	4510.8	-	22.52	22.52	0.66
Average	3653.99	-	19.46	19.30	0.61

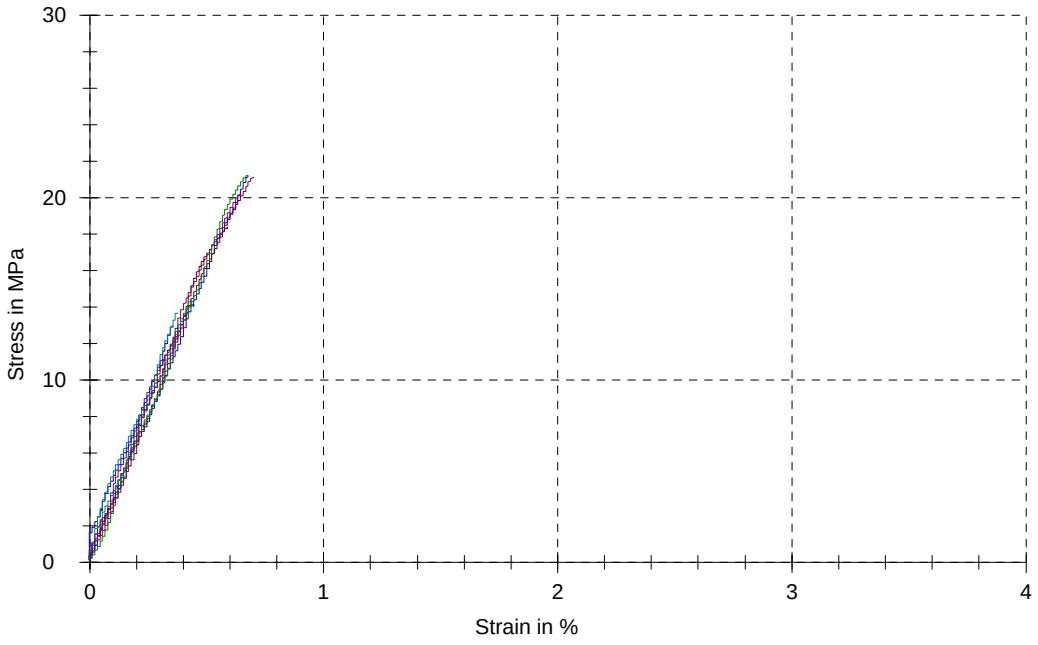

Figure 3.12. The stress-strain diagram of PS for β=90 (Mode-I) and a/w=0.1

Table 3.7. Results for PS at β=90 (Mode-I) and a/w=0.1

Specimen Number	Modulus of Elasticity $E\,(MPa)$	Yield Strength $\sigma_Y\,(MPa)$	Ultimate Stress $\sigma_M\,(MPa)$	Stress at Break $\sigma_B\,(MPa)$	Elongation at Break $\varepsilon_B\,(\%)$
1	3670.44	-	18.36	18.32	0.59
2	3512.69	-	14.13	14	0.44
3	3010.65	-	21.21	21.21	0.68
4	2801.8	-	14.38	14.38	0.43
5	3716.93	-	20.21	20.17	0.64
6	2912.21	-	21.09	21.09	0.7
7	3709.14	-	21.2	21.2	0.68
8	3007.71	-	12.95	12.95	0.36
9	2923.83	-	13.66	13.66	0.38
10	3623.3	-	13.57	13.57	0.41
Average	3288.87	-	17.08	17.06	0.53

Using these results, the ultimate strength, σ_c of PMMA plates which contains a central crack under pure mode-I loading is determined as an average value of 19.46 MPa. For PS plates, the ultimate strength is 17.08 MPa.

As seen from Figures 3.11 and 3.12, Brittle materials do not yield. For these materials the stress at break (rupture stress) and the ultimate strength are the almost same.

The critical fracture toughness for both PMMA and PS containing a crack length of $2a = 5$ mm can be found by using equation 3.5 and the values of ultimate strength.

For PMMA, the critical fracture toughness;

$$K_{Ic} = 1.006\sigma_c\sqrt{\pi a} = 1.73\,MPa\sqrt{m}$$

for PS,

$$K_{Ic} = 1.006\sigma_c\sqrt{\pi a} = 1.52\,MPa\sqrt{m}$$

3.4. Crack Initiation Angle Measurements

To study crack propagation direction under mixed-mode loading, PMMA and PS plates with central angled crack were loaded under tension. PMMA and PS specimens with various crack angles, $\beta = 90^{\circ}, 80^{\circ}, 75^{\circ}, 70^{\circ}, 60^{\circ}, 50^{\circ}, 45^{\circ}, 40^{\circ}, 30^{\circ}$ and 15° with $a/W = 0.1$. 10 specimens with same geometry are tested. Before tensile testing, PMMA and PS specimens with a central crack $\beta = 80^{\circ}$ and $a/W = 0.1$ are shown in Figures 3.13(a) and 3.13(b). All testing under mixed-mode loading are performed using a Zwick/Roell Z010 tensile testing machine at room temperature.

(a) (b)

Figure 3.13. (a) PMMA specimens with an inclined crack, $\beta = 80^{\circ}$ before tensile testing (b) PS specimens with an inclined crack, $\beta = 80^{\circ}$ before tensile testing

A sudden propagation of the crack occurred and no stable crack growth was observed in this study for each PMMA and PS specimens. The catastrophic propagation of the crack for PMMA and PS specimens under mixed-mode loading after testing are seen in Figures 3.14(a) and 3.14(b).

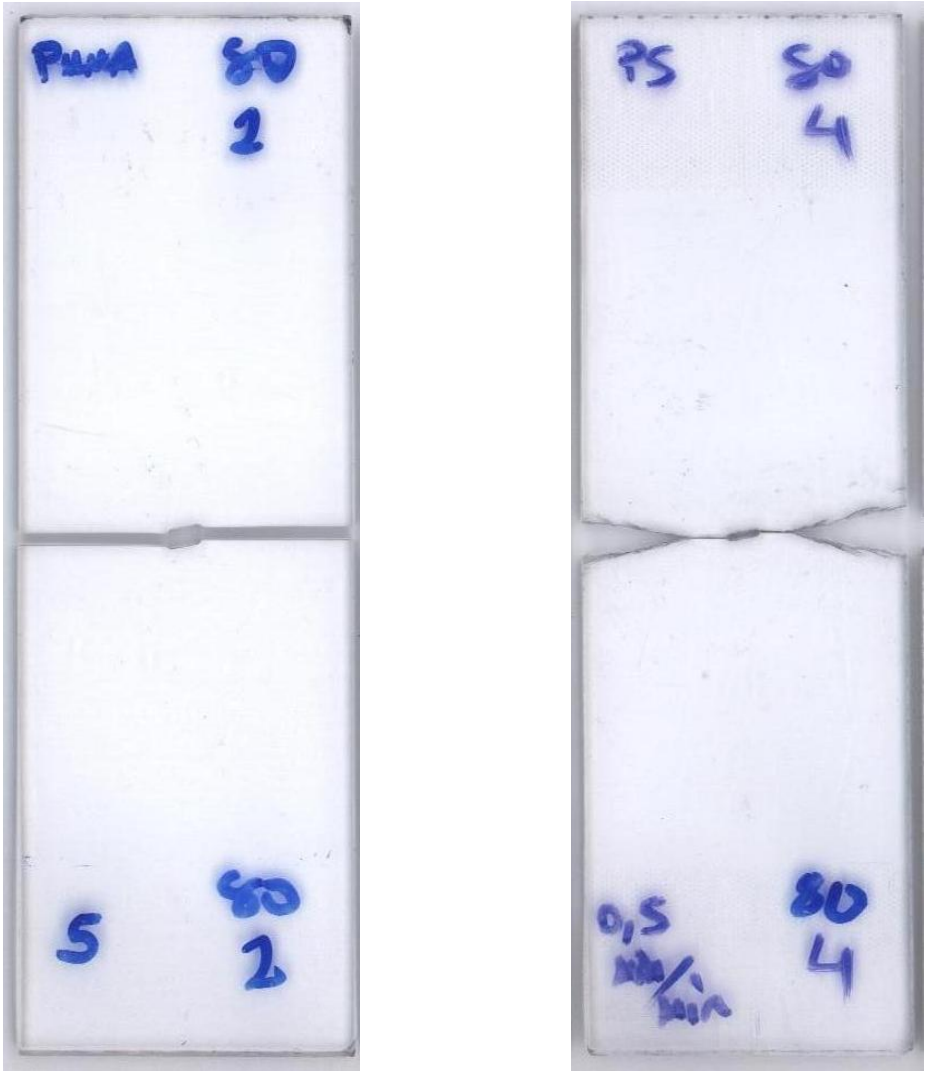

(a) (b)

Figure 3.14. (a) PMMA specimens with an inclined crack, $\beta = 80^{\circ}$ after tensile testing

(b) PS specimens with an inclined crack, $\beta = 80^{\circ}$ after tensile testing

PMMA specimens with crack angles, β=90^o, 80^o, 75^o, 70^o, 60^o, 50^o, 45^o, 40^o, 30^o and 15^o are tested. The failure under tensile testing can be seen in Figures 3.15-3.19 and PS specimens after failure under tensile testing are given in Figures 3.20-3.24.

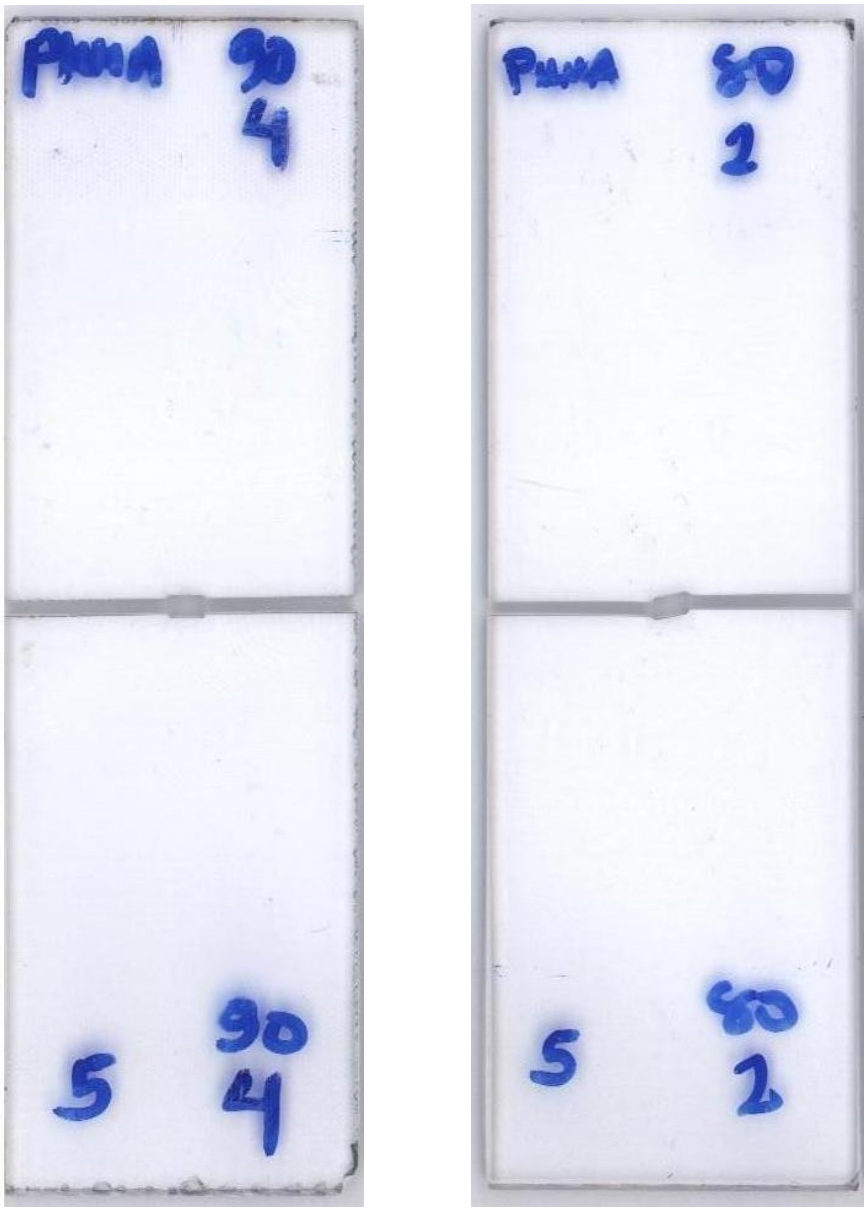

(a) (b)

Figure 3.15. (a) PMMA specimens with an inclined crack, $\beta = 90^\circ$ and $a/W = 0.1$

(b) PMMA specimens with an inclined crack, $\beta = 80^\circ$ and $a/W = 0.1$

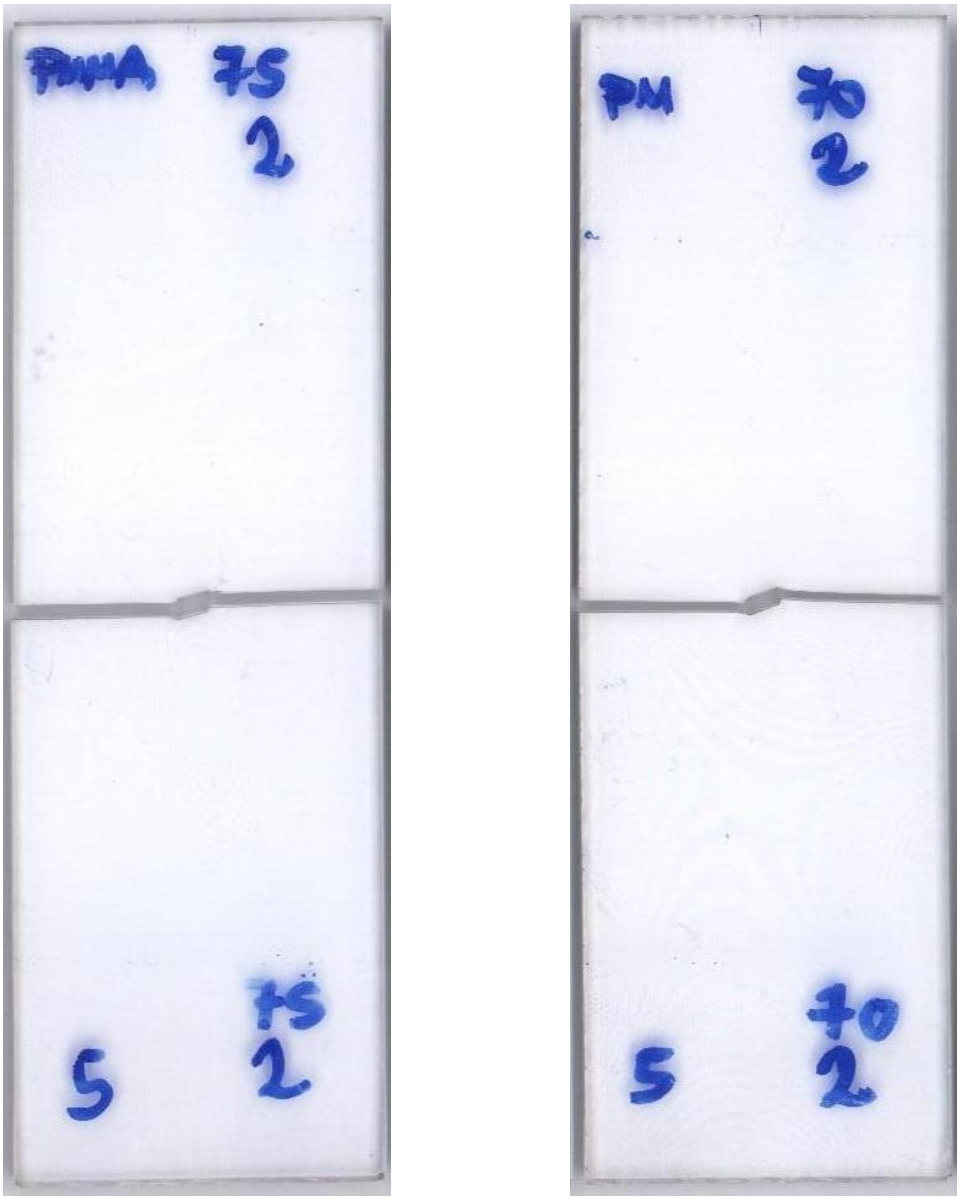

(a) (b)

Figure 3.16. (a) PMMA specimens with an inclined crack, $\beta = 75^{\circ}$ and $a/W = 0.1$

(b) PMMA specimens with an inclined crack, $\beta = 70^{\circ}$ and $a/W = 0.1$

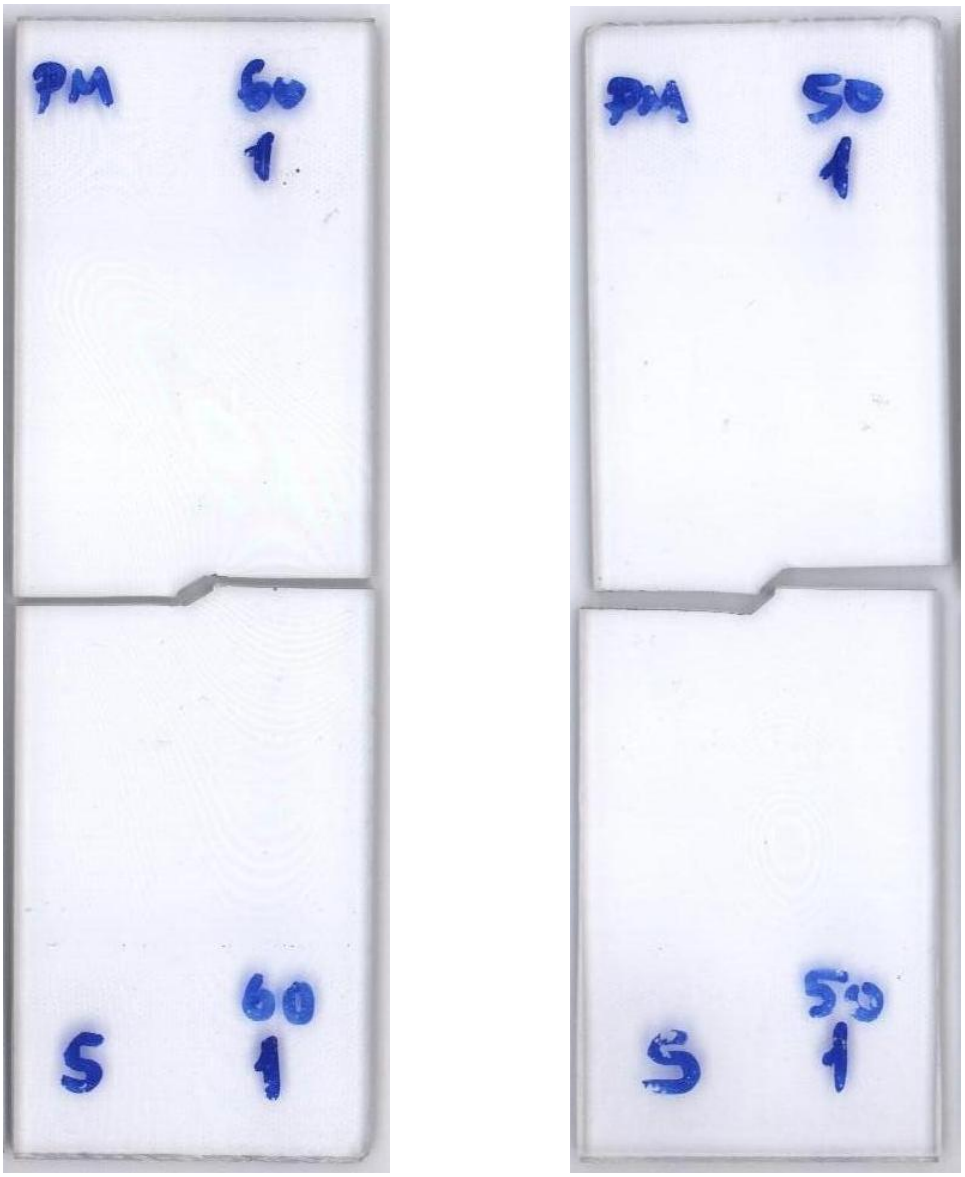

(a) (b)

Figure 3.17. (a) PMMA specimens with an inclined crack, $\beta = 60^{\circ}$ and $a/W = 0.1$

(b) PMMA specimens with an inclined crack, $\beta = 50^{\circ}$ and $a/W = 0.1$

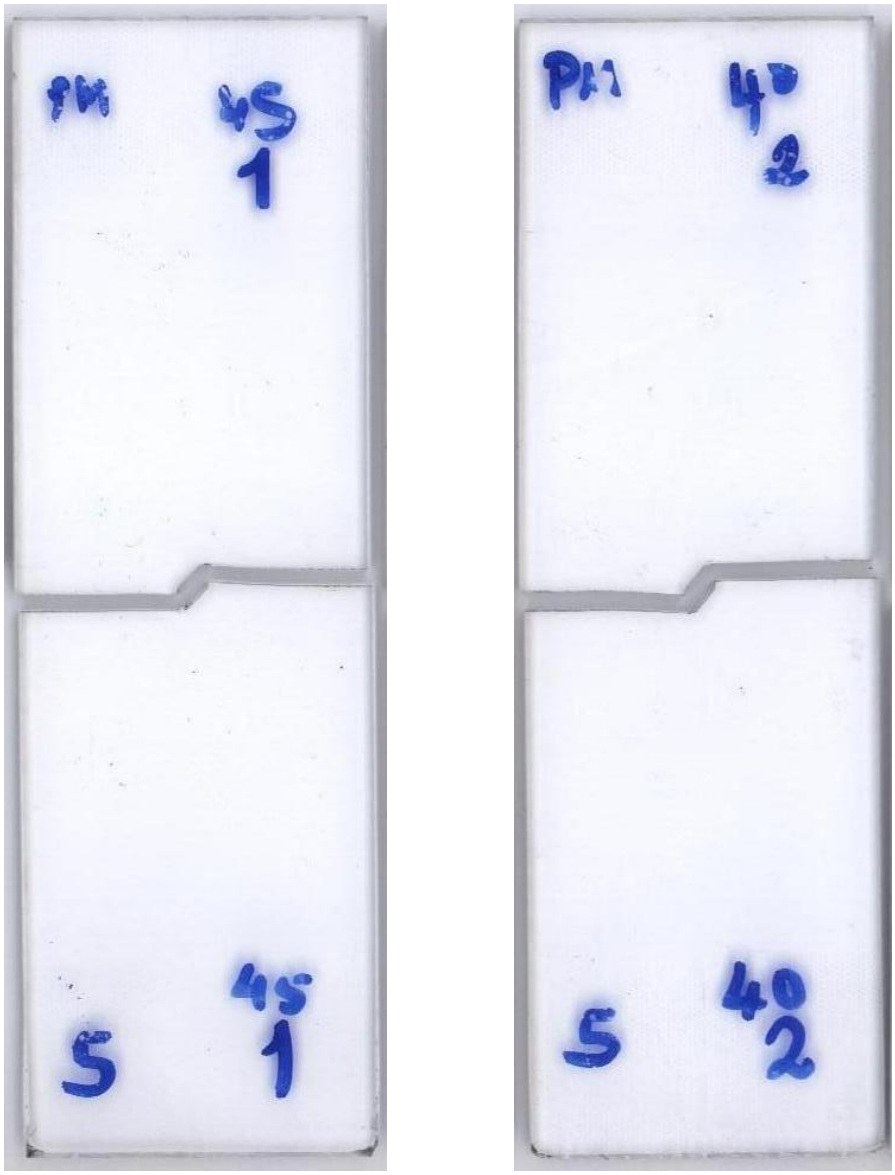

(a) (b)

Figure 3.18. (a) PMMA specimens with an inclined crack, $\beta = 45^{\circ}$ and $a/W = 0.1$

(b) PMMA specimens with an inclined crack, $\beta = 40^{\circ}$ and $a/W = 0.1$

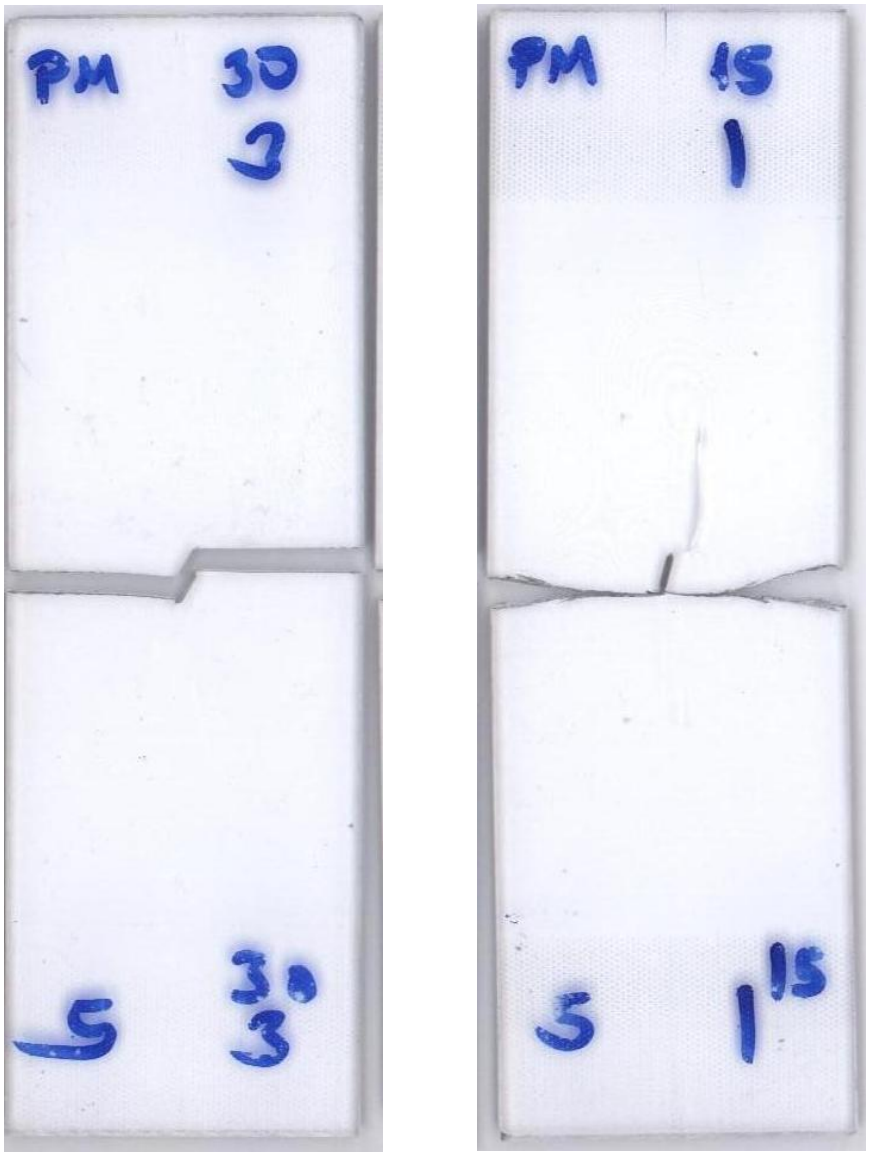

(a) (b)

Figure 3.19. (a) PMMA specimens with an inclined crack, $\beta = 30^{\circ}$ and $a/W = 0.1$

(b) PMMA specimens with an inclined crack, $\beta = 15^{\circ}$ and $a/W = 0.1$

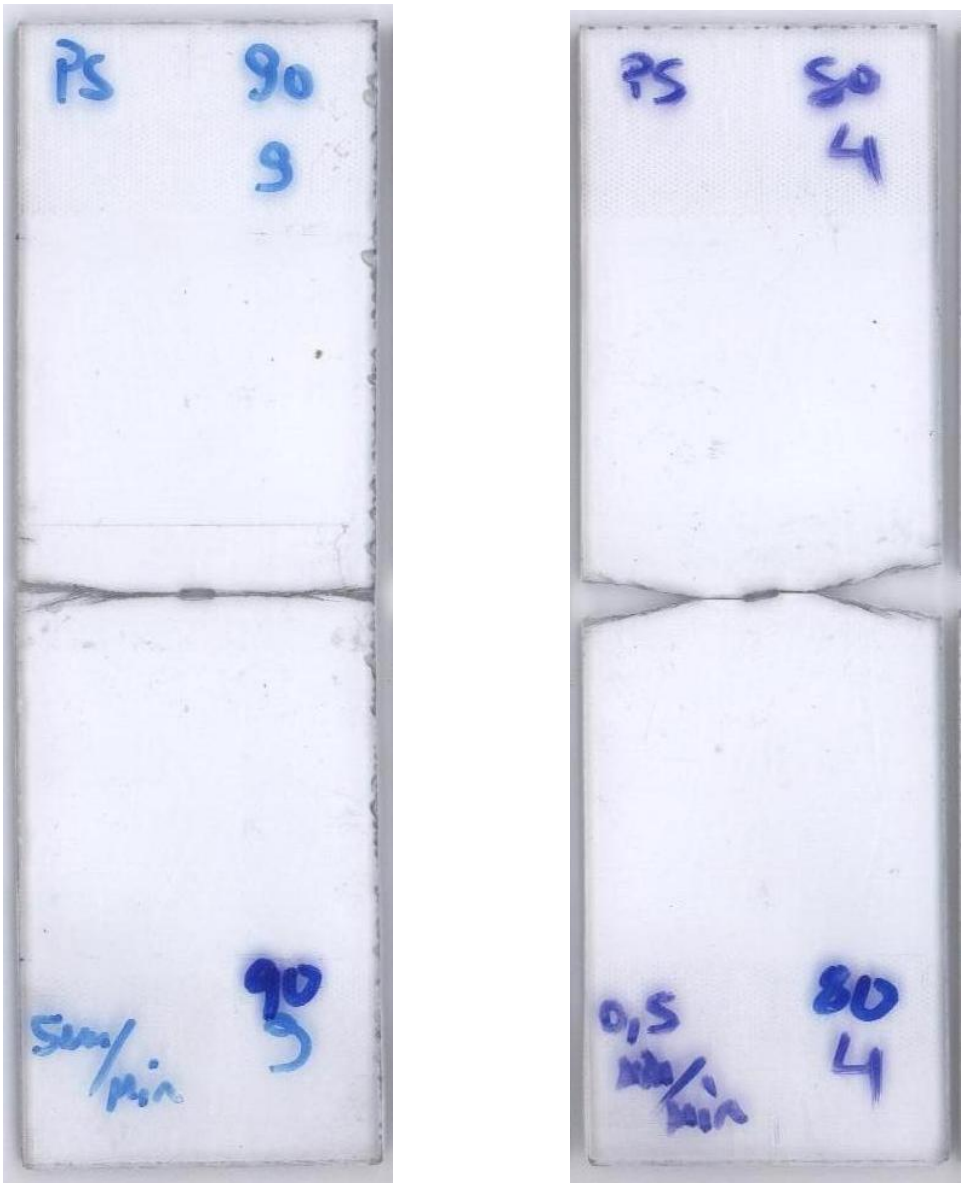

(a) (b)

Figure 3.20. (a) PS specimens with an inclined crack, $\beta = 90^{\circ}$ and $a/W = 0.1$

(b) PS specimens with an inclined crack, $\beta = 80^{\circ}$ and $a/W = 0.1$

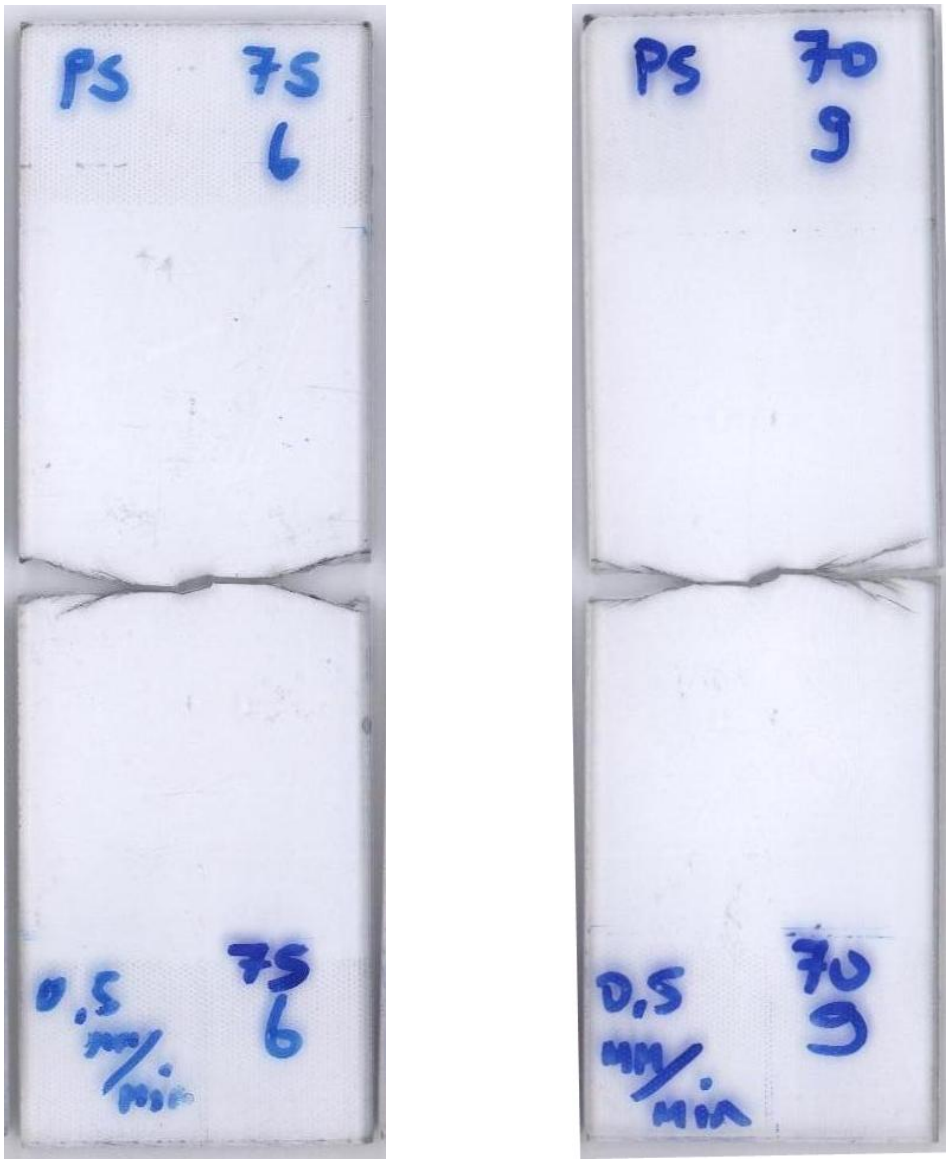

(a) (b)

Figure 3.21. (a) PS specimens with an inclined crack, $\beta = 75^{\circ}$ and $a/W = 0.1$

(b) PS specimens with an inclined crack, $\beta = 70^{\circ}$ and $a/W = 0.1$

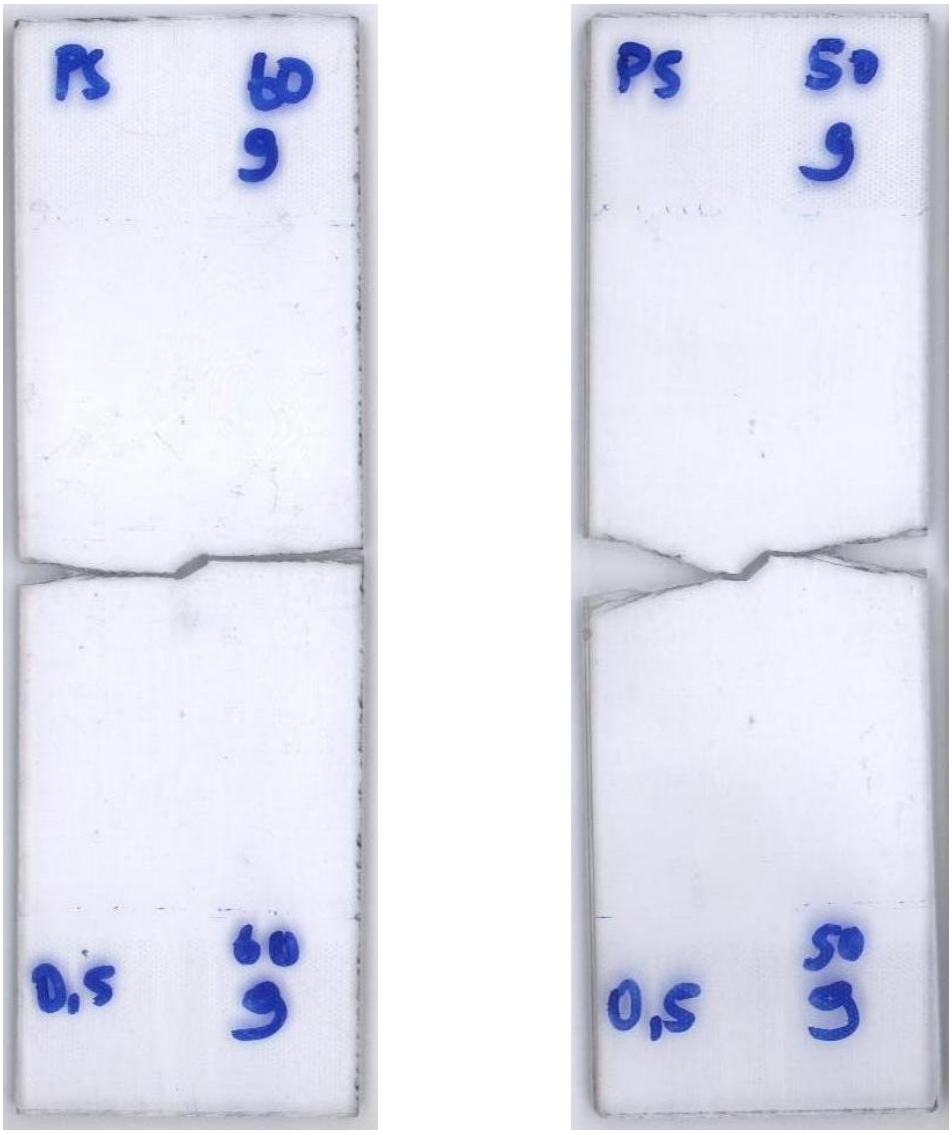

(a) (b)

Figure 3.22. (a) PS specimens with an inclined crack, $\beta = 60^{\circ}$ and $a/W = 0.1$

(b) PS specimens with an inclined crack, $\beta = 50^{\circ}$ and $a/W = 0.1$

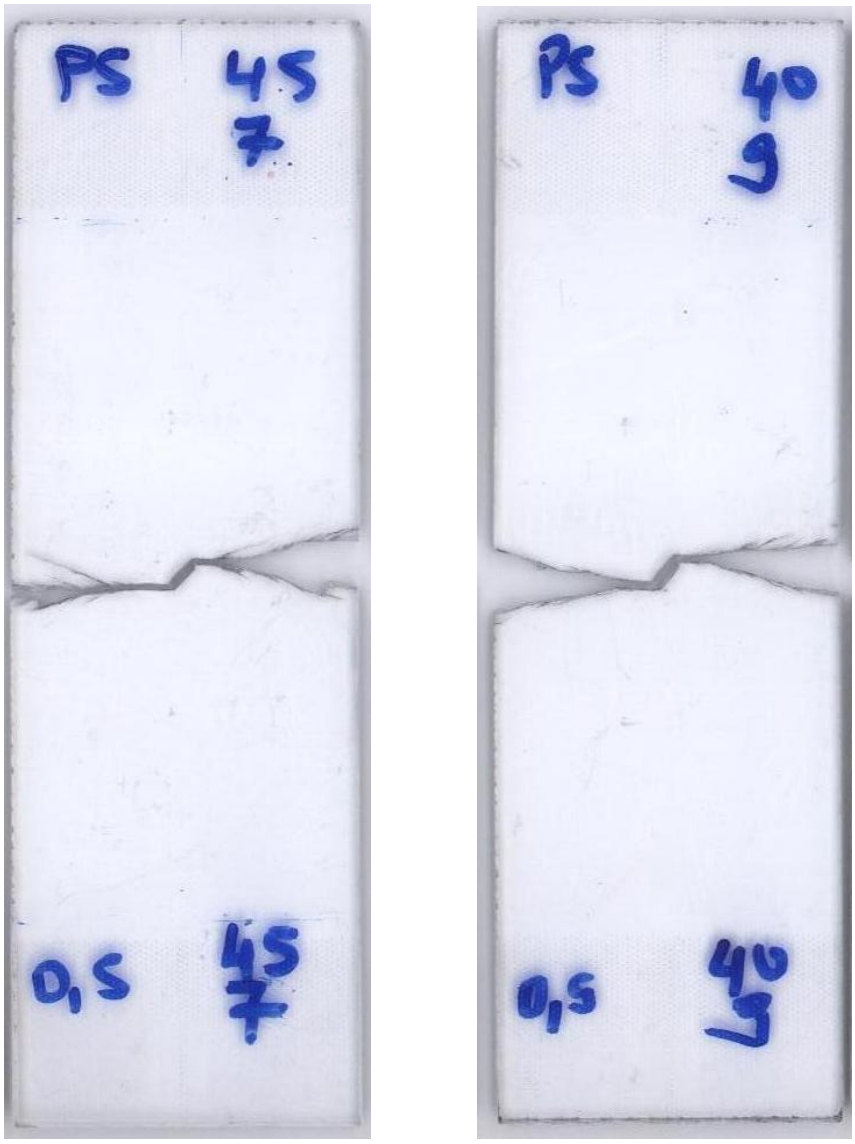

(a) (b)

Figure 3.23. (a) PS specimens with an inclined crack, $\beta = 45^{\circ}$ and $a/W = 0.1$

(b) PS specimens with an inclined crack, $\beta = 40^{\circ}$ and $a/W = 0.1$

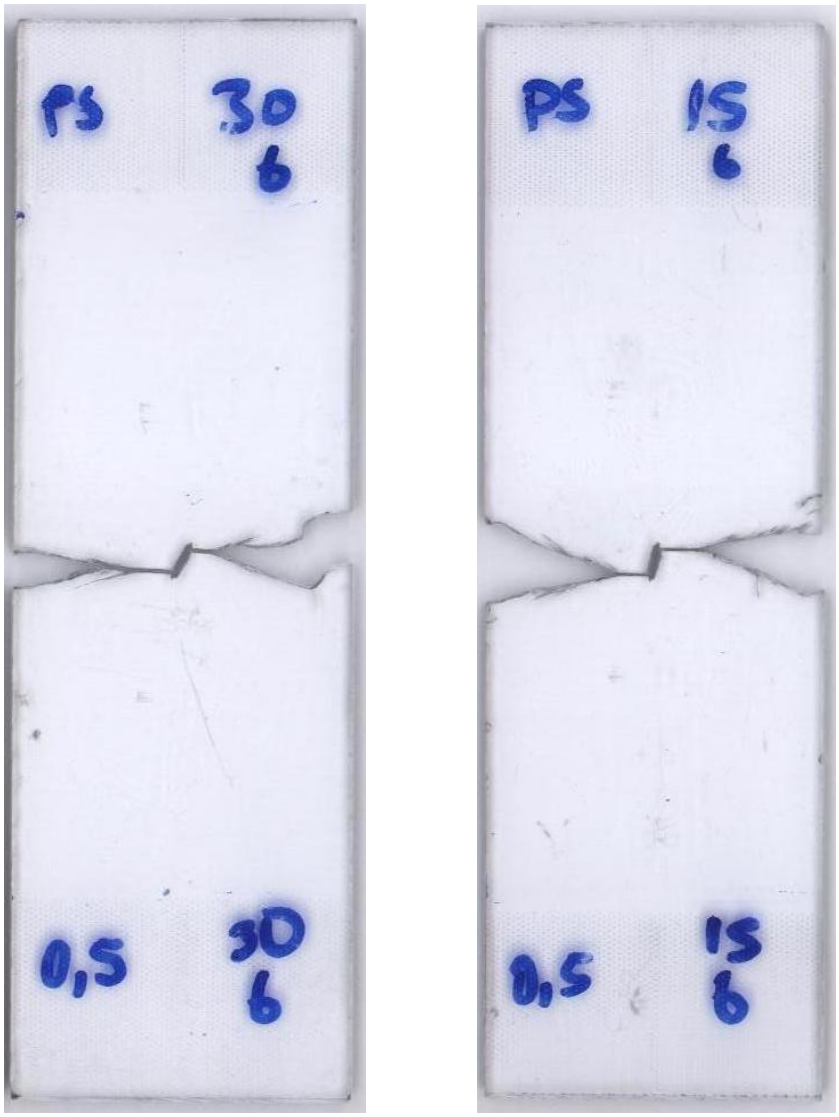

(a) (b)

Figure 3.24. (a) PS specimens with an inclined crack, $\beta = 30^{\circ}$ and $a/W = 0.1$

(b) PS specimens with an inclined crack, $\beta = 15^{\circ}$ and $a/W = 0.1$

In this work, a total of 100 PMMA specimens are used. 10 specimens for each crack angle β which consists of 15^o, 30^o, 40^o, 45^o, 50^o, 60^o, 70^o, 75^o, 80^o and 90^o are tested using Zwick/Roel Z10 tensile testing machine at 5 mm/min loading rate. The obtained crack initiation angles are given in Table 3.8 with $(\theta_c)_{avg.}$ being the average crack initiation angle of all measured values. In this experiments, the ratio of a/W is 0.1. Same procedure is done for a total 100 PS specimens for different crack angles. The crack initiation angles for PS specimens are also illustrated in Table 3.9.

The initial fracture angles θ_c at both ends of the crack giving in Figure 3.25 are measured. The crack initiation angles were measured from the image magnified 250 times. The average fracture angle of all measured values is calculated.

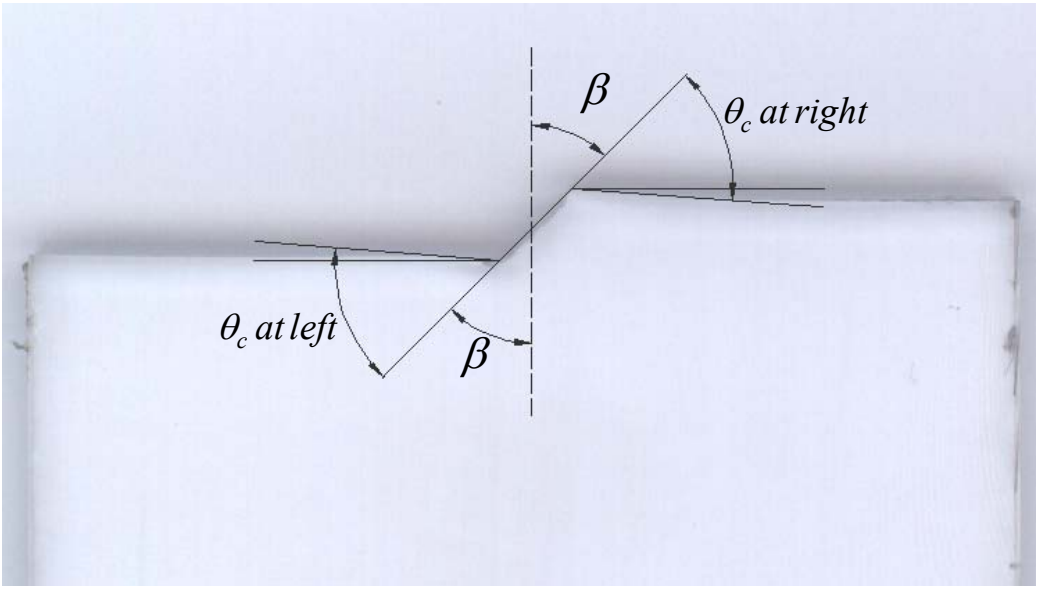

Figure 3.25. The measurement of the crack initiation angles θ_c

Table 3.8. Crack initiation angle, θ_c for PMMA

Specimen Number		Crack Angle, β									
		15	30	40	45	50	60	70	75	80	90
θ_c $x' = a$	1	-82.2	N/A	N/A	-50.3	-49.6	-41.4	N/A	-20.8	N/A	0.0
	2	-81.1	N/A	-57.1	-52.1	-52.4	-37.3	-28.1	-23.1	-15.0	0.0
	3	N/A	-63.7	-56.2	-53.3	N/A	-37.4	-24.8	N/A	-15.8	0.0
	4	N/A	-62.2	N/A	-53.6	-52.4	-37.9	-25.6	N/A	N/A	0.0
	5	-78.5	-62.0	-55.5	-51.6	-52.8	-38.6	-27.4	N/A	N/A	0.0
	6	N/A	N/A	-57.5	-54.8	-47.6	-42.1	-28.2	-19.3	-15.9	0.0
	7	-83.6	N/A	N/A	N/A	-48.0	-37.9	-29.1	N/A	-15.0	0.0
	8	-80.1	-62.9	N/A	-52.7	-52.5	-38.2	-28.5	-19.6	N/A	0.0
	9	N/A	-62.2	-54.7	-54.6	-49.5	N/A	N/A	N/A	-12.6	0.0
	10	N/A	-62.0	N/A	N/A	-50.6	N/A	N/A	-21.1	N/A	0.0
Average		-81.1	-62.5	-56.2	-52.9	-50.6	-38.8	-27.4	-20.8	-14.9	0.0
θ_c $x' = -a$	1	-82.7	N/A	-56.2	-49.2	-49.4	-42.2	-32.3	-23.1	N/A	0.0
	2	N/A	N/A	-59.0	-57.7	-52.6	-36.7	-28.1	-20.2	-14.5	0.0
	3	N/A	-65.0	-58.9	-53.7	N/A	-42.8	-25.3	-21.9	-16.7	0.0
	4	N/A	-62.9	N/A	N/A	N/A	-40.7	-26.6	N/A	-16.7	0.0
	5	-79.4	-63.0	-57.8	-52.4	-49.2	-41.7	-30.2	-20.2	-14.2	0.0
	6	N/A	N/A	-59.7	-51.8	-51.4	-35.8	-27.7	-19.1	-14.5	0.0
	7	-79.6	-63.0	N/A	N/A	-49.2	-39.9	N/A	N/A	-15.8	0.0
	8	-78.9	-63.3	N/A	-55.4	-48.7	N/A	-27.6	-22.9	-14.4	0.0
	9	-81.8	-61.4	-54.2	-54.9	-49.8	N/A	-31.0	-22.0	-17.7	0.0
	10	N/A	-63.0	N/A	N/A	-49.9	N/A	-26.6	N/A	-16.9	0.0
Average		-80.5	-63.1	-57.6	-53.6	-50.0	-40.0	-28.4	-21.3	-15.7	0.0
$(\theta_c)_{avg.}$		-80.8	-62.8	-56.9	-53.2	-50.3	-39.4	-27.9	-21.1	-15.3	0.0

Table 3.9. Crack initiation angle, θ_c for PS

Specimen Number		Crack Angle, β									
		15	30	40	45	50	60	70	75	80	90
θ_c $x' = a$	1	-77.4	-64.8	-61.5	N/A	N/A	-36.5	N/A	-18.5	-13.9	0.0
	2	-72.7	-65.2	N/A	N/A	N/A	N/A	-24.5	-19.0	-13.7	0.0
	3	-77.4	-64.7	-57.2	-51.8	N/A	-36.0	N/A	-20.7	-14.1	0.0
	4	-77.8	-67.1	-55.4	N/A	-47.5	-38.3	-24.4	-19.5	-12.8	0.0
	5	-75.5	-69.3	-54.4	-53.6	-45.1	N/A	-23.8	-20.3	-14.1	0.0
	6	-75.9	-67.0	-63.2	-52.8	-48.7	-38.1	-25.2	-20.4	-13.5	0.0
	7	-75.7	-68.9	-55.9	-53.3	-47.0	-38.2	N/A	N/A	-13.6	0.0
	8	-74.9	N/A	-62.7	-51.0	-46.1	-36.6	-26.9	-19.3	-14.7	0.0
	9	-77.5	N/A	-61.1	N/A	-47.5	N/A	-22.9	N/A	-14.5	0.0
	10	N/A	N/A	N/A	N/A	N/A	-34.2	-23.7	N/A	N/A	0.0
Average		-76.1	-66.7	-58.9	-52.5	-47.0	-36.8	-24.5	-19.6	-13.9	0.0
θ_c $x' = -a$	1	-77.5	-65.3	-55.1	-52.2	N/A	-34.5	N/A	-19.5	-12.1	0.0
	2	-73.0	-66.9	-57.5	N/A	N/A	N/A	-26.3	-18.8	-12.7	0.0
	3	-75.6	-65.8	-60.0	-53.3	-44.5	-36.8	-24.8	-20.0	-12.2	0.0
	4	-76.6	-66.6	-57.1	-53.4	-47.8	-37.7	-25.9	-20.5	-12.8	0.0
	5	-75.9	-65.8	-55.9	-49.8	-44.5	N/A	-22.8	-17.9	N/A	0.0
	6	-72.7	-67.8	-56.6	-52.7	-48.8	-35.1	-24.8	-20.1	-13.3	0.0
	7	-76.6	-65.9	-54.7	-53.7	-47.0	-36.0	N/A	N/A	-12.3	0.0
	8	-73.6	N/A	-56.1	-52.7	-47.4	-35.2	-27.1	-19.8	-16.5	0.0
	9	-76.8	N/A	-60.5	N/A	-46.6	N/A	-21.9	N/A	-14.9	0.0
	10	N/A	N/A	N/A	-54.2	N/A	-35.4	-23.5	N/A	N/A	0.0
Average		-75.4	-66.3	-57.1	-52.8	-46.6	-35.8	-24.6	-19.5	-13.4	0.0
$(\theta_c)_{avg.}$		-75.7	-66.5	-58.0	-52.6	-46.8	-36.3	-24.6	-19.6	-13.6	0.0

The initial fracture angles θ_c at both left and right ends of the crack were measured. The image of the end of the crack usually showed a band with upper and lower edges giving different values of θ_c . The variation between these angles was at most 3^o. The reason for this difference is that if the initial crack front is not precisely normal to sheet surface then one side moves before the other end and a distorted angle is produced.

At some points, it was not possible to measure the crack initiation angles, θ_c. N/A in Tables 3.8 and 3.9 represents these points. At these points, linear crack propagation is

observed and the crack initiation angle did not occur. When we check measured values obtained from the image magnified 250 times, the difference between image and magnified image is approximately $\pm 1^{\circ}$. Therefore, we assumed that the error in our measurements is approximately $\pm 1^{\circ}$.

4. COMPARISON OF EXPERIMENTAL RESULTS WITH COMPUTATIONAL RESULTS

Calculated results of θ_c for different β using MTS, GMTS, S and M-criteria under mixed-mode loading and experimental results obtained from present work for PMMA and PS specimens are compared in Figures 4.1 to 4.16 for different r_c. As we mentioned in section 2.4, the critical radius r_c can be represented in the following dimensionless form of:

$$\alpha = \sqrt{\frac{2r_c}{a}} \tag{4.1}$$

where *a* is crack length. The mode mixity parameter M^e is given by

$$M^e = \frac{2}{\pi}\tan^{-1}\left(\frac{K_I}{K_{II}}\right) \tag{4.2}$$

The value of M^e is 1 for pure mode-I and zero for pure mode-II. For mixed –mode, the parameter takes values between 0 and 1. The predictions obtained using MTS-criterion and the generalized MTS-criterion are shown on the same figures for comparison. MTS-criterion assumes a constant radius for the core region and uses only the singular elastic stress field to define stresses at the crack tip without including T-stress, the value of radius r_c does not affect the crack initiation angle. However, in GMTS-criterion, the non- singular term, T-stress, is added to elastic stress field, then the value of r_c affects the crack initiation angle which is shown in Figure 4.1 and 4.2. Experimental results given in Figures 4.1 and 4.2 show that T-stress has an influence on mixed-mode fracture whether it is positive or negative. And also, it can be seen that, for the PMMA plate containing a central crack, the value of α which is the dimensionless form of critical radius r_c gives a better fit for 0.1.

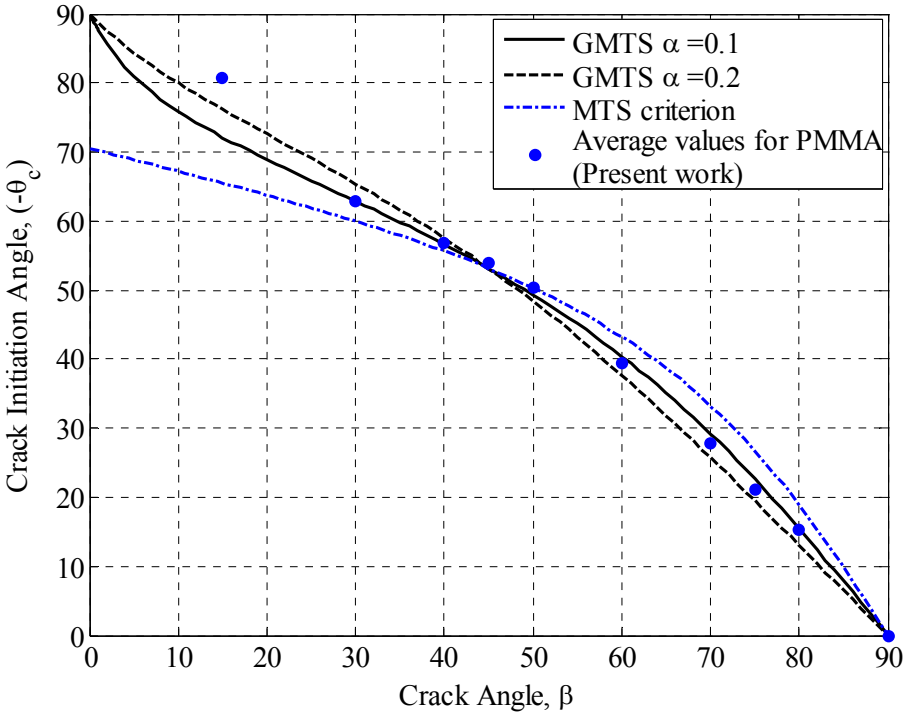

Figure 4.1. Crack initiation angle vs crack angle for PMMA under tension, $a/w = 0.1 \text{and} \alpha = \sqrt{2r_c/a}$

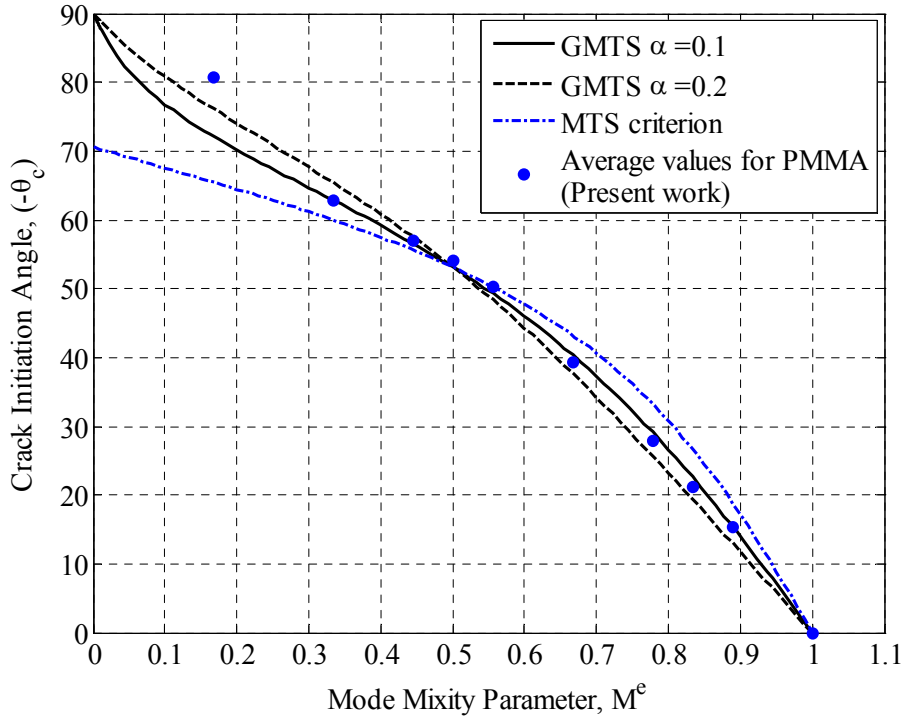

Figure 4.2. Crack initiation angle vs mode mixity parameter M^e for PMMA, $a/w = 0.1 \text{and} \alpha = \sqrt{2r_c/a}$

For central cracked PMMA plate under mixed-mode loading, Figures 4.3 and 4.4 present predictions of strain energy density (S-criterion) criterion for $0.3 < \nu < 0.4$. The effects of the plane-strain and plane stress are shown on the same figures. From these figures, it can be concluded that in mixed-mode fracture, as Poisson's ratio ν increases the crack initiation angle $(-\theta_c)$ increases and ν has a greater influence on plane-strain than it has influence on plane-stress. The S-criterion gives $\theta_c = -83.4$ for plane strain and $\theta_c = -80.3$ for plane stress at $\beta = 0$ pure mode-II and $\nu = 0.33$.

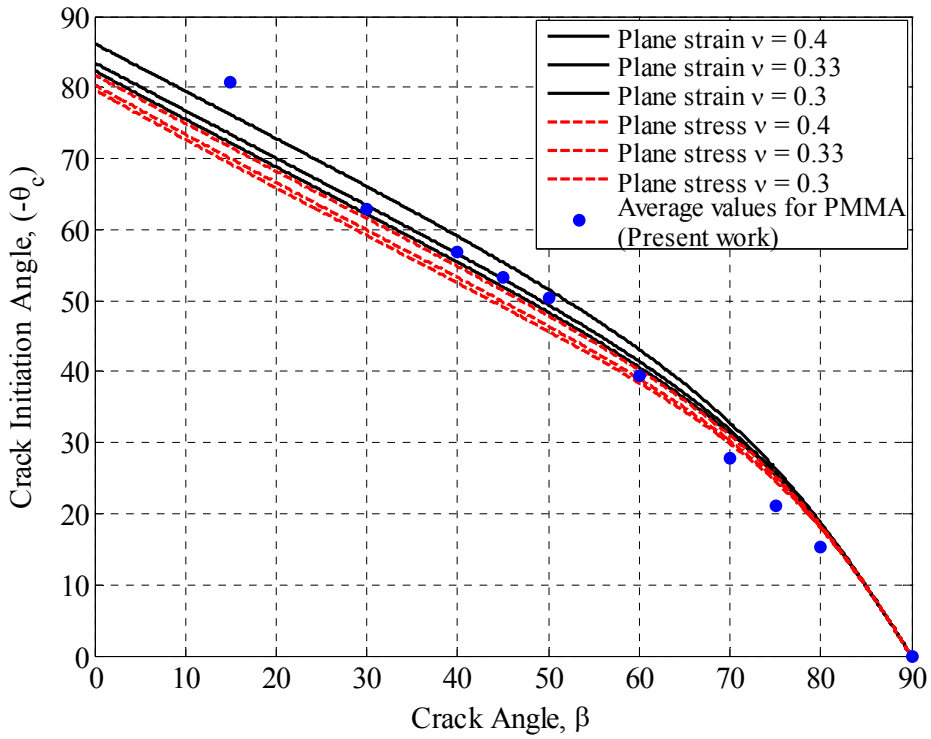

Figure 4.3. Crack initiation angle vs crack angle for PMMA under tension based on S-criterion, $a/w = 0.1$

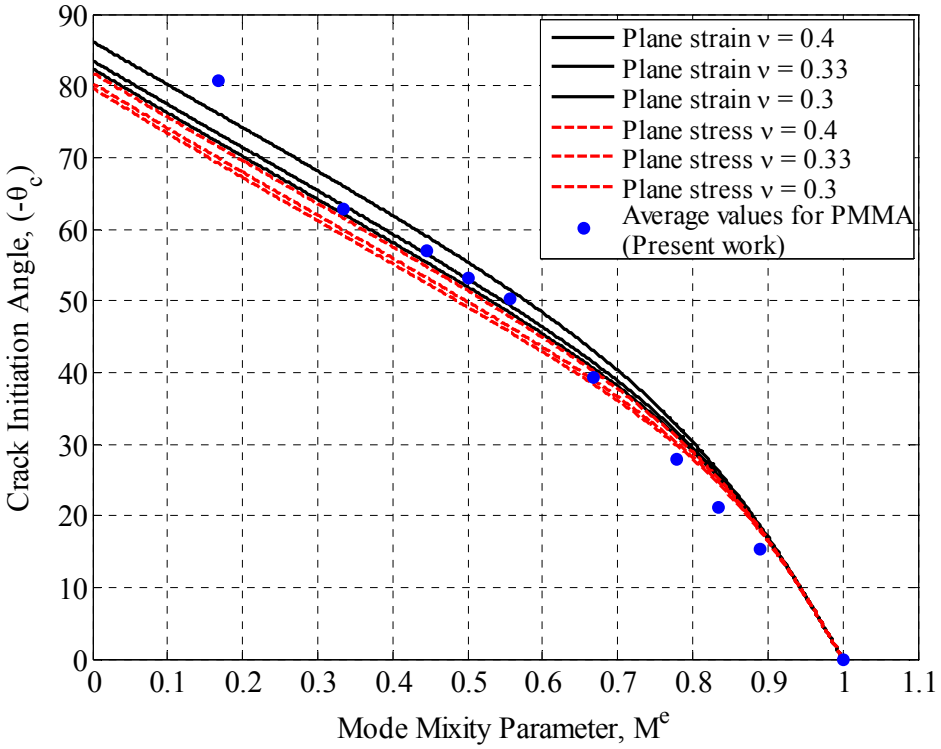

Figure 4.4. Crack initiation angle vs mode mixity parameter M^e for PMMA under tension based on S-criterion, $a/w = 0.1$

For PMMA, as seen in Figure 4.1 and 4.2, the experimentally obtained values of crack initiation angle $(-\theta_c)$ are in very good agreement with the prediction of the generalized MTS-criterion for mixed-mode loading. In contrast, the curve obtained from S-criterion as seen in Figure 4.3 and 4.4 does not appear to show agreement in the range of large crack angle β.

Experimental results on crack initiation angle for center cracked PS are given in Figures 4.5 to 4.8. Figures 4.5 and 4.6 show that as the crack angle β increases, the effect of T-stress increases and it is apparent that the predictions from generalized MTS-criterion for $\alpha = 0.2$ are quite close to experimental points for central cracked PS under mixed-mode loading.

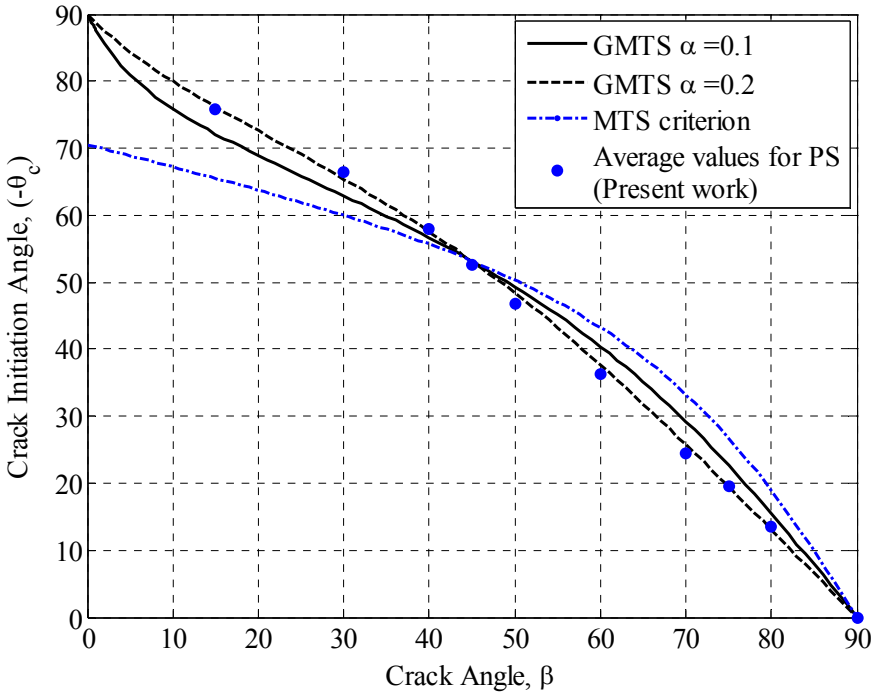

Figure 4.5. Crack initiation angle vs crack angle for PS under tension, $a/w = 0.1 \text{and} \alpha = \sqrt{2r_c/a}$

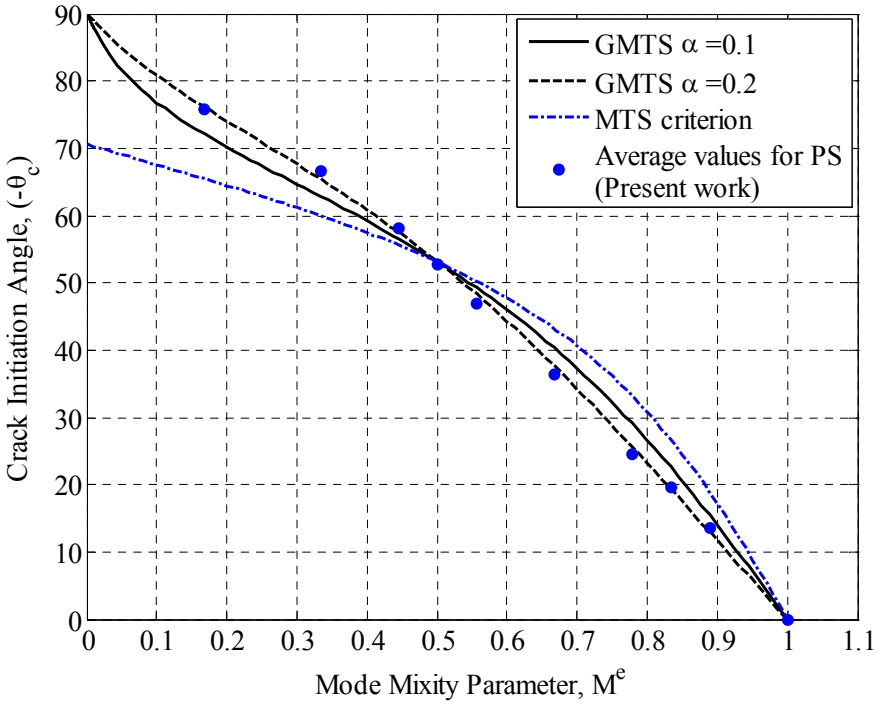

Figure 4.6. Crack initiation angle vs mode mixity parameter M^e for PS, $a/w = 0.1 \text{and} \alpha = \sqrt{2r_c/a}$

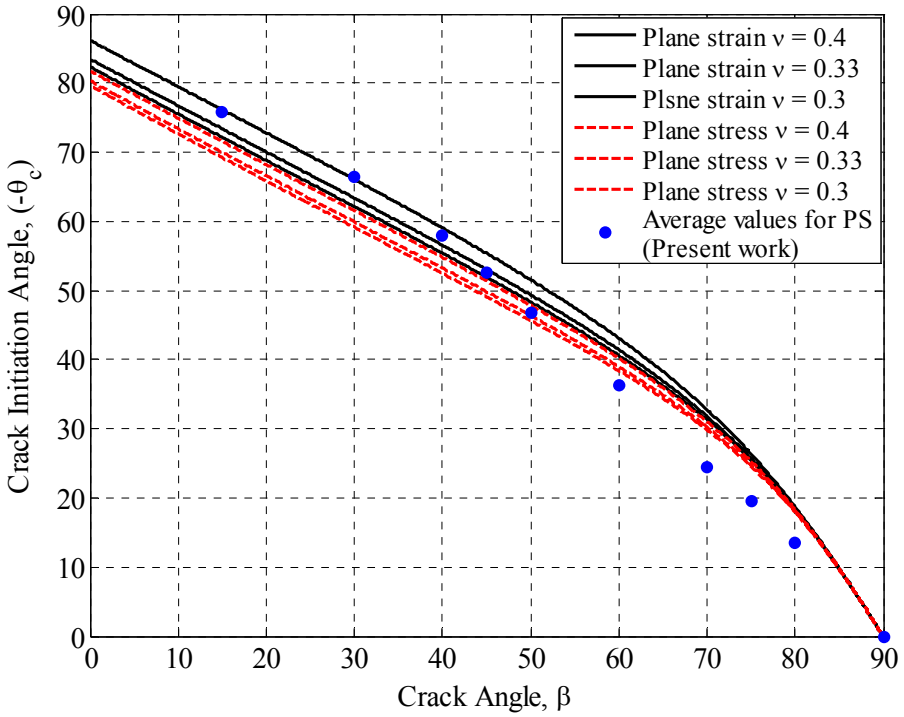

Figure 4.7. Crack initiation angle vs crack angle for PMMA under tension based on S-criterion, $a/w = 0.1$

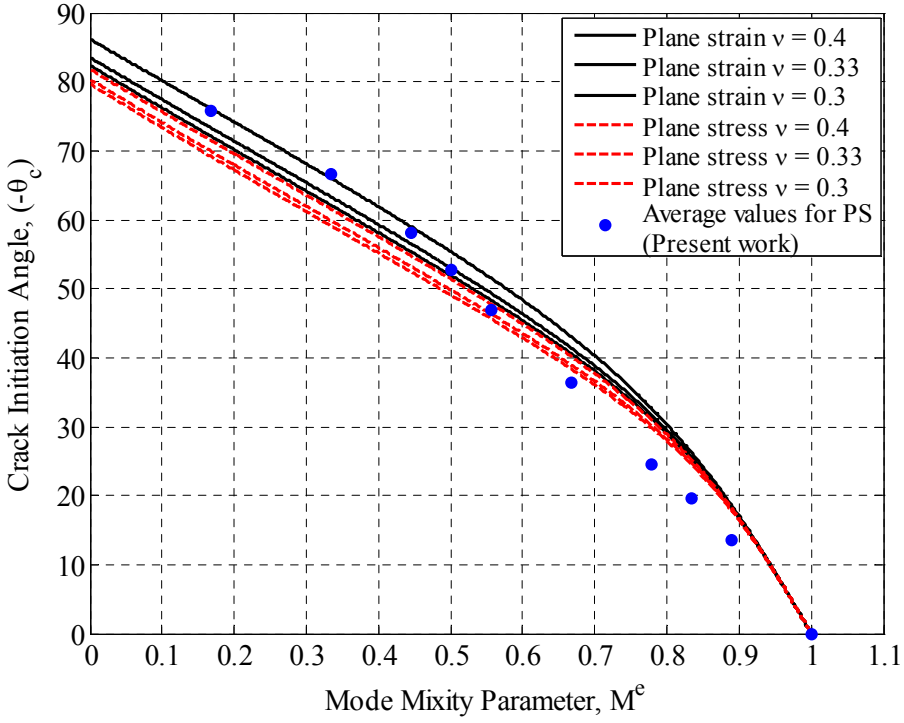

Figure 4.8. Crack initiation angle vs mode mixity parameter M^e for PS under tension based on S-criterion, $a/w = 0.1$

The experimental results on crack initiation angles for PMMA presented by William and Ewing [7], Ueda et al [8], and present work are shown in Figure 4.9. If the crack length does not vary, α is as a constant. Consequently, the prediction using the generalized MTS-criterion reflects the variation of T-stress. Thus, for $0 \le \beta \le 45$, the T-stress is positive and the magnitude of the fracture angle is higher than that predicted by the conventional MTS-criterion. For $45 \le \beta \le 90$, T-stress is negative and the magnitude of the fracture angle is less than the predicted value of the conventional MTS-criterion. All experimental results as seen in Figure 4.9 show that the T-stress has an important effect on mixed-mode fracture.

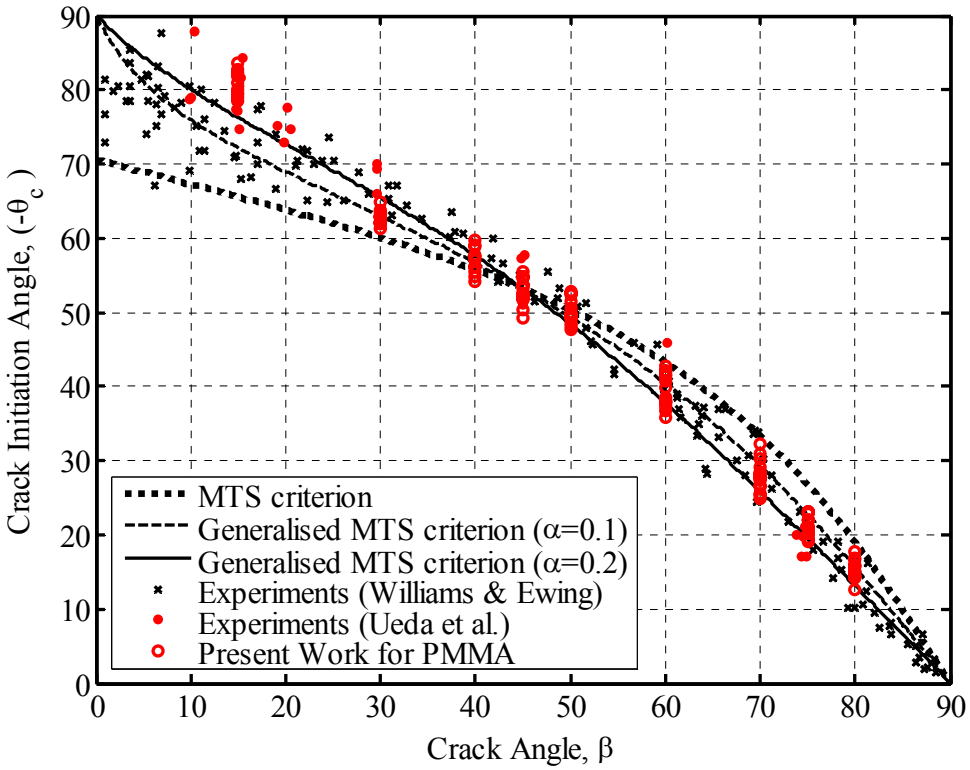

Figure 4.9. Experimental results for crack initiation angle for PMMA

For PMMA specimens, the MTS-criterion presented by Erdogan and Sih [6] and the generalized MTS-criterion are shown together in Figure 4.10. It can be seen that the line tends to $\theta = 90^o$ and not to 70.5^o. For $\alpha = 0.1$, GMTS-criterion gives a better fit to experimental points for $\beta > 30^o$ and $\alpha = 0.1$ is chosen as the best fit to the experimental results. For $\beta = 15$, the crack initiation angles θ_c are greater than the prediction of the

conventional MTS-criterion. The critical distance of ahead of the crack tip r_c plays an important role in predicting crack growth direction. It is assumed that r_c is a critical distance in front of the crack tip where the fracture would occur. The critical radius r_c was determined by using the dimensionless parameter α .

$$\alpha = \left(\frac{2r_c}{a} \right)^{1/2} \quad \text{for } \alpha = 0.1 \text{and } 2a = 5\,mm \tag{4.3}$$

$$\Rightarrow \left(\frac{2r_c}{a} \right)^{1/2} = 0.1$$

$$\Rightarrow r_c = \frac{0.1^2 a}{2}$$

$$\Rightarrow r_c \simeq 0.01$$

For PMMA specimens, a value of critical radius r_c is 0.01mm is obtained.

The experimental results about crack initiation angle about center cracked PS specimens are illustrated in Figure 4.11. A value of 0.2 for α gives good results for prediction of crack initiation angle. For PS specimens, a value of critical radius r_c is 0.05mm is obtained. Therefore In this study, we assumed that the critical radius r_c is a material constant that can be determined form experiments.

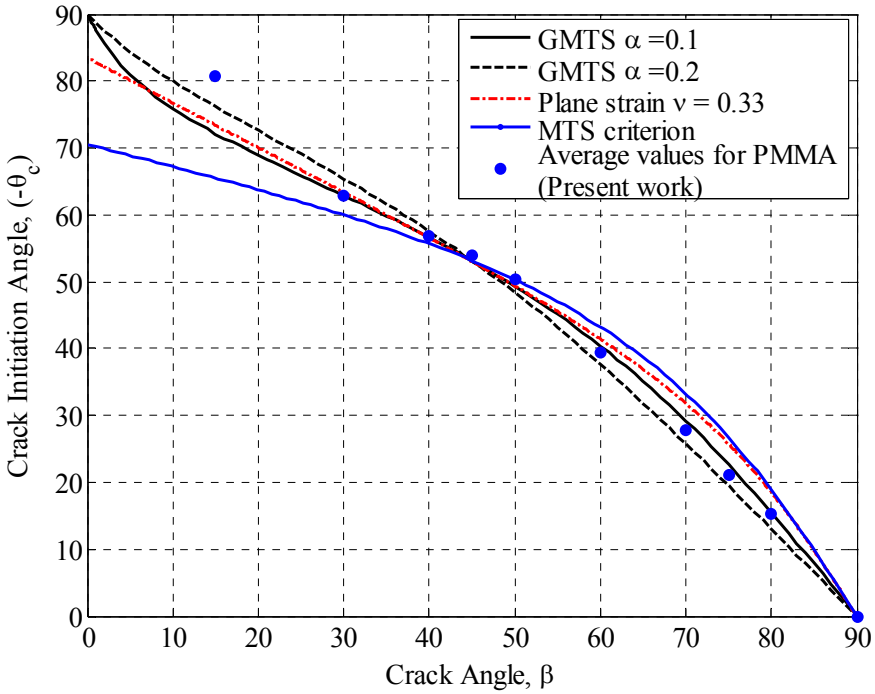

Figure 4.10. Crack initiation angle vs crack angle for PMMA under tension, $a/w = 0.1 \text{and} \, \alpha = \sqrt{2r_c/a}$

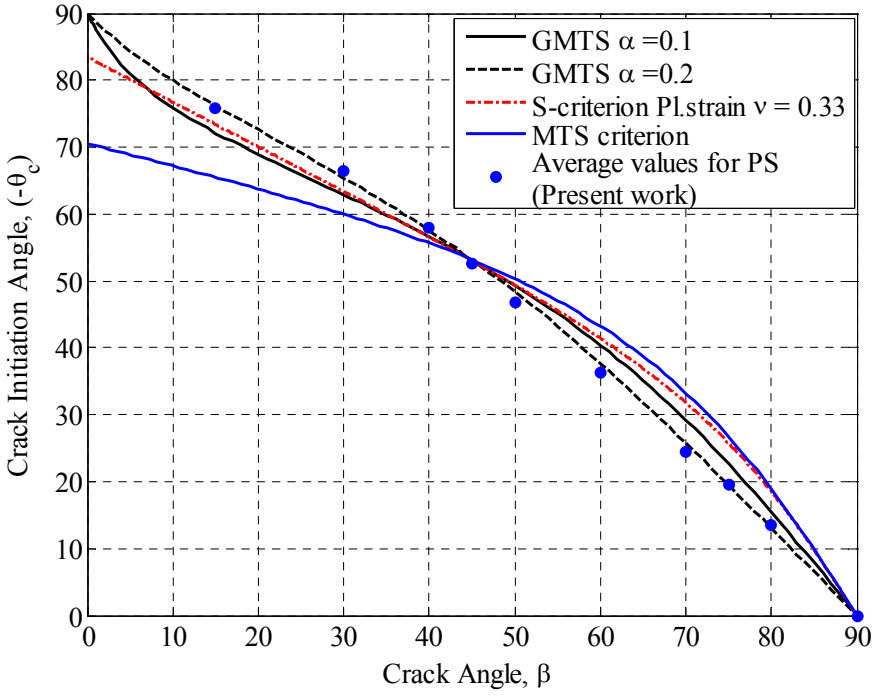

Figure 4.11. Crack initiation angle vs crack angle for PS under tension, $a/w = 0.1 \text{and} \, \alpha = \sqrt{2r_c/a}$

M-criterion assumes that the crack starts to grow from where the triaxiality ratio is maximum around the crack tip and uses only the singular elastic stress field to define stresses at the crack tip, and then the value of that radius r_c does not affect the crack initiation angle. However, in the modified M-criterion, we inserted T-stress term into stress field equations and modified the M-criterion. For PMMA and PS specimens, the M-criterion $(\alpha = 0)$ presented by Kong and the modified M-criterion are shown together in Figure 4.12 to 4.14. Therefore, from Figures 4.12 to 4.14, the value of the critical radius r_c affects the crack initiation angle. It can be seen that the line tends to $\theta = 109.2^o$ and not to 98.91^o for pure mode-II loading. As seen in Figures 4.12- 4.14, the experimental results of PMMA and PS specimens for this study do not show a good agreement with the theoretical results in a large range of crack angle β with M-criterion.

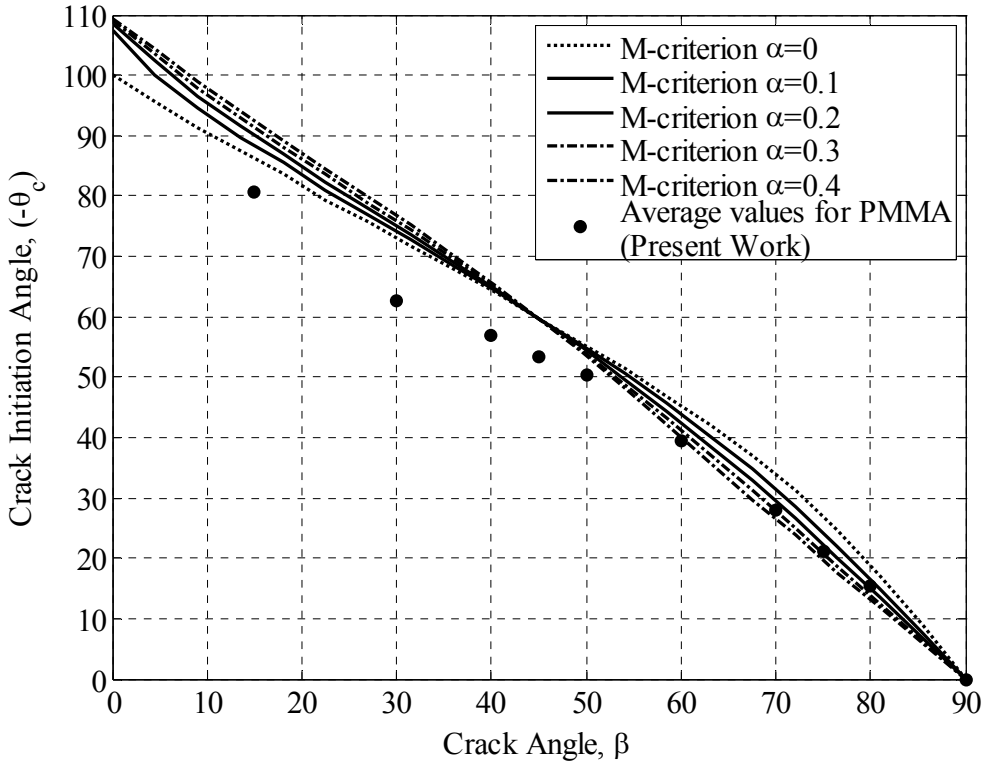

Figure 4.12. Crack initiation angle vs crack angle for PMMA based on M-criterion, $a/w = 0.1$ and $\alpha = \sqrt{2r_c/a}$

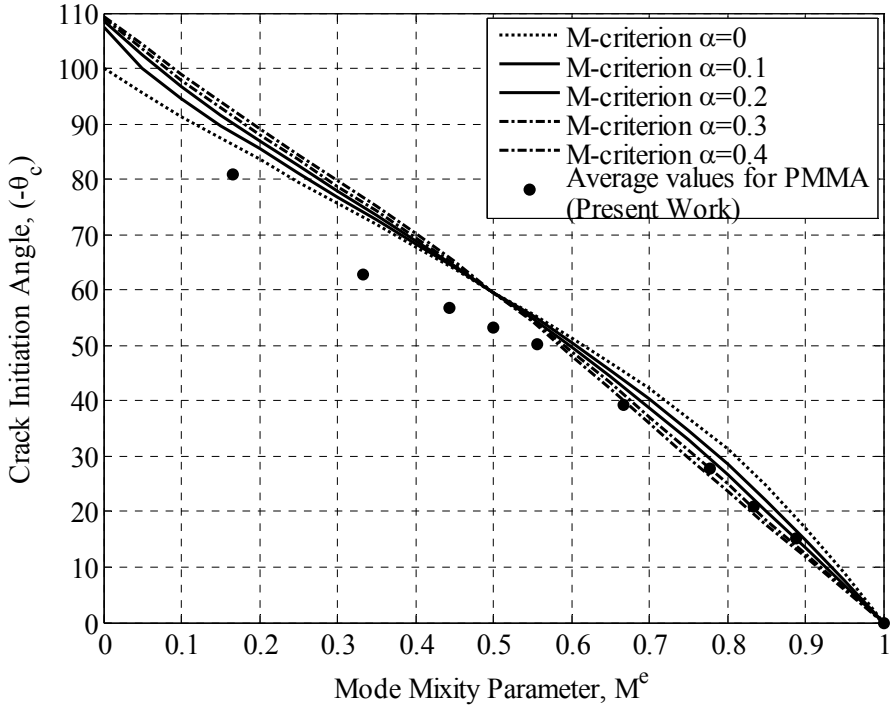

Figure 4.13. Crack initiation angle vs mode mixity parameter M^e for PMMA based on M-criterion, $a/w = 0.1$ and $\alpha = \sqrt{2r_c/a}$

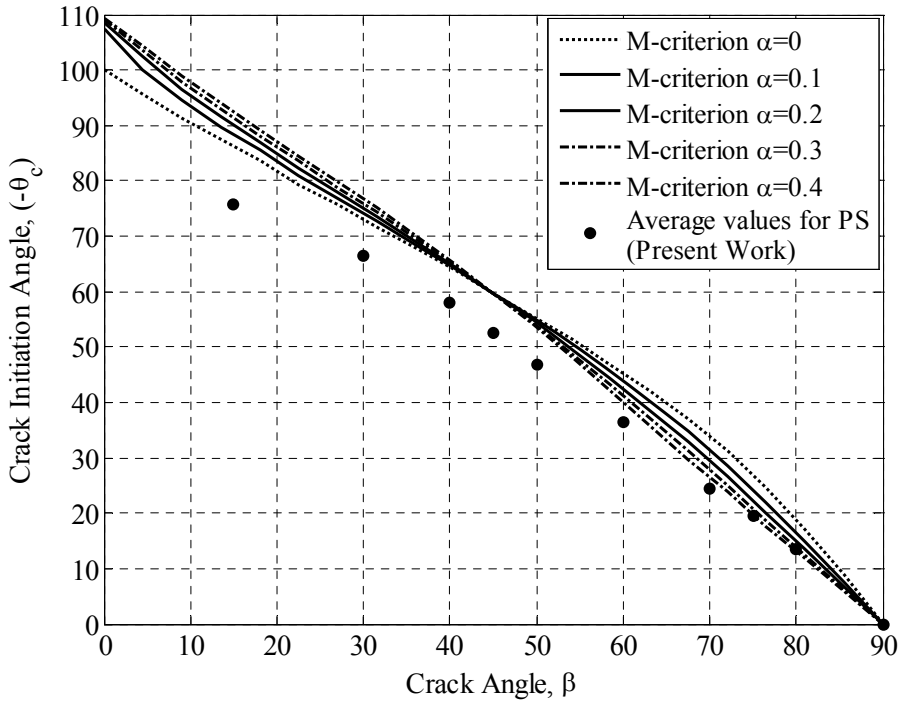

Figure 4.14. Crack initiation angle vs crack angle for PS based on M-criterion, $a/w = 0.1$ and $\alpha = \sqrt{2r_c/a}$

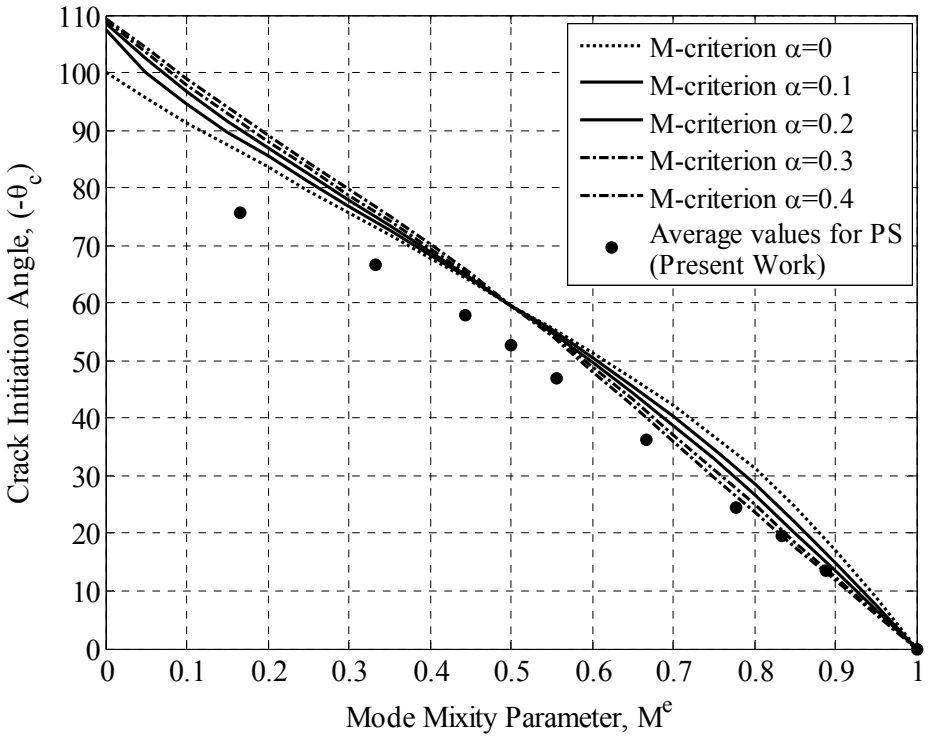

Figure 4.15. Crack initiation angle vs mode mixity parameter M^e for PMMA based on M-criterion, $a/w = 0.1$ and $\alpha = \sqrt{2r_c/a}$

For a cracked body under mixed-mode loading conditions, using the stress field equations in conjunction with a given crack initiation criterion, the angle θ_c defines the crack initiation angle and *r* defines the critical radius. As discussed earlier, there are two approaches to define this radius r: one is to assume a constant radius and the other is to define a variable radius based on some yield function. In M-criterion, the Von Misses yield criterion is used to define the equivalent stress σ_{eq}. Von Misses yield criterion is often applied for ductile materials that yielding occurs. For mixed-mode loading of PMMA and PS which are brittle material, as seen in Figures 4.12 to 4.15, the experimental points are very scattered and do not favor M-criterion and the modified M-criterion.

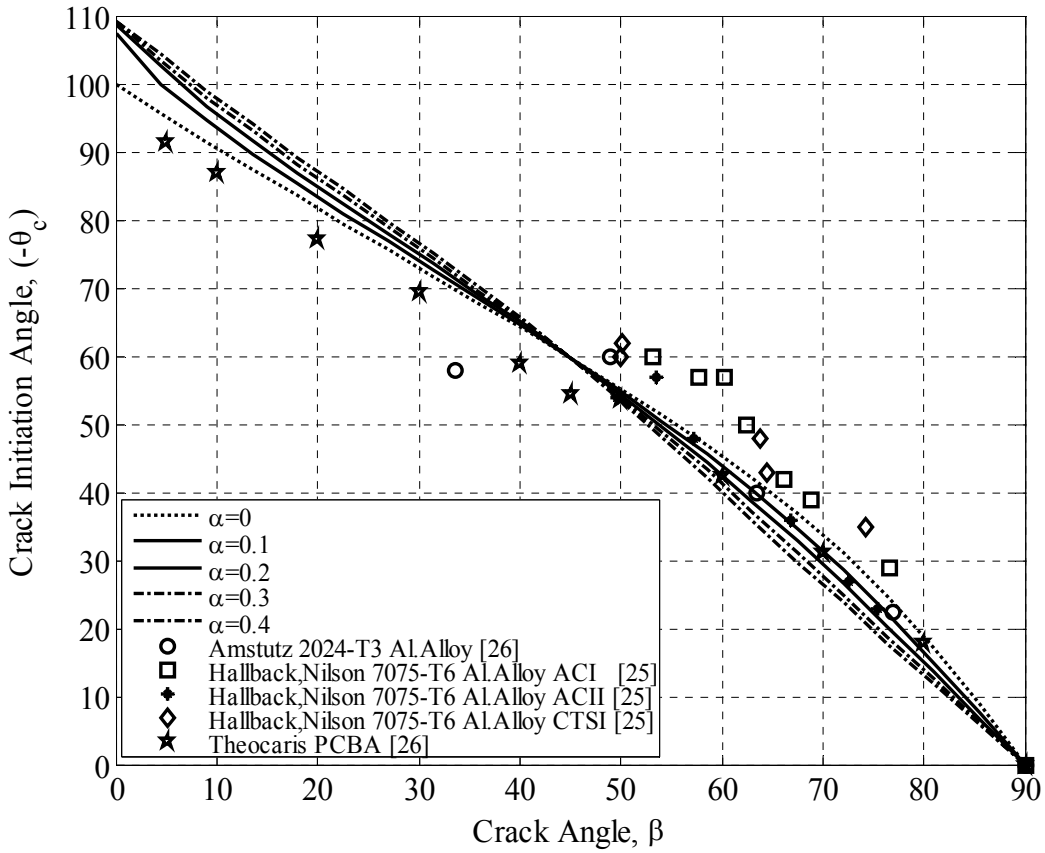

Figure 4.16. Experimental results for crack initiation angle for ductile materials based on M-criterion, $a/w = 0.1$ and $\alpha = \sqrt{2r_c/a}$

In Figure 4.16, the experimental data for ductile materials is shown. Amstutz used 2024-T3 aluminum alloy central crack specimens in his study. Hallback and Nilson performed on their experiments with 7075-T6 aluminum alloy specimens [25] and Theocaris [26] tested polycarbonate (PCBA) specimens containing a slant internal crack in his experiments. As seen in figure 4.16, for $45^\circ < \beta < 90^\circ$, ductile materials show a better agreement with M-criterion. We concluded that the predictions of M-criterion and the modified M-criterion are available for ductile materials under uniaxial tension.

5. CONCLUSION

The purpose of this study was to determine crack initiation angles, the effect of critical radius r_c and T-stress on crack initiation angles using experimental and analytical techniques. The maximum tangential stress (MTS-criterion), the generalized maximum tangential stress (GMTS-criterion), the minimum strain energy density (S-criterion) and the maximum triaxial stress (M-criterion) criteria were analyzed. Analytical results were compared to experimental results of PMMA and PS with an inclined central crack under mixed-mode loading.

In this study, a sudden propagation of the crack and no stable crack growth was observed in testing of PMMA and PS specimens. In this work, a total of 100 specimens for both PMMA and PS are used. 10 specimens for each crack angle β which consists of 15^o, 30^o, 40^o, 45^o, 50^o, 60^o, 70^o, 75^o, 80^o and 90^o are tested using Zwick/Roel Z10 tensile testing machine. The initial fracture angles θ_c at both ends of the crack are measured. The crack initiation angles were measured from the image magnified 250 times.

M-criterion was modified by inserting T-stress term into the stress field equations. The analytical results of the modified M-criterion do not give a good agreement with the experimental results as expected. We concluded that, M-criteria is proper for prediction of crack initiation angle of ductile materials.

For both PMMA and PS, measured crack initiation angles, $-\theta_c$ versus crack angles β and the mode mixity parameter M^e were plotted in figures for each criterion used. The generalized MTS-criterion is in a better agreement with our experimental results for both central cracked PMMA and PS specimens than other criteria. Similar to earlier results in literature, the experimental results show the importance of the non-singular term, T-stress, and the critical radius r_c which is a material property. The reason of the difference between the conventional MTS-criterion and experimental results is the presence of the T-stress and the critical radius r_c .

The critical radius r_c which is assumed to be material property was determined for central cracked PMMA and PS specimens. The critical radius $r_c = 0.01$ for PMMA and 0.05 for PS is reasonable.

APPENDIX A: RESULTS OF TENSILE TESTING FOR PMMA

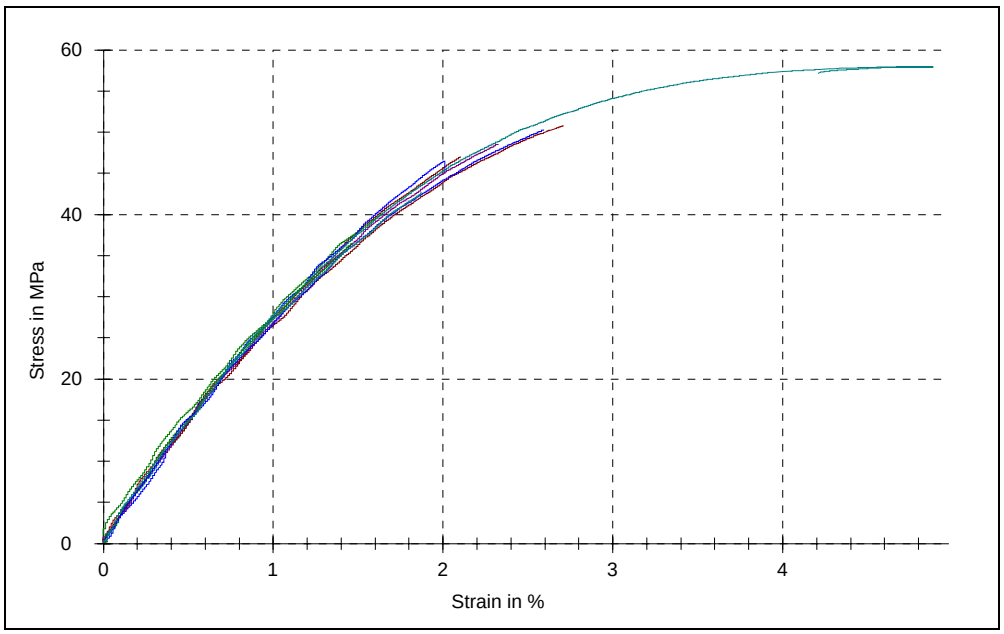

Figure A.1.The stress-strain diagram of PMMA for β=15 and a/w=0.1

Table A.1. The results of PMMA for β=15 and a/w=0.1

Specimen Number	Modulus of Elasticity $E\,(MPa)$	Ultimate Stress $\sigma_M\,(MPa)$	Stress at Break $\sigma_B\,(MPa)$	Elongation at Break $\varepsilon_B\,(\%)$
1	2670.87	47.03	47.03	2.1
2	2767.90	40	39.86	1.63
3	2583.40	46.46	44.95	2.01
4	2884.61	57.96	57.11	4.21
5	2957.60	48.53	48.53	2.32
6	3346.16	50.76	50.75	2.71
7	3012.19	36.48	36.45	1.47
8	3028.93	50.27	50.27	2.59
9	3037.10	42.64	42.64	1.88
Average	2920.97	46.68	46.40	2.32

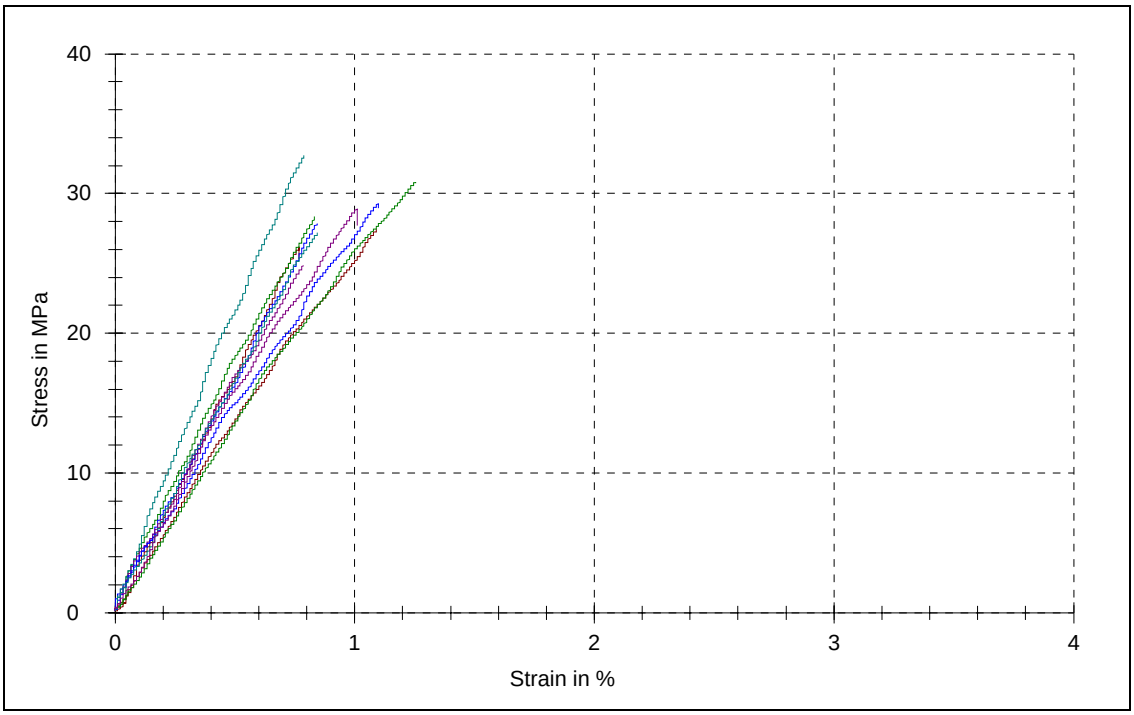

Figure A.2. The stress-strain diagram of PMMA for β=30 and a/w=0.1

Table A.2. The results of PMMA for β=30 and a/w=0.1

Specimen Number	Modulus of Elasticity $E\,(MPa)$	Ultimate Stress $\sigma_M\,(MPa)$	Stress at Break $\sigma_B\,(MPa)$	Elongation at Break $\varepsilon_B\,(\%)$
1	3496.97	26.21	25.3	0.77
2	3365.91	28.34	28.34	0.83
3	3230.31	27.84	27.84	0.84
4	4454.43	32.73	32.73	0.79
5	2743.5	24.81	24.81	0.79
6	2736.36	27.45	27.45	1.09
7	2737.95	30.84	30.84	1.26
8	2526.19	29.26	28.95	1.1
9	3234.96	27.2	27.2	0.84
10	3232.53	28.92	27.68	1.01
Average	3175.91	28.36	28.11	0.93

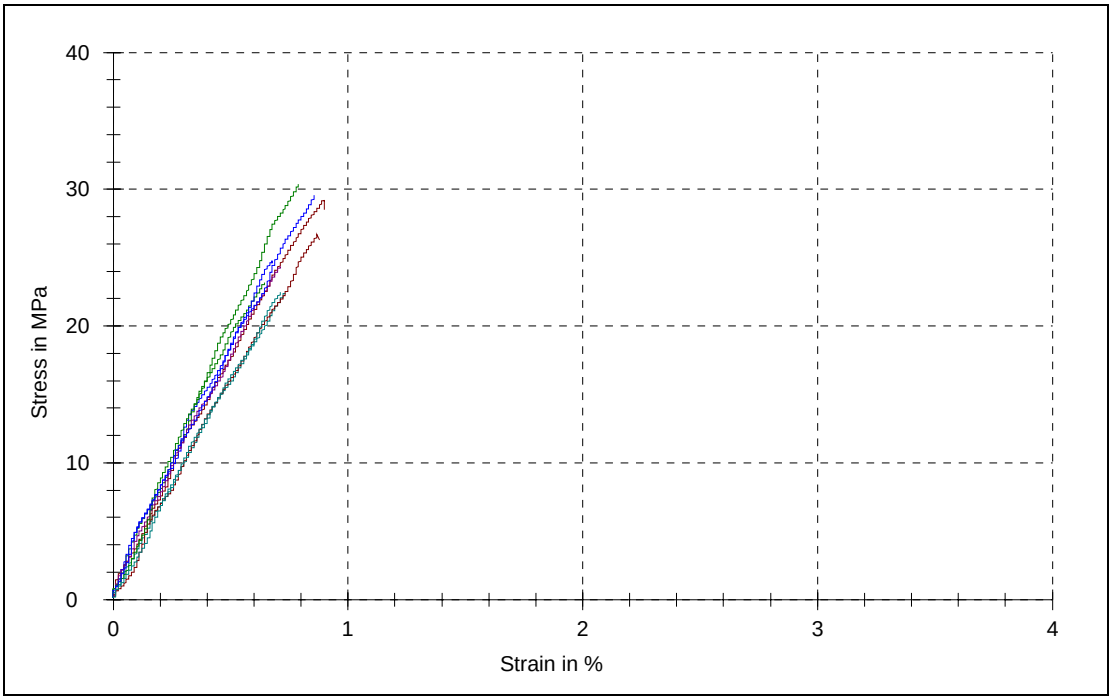

Figure A.3. The stress-strain diagram of PMMA for β=40 and a/w=0.1

Table A.3. The results of PMMA for β=40 and a/w=0.1

Specimen Number	Modulus of Elasticity $E\,(MPa)$	Ultimate Stress $\sigma_M\,(MPa)$	Stress at Break $\sigma_B\,(MPa)$	Elongation at Break $\varepsilon_B\,(\%)$
1	3457.42	29.21	28.51	0.9
2	3422.67	23.15	23.15	0.64
3	3328.26	24.8	24.6	0.68
4	3280.28	22.42	22.42	0.73
5	3521.54	24.31	24.3	0.71
6	3879.7	26.69	26.29	0.88
7	4715.97	30.36	30.36	0.79
8	3612.99	29.58	29.58	0.86
9	3537.4	22.47	22.47	0.71
Average	3639.58	25.89	25.74	0.77

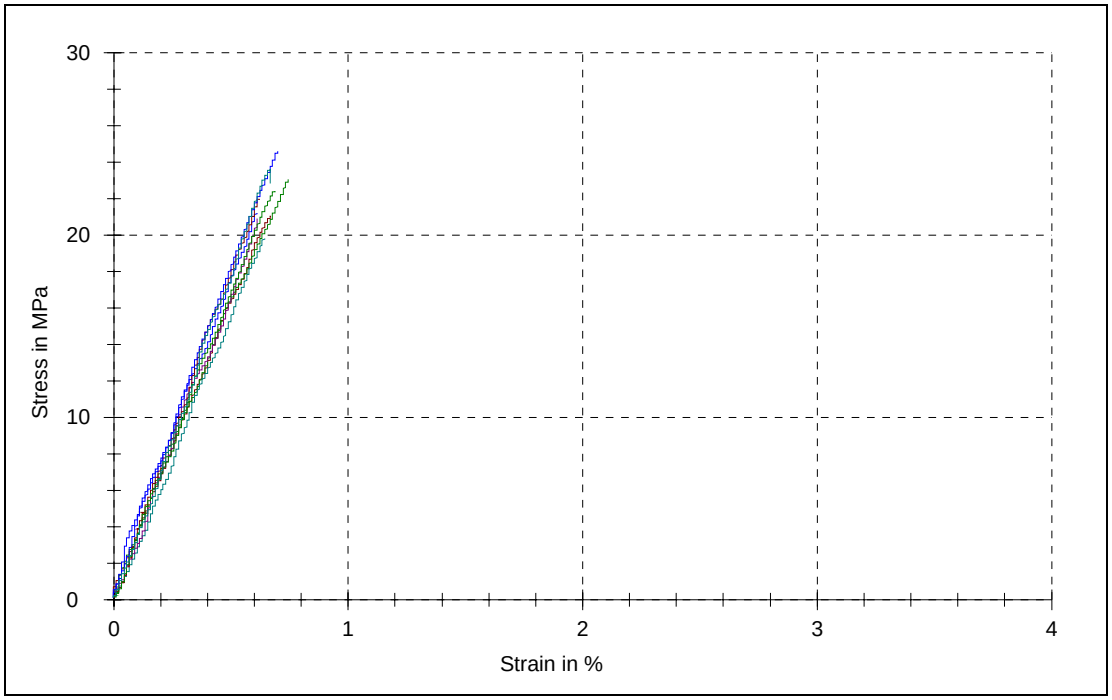

Figure A.4. The stress-strain diagram of PMMA for β=45 and a/w=0.1

Table A.4. The results of PMMA for β=45and a/w=0.1

Specimen Number	Modulus of Elasticity $E\,(MPa)$	Ultimate Stress $\sigma_M\,(MPa)$	Stress at Break $\sigma_B\,(MPa)$	Elongation at Break $\varepsilon_B\,(\%)$
1	3196.46	21.05	20.99	0.67
2	3337.63	23.05	23.05	0.74
3	3526.18	21.18	21.18	0.61
4	3088.53	19.78	19.78	0.64
5	3603.21	20.9	20.9	0.61
6	3726.1	21.96	21.96	0.62
7	3382.53	22.4	22.4	0.69
8	2988.79	24.58	24.58	0.7
9	3530.1	23.6	22.82	0.67
Average	3375.50	22.06	21.96	0.66

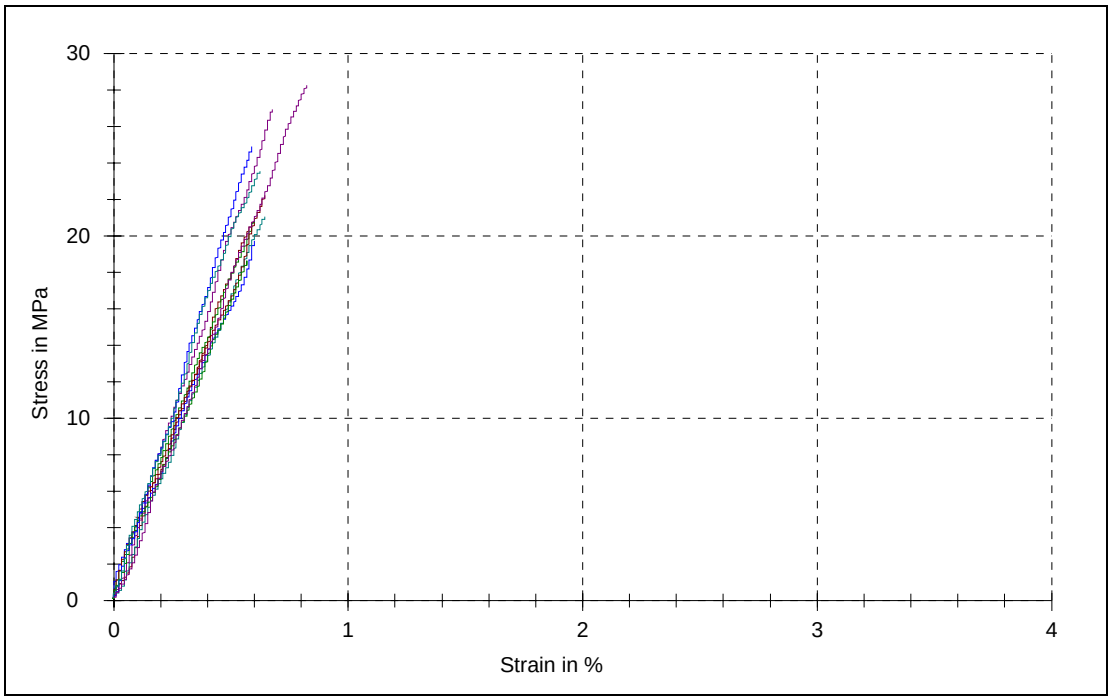

Figure A.5. The stress-strain diagram of PMMA for β=50 and a/w=0.1

Table A.5. The results of PMMA for β=50 and a/w=0.1

Specimen Number	Modulus of Elasticity $E\,(MPa)$	Ultimate Stress $\sigma_M\,(MPa)$	Stress at Break $\sigma_B\,(MPa)$	Elongation at Break $\varepsilon_B\,(\%)$
1	4106.26	22.2	22.2	0.64
2	3499.24	20.8	20.8	0.6
3	2810.04	19.73	19.73	0.6
4	3411.87	21.04	21.04	0.64
5	4398.23	26.91	26.91	0.68
6	2912.26	20.69	20.69	0.6
7	2994.4	18.62	18.39	0.57
8	3953.33	24.89	24.89	0.59
9	3644.94	23.54	23.54	0.62
10	3906.11	28.24	28.24	0.82
Average	3563.67	22.64	22.64	0.64

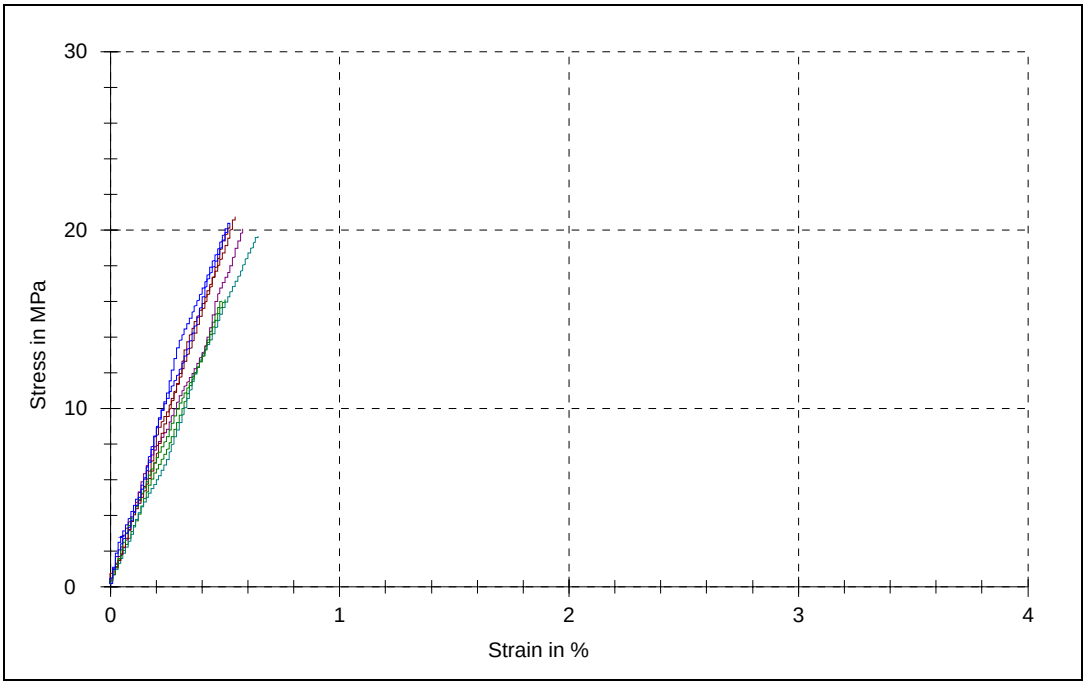

Figure A.6. The stress-strain diagram of PMMA for β=60 and a/w=0.1

Table A.6. The results of PMMA for β=60 and a/w=0.1

Specimen Number	Modulus of Elasticity $E\,(MPa)$	Ultimate Stress $\sigma_M\,(MPa)$	Stress at Break $\sigma_B\,(MPa)$	Elongation at Break $\varepsilon_B\,(\%)$
1	3551.84	14.02	14.02	0.4
2	3979.02	15.78	15.78	0.41
3	3974.44	15.62	15.09	0.41
4	2879.93	14.91	14.91	0.43
5	3075.63	15.13	15.13	0.46
6	4217.96	19.08	19.08	0.48
7	2958.91	15.19	15.19	0.41
8	3224.25	16.15	15.62	0.44
9	4007.96	15.8	15.8	0.41
10	4316.18	18.6	18.6	0.46
Average	3618.61	16.03	15.92	0.43

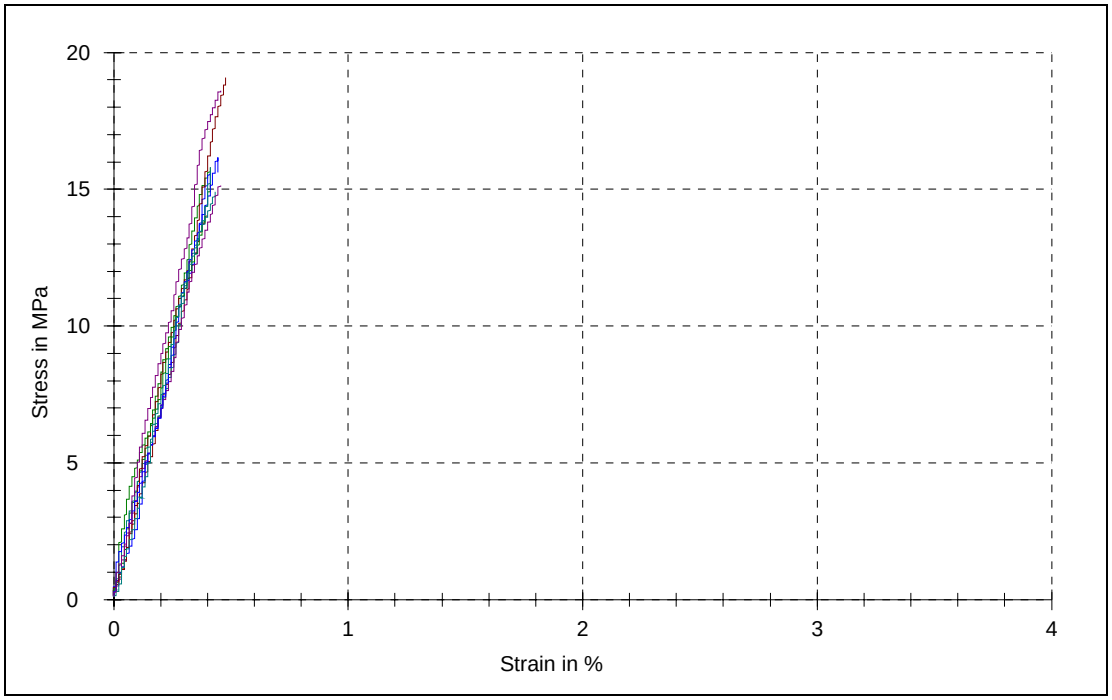

Figure A.7. The stress-strain diagram of PMMA for β=70 and a/w=0.1

Table A.7. The results of PMMA for β=70 and a/w=0.1

Specimen Number	Modulus of Elasticity $E\,(MPa)$	Ultimate Stress $\sigma_M\,(MPa)$	Stress at Break $\sigma_B\,(MPa)$	Elongation at Break $\varepsilon_B\,(\%)$
1	2682.02	13.73	13.28	0.47
2	3201.06	15.62	15.62	0.46
3	3158.15	14.24	14.23	0.42
4	3132.28	13.02	12.94	0.4
5	4751.9	17.61	17.3	0.43
6	3193.86	17.66	17.66	0.51
7	2704.01	14.97	14.66	0.43
8	4040.61	18.6	18.6	0.5
9	3518.38	19.77	19.77	0.54
10	3483.92	15.67	15.67	0.52
Average	3386.62	16.09	15.97	0.47

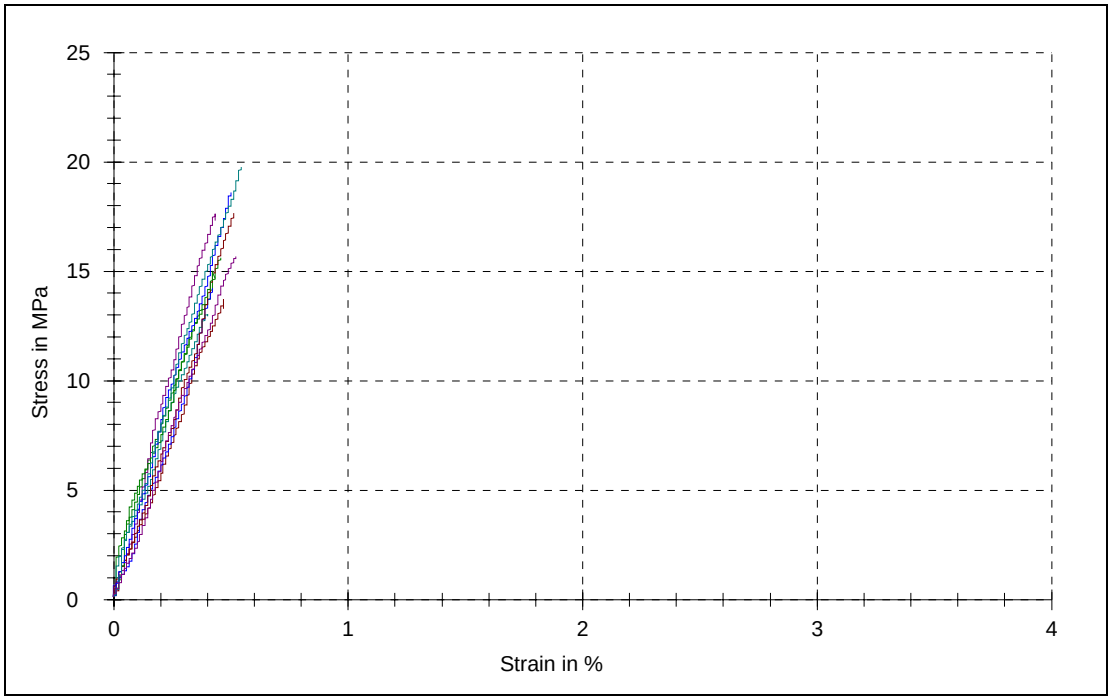

Figure A.8. The stress-strain diagram of PMMA for β=75 and a/w=0.1

Table A.8. The results of PMMA for β=75 and a/w=0.1

Specimen Number	Modulus of Elasticity $E\,(MPa)$	Ultimate Stress $\sigma_M\,(MPa)$	Stress at Break $\sigma_B\,(MPa)$	Elongation at Break $\varepsilon_B\,(\%)$
1	3448.46	14.97	14.97	0.42
2	2991.79	13.88	13.88	0.42
3	3420.57	18.97	18.57	0.54
4	3793.9	15.51	15.51	0.42
5	4108.11	16.39	16.39	0.46
6	3784.25	16.38	16.36	0.46
7	2976.82	18.23	17.66	0.5
8	3478.86	23.66	23.66	0.66
9	3799.02	19.84	19.84	0.53
10	3088.54	16.5	16.04	0.46
Average	3489.03	17.43	17.29	0.49

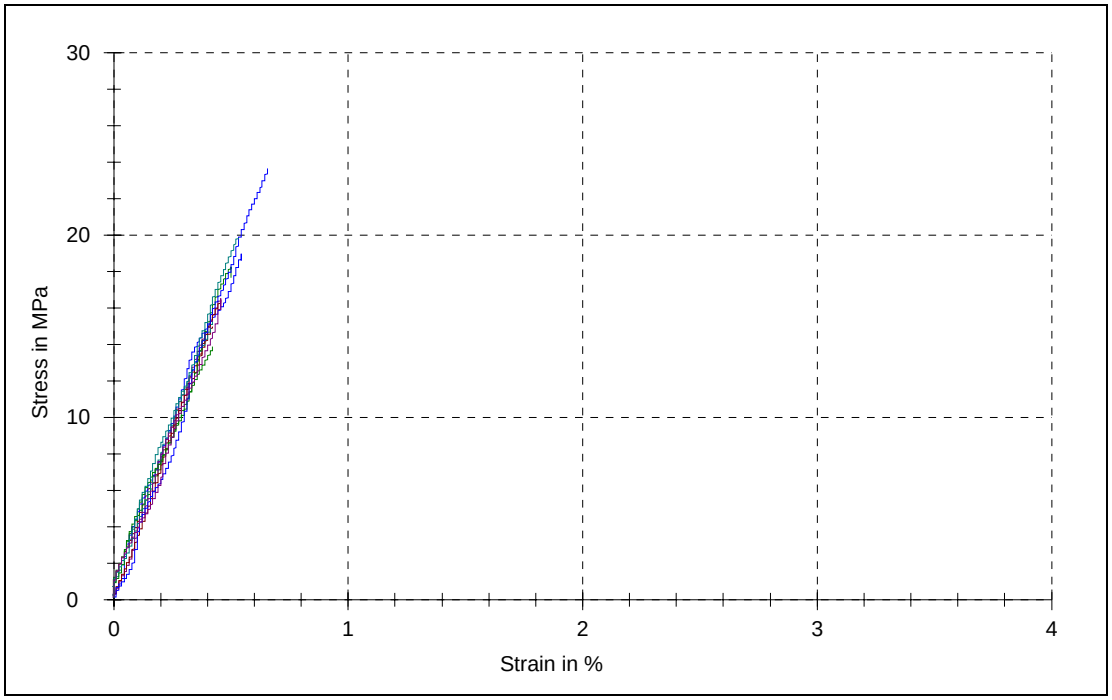

Figure A.9. The stress-strain diagram of PMMA for β=80 and a/w=0.1

Table A.9. The results of PMMA for β=80 and a/w=0.1

Specimen Number	Modulus of Elasticity $E\,(MPa)$	Ultimate Stress $\sigma_M\,(MPa)$	Stress at Break $\sigma_B\,(MPa)$	Elongation at Break $\varepsilon_B\,(\%)$
1	3448.46	14.97	14.97	0.42
2	2991.79	13.88	13.88	0.42
3	3420.57	18.97	18.57	0.54
4	3793.9	15.51	15.51	0.42
5	4108.11	16.39	16.39	0.46
6	3784.25	16.38	16.36	0.46
7	2976.82	18.23	17.66	0.5
8	3478.86	23.66	23.66	0.66
9	3799.02	19.84	19.84	0.53
10	3088.54	16.5	16.04	0.46
Average	3489.03	17.43	17.29	0.49

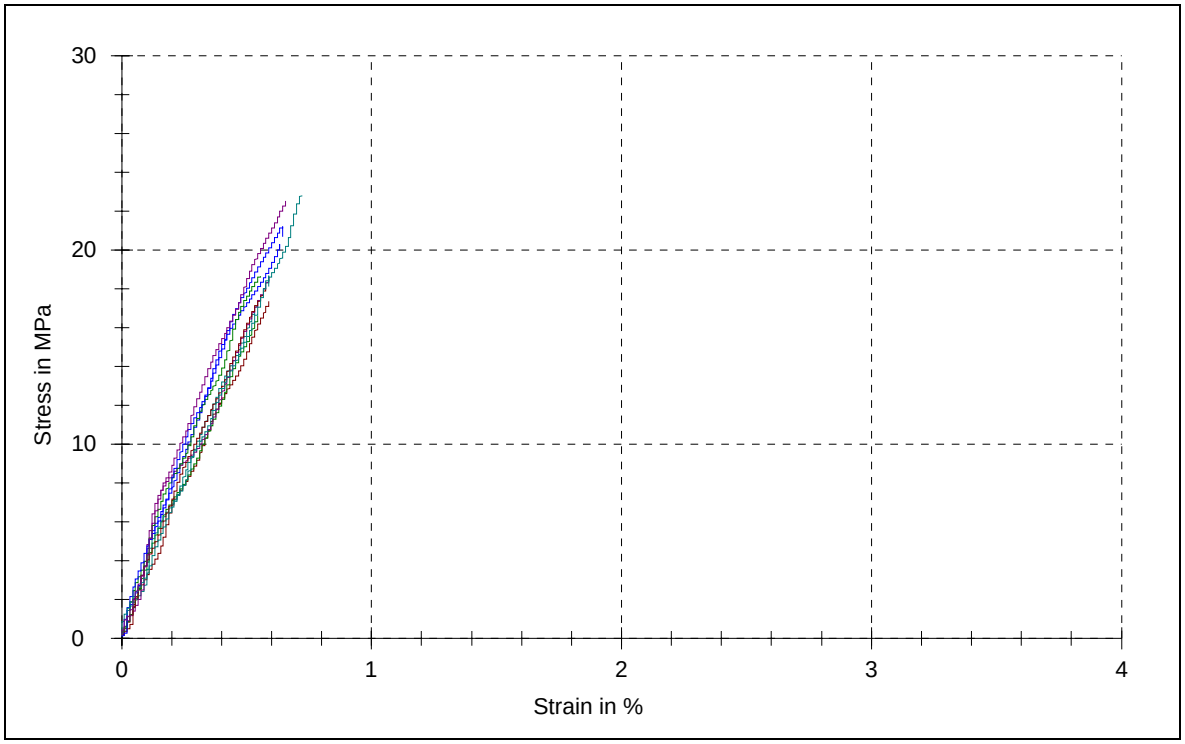

Figure A.10. The stress-strain diagram of PMMA for β=90 and a/w=0.1

Table A.10. The results of PMMA for β=90 and a/w=0.1

Specimen Number	Modulus of Elasticity $E\,(MPa)$	Ultimate Stress $\sigma_M\,(MPa)$	Stress at Break $\sigma_B\,(MPa)$	Elongation at Break $\varepsilon_B\,(\%)$
1	3192.26	17.32	17.32	0.59
2	3344.33	16.6	16.6	0.54
3	3623.72	20.27	20.04	0.63
4	3329.13	22.78	22.78	0.72
5	4635.98	18.58	18.38	0.59
6	3430.92	18.01	18.01	0.58
7	3694.37	18.62	18.62	0.56
8	3601.18	21.2	20.68	0.64
9	3177.22	18.68	18.09	0.59
10	4510.8	22.52	22.52	0.66
Average	3653.99	19.46	19.30	0.61

APPENDIX B: RESULTS OF TENSILE TESTING FOR PS

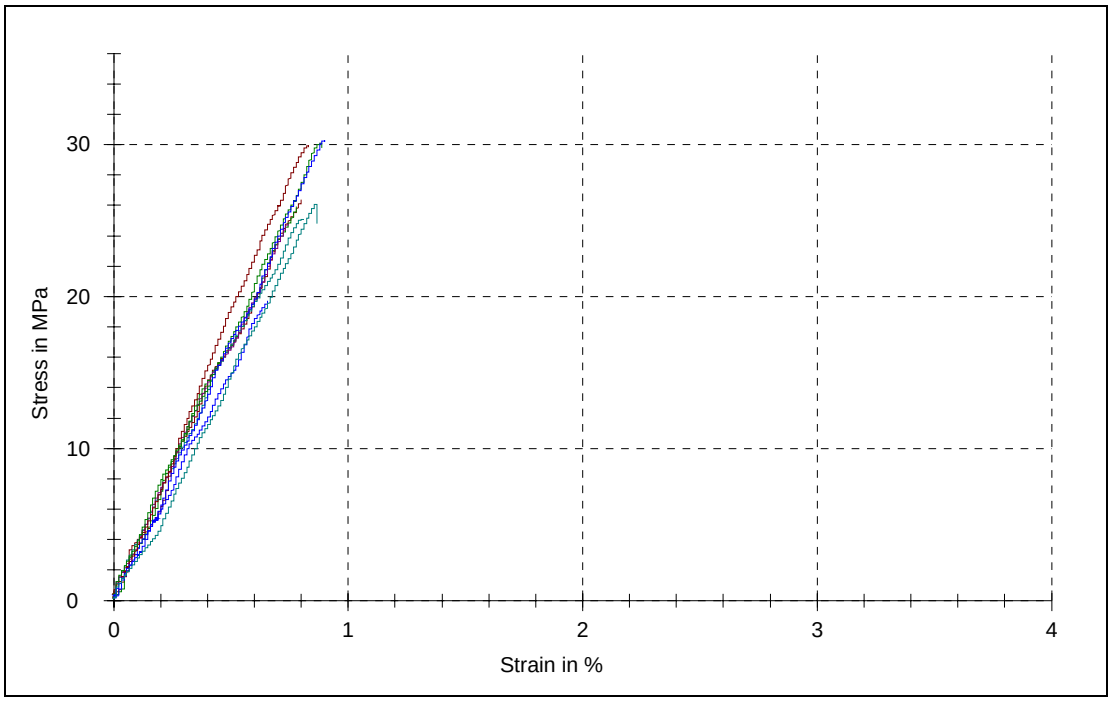

Figure B.1. The stress-strain diagram of PS for β=15 and a/w=0.1

Table B.1. The results of PS for β=15 and a/w=0.1

Specimen Number	Modulus of Elasticity $E\,(MPa)$	Ultimate Stress $\sigma_M\,(MPa)$	Stress at Break $\sigma_B\,(MPa)$	Elongation at Break $\varepsilon_B\,(\%)$
1	2980.71	26.36	26.36	0.8
2	3579.16	25.93	25.93	0.78
3	2763.28	19.72	19.72	0.66
4	3277.81	25.09	25.05	0.81
5	3504.56	24.81	24.81	0.74
6	3591.48	29.93	29.83	0.83
7	3739.59	30.08	29.79	0.89
8	3277.83	30.25	30.18	0.9
9	2320.61	26.06	24.77	0.87
Average	3226.11	26.47	26.27	0.81

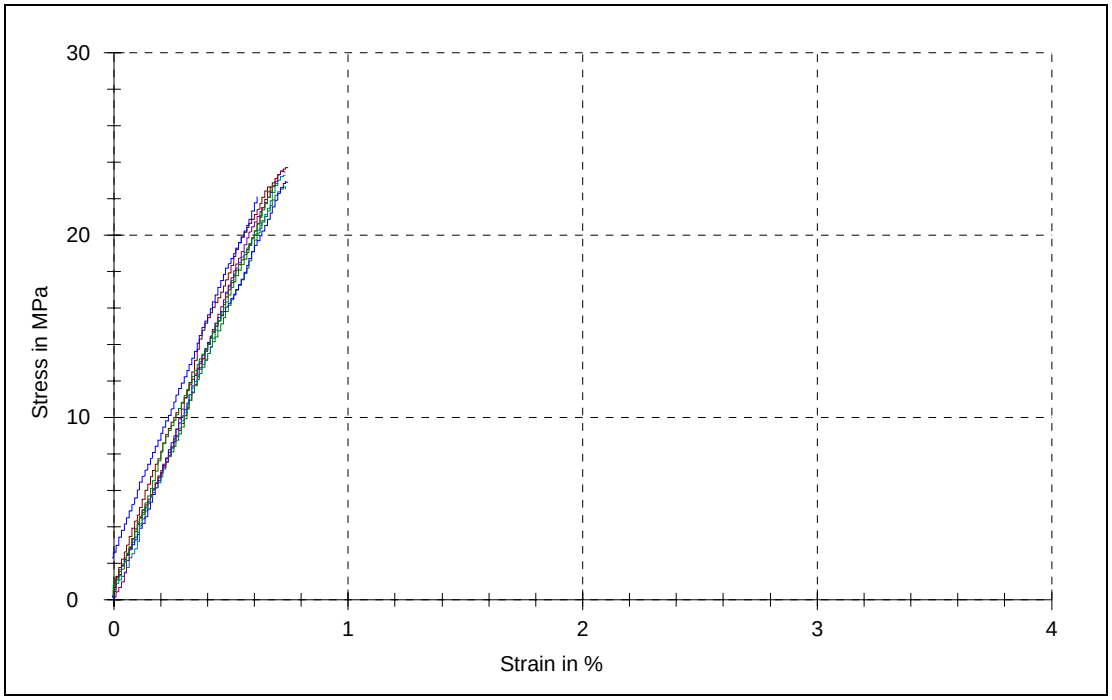

Figure B.2. The stress-strain diagram of PS for β=30 and a/w=0.1

Table B.2. The results of PS for β=30 and a/w=0.1

Specimen Number	Modulus of Elasticity $E\,(MPa)$	Ultimate Stress $\sigma_M\,(MPa)$	Stress at Break $\sigma_B\,(MPa)$	Elongation at Break $\varepsilon_B\,(\%)$
1	3086.91	23.67	23.67	0.74
2	3065.04	22.62	22.51	0.73
3	3268.28	22.91	22.89	0.74
4	3458.29	23.28	23.27	0.73
5	3200.5	23.51	23.4	0.73
6	3556.66	22.62	22.6	0.67
7	3830.26	22.81	22.77	0.7
8	3160.79	22.1	22.1	0.61
Average	3328.34	22.94	22.90	0.71

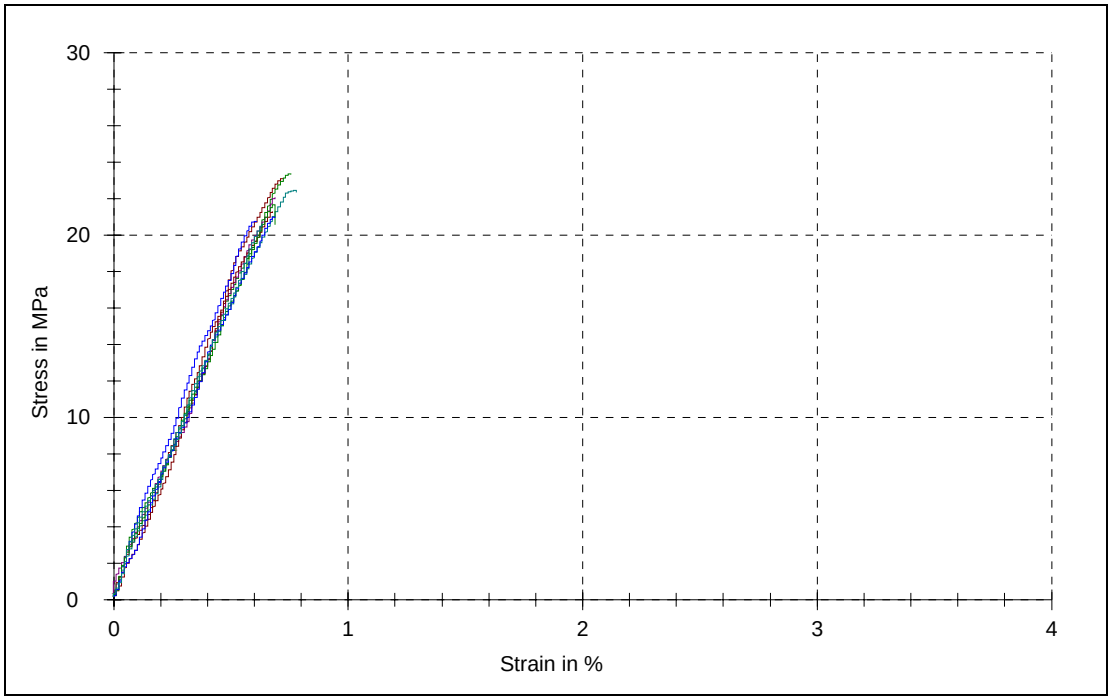

Figure B.3. The stress-strain diagram of PS for β=40 and a/w=0.1

Table B.3. The results of PS for β=40 and a/w=0.1

Specimen Number	Modulus of Elasticity $E\,(MPa)$	Ultimate Stress $\sigma_M\,(MPa)$	Stress at Break $\sigma_B\,(MPa)$	Elongation at Break $\varepsilon_B\,(\%)$
1	3122.36	23.09	23.07	0.72
2	2669.87	23.35	23.31	0.76
3	3363.34	20.74	20.72	0.61
4	3002.63	22.43	22.32	0.78
5	2983.99	22.04	22.04	0.69
6	2954.37	21.26	21.22	0.68
7	2901.59	21.63	20.56	0.69
8	3498.52	20.96	20.94	0.69
9	2931.69	20.61	20.61	0.63
Average	3047.60	21.79	21.64	0.69

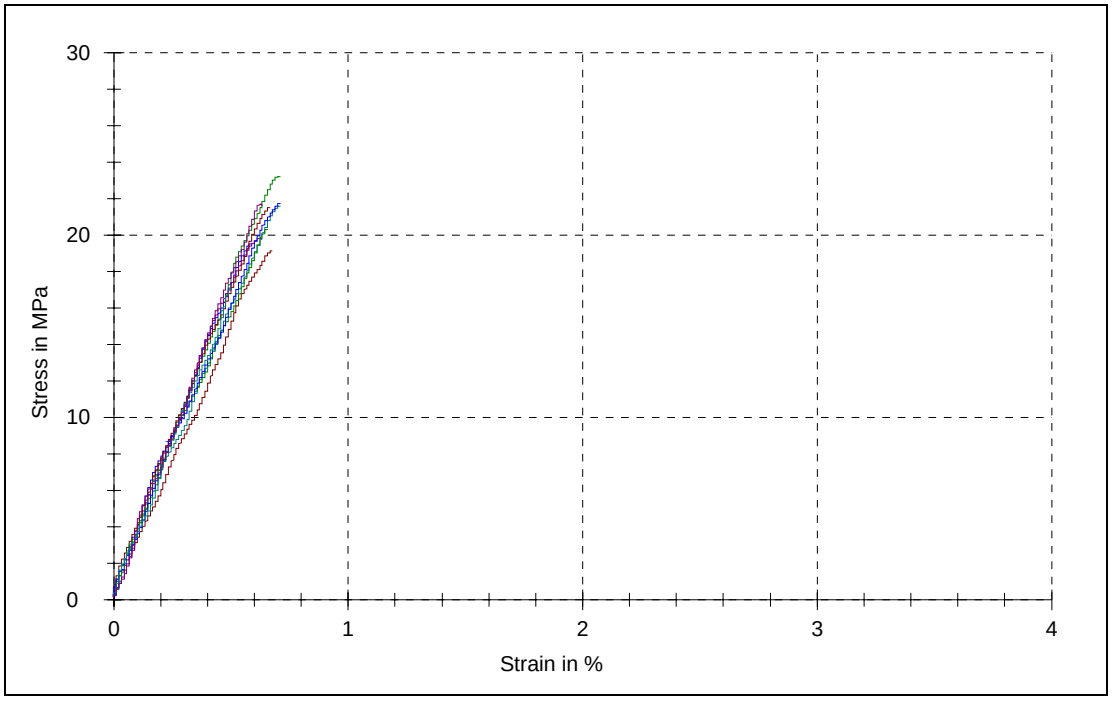

Figure B.4. The stress-strain diagram of PS for β=45 and a/w=0.1

Table B.4. The results of PS for β=45 and a/w=0.1

Specimen Number	Modulus of Elasticity E (Mpa)	Ultimate Strength σM (Mpa)	Stress at Break σB (Mpa)	Elongation at Break εB (%)
1	2768.7	19.11	19.1	0.68
2	3311.11	23.21	23.18	0.71
3	3653.11	19.53	19.53	0.59
4	3427.44	21.56	21.55	0.71
5	3859.48	19.8	19.78	0.63
6	3423.9	21.51	21.51	0.67
7	3342.21	20.34	20.32	0.66
8	3513.4	21.7	21.7	0.71
9	3313.9	17.16	17.16	0.5
10	3562.58	21.69	21.58	0.63
Average	3417.58	20.56	20.54	0.65

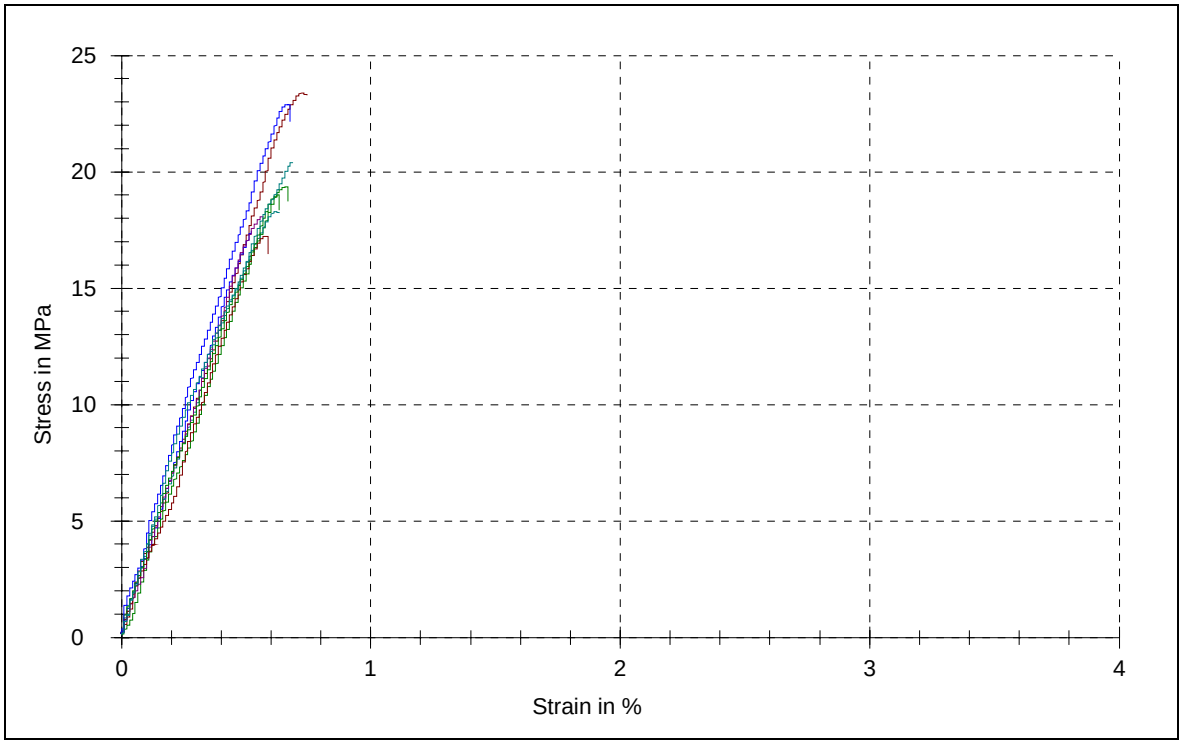

Figure B.5. The stress-strain diagram of PS for β=50 and a/w=0.1

Table B.5. The results of PS for β=50 and a/w=0.1

Specimen Number	Modulus of Elasticity E (Mpa)	Ultimate Strength σM (Mpa)	Stress at Break σB (Mpa)	Elongation at Break εB (%)
1	3220.49	23.39	23.29	0.74
2	3325.55	19.36	18.71	0.67
3	3437.71	17.48	17.48	0.52
4	3187.07	18.3	18.24	0.63
5	3529.09	18.07	18.05	0.57
6	2589.55	17.23	16.46	0.59
7	3287.86	19.01	18.34	0.63
8	3850.24	22.89	22.16	0.68
9	3832.08	20.38	20.38	0.69
Average	3362.18	19.57	19.23	0.64

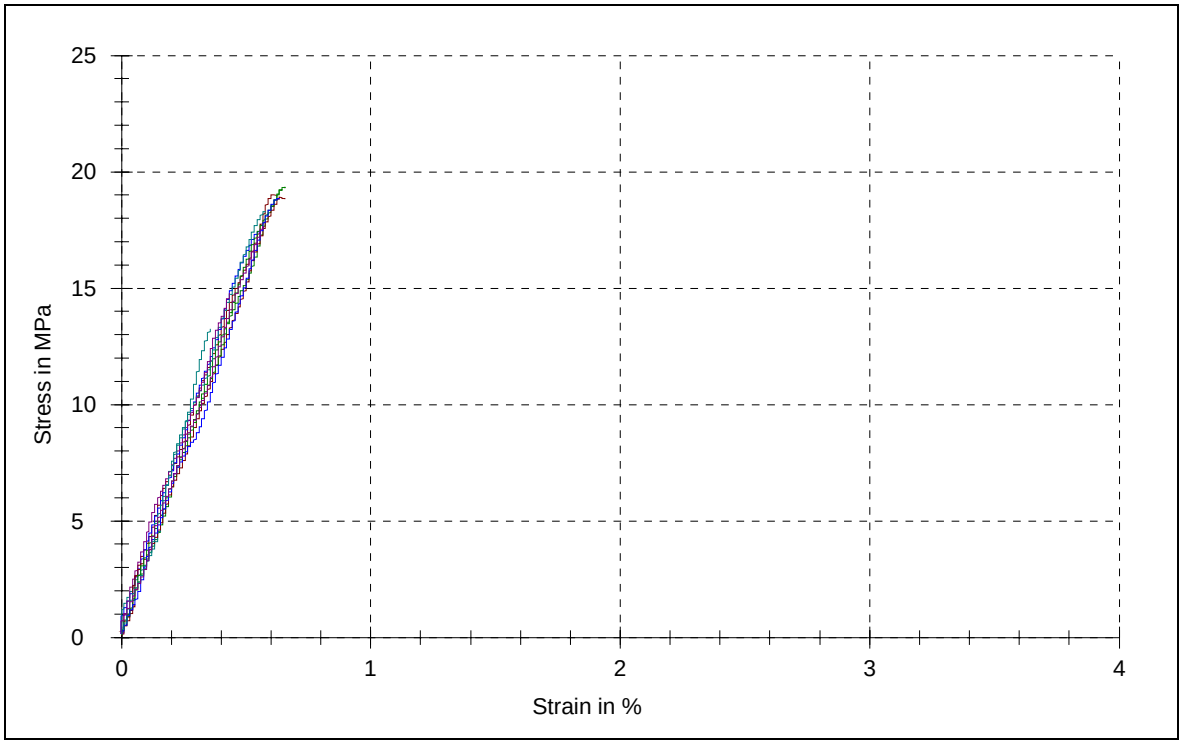

Figure B.6. The stress-strain diagram of PS for β=60 and a/w=0.1

Table B.6. The results of PS for β=60 and a/w=0.1

Specimen Number	Modulus of Elasticity $E\,(MPa)$	Ultimate Stress $\sigma_M\,(MPa)$	Stress at Break $\sigma_B\,(MPa)$	Elongation at Break $\varepsilon_B\,(\%)$
1	3314.99	19.02	18.94	0.62
2	3156.98	19.26	19.26	0.64
3	3141.79	17.43	17.38	0.56
4	3814.99	18.3	18.27	0.58
5	3033.2	14.8	14.8	0.43
6	2691.51	18.9	18.81	0.66
7	3056.97	19.34	19.31	0.66
8	3325.06	18.85	18.82	0.63
9	3824.18	13.26	13.26	0.36
10	3273.53	17.67	17.56	0.57
Average	3263.32	17.68	17.64	0.57

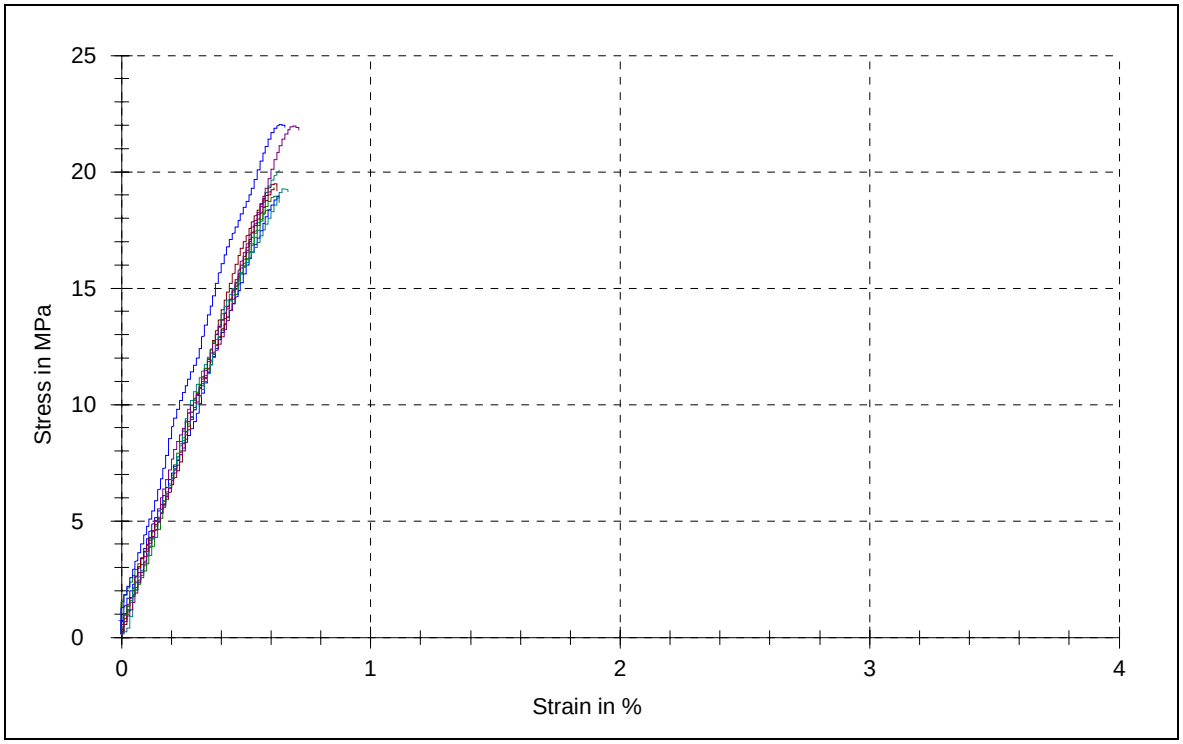

Figure B. 7. The stress-strain diagram of PS for β=70 and a/w=0.1

Table B.7. The results of PS for β=70 and a/w=0.1

Specimen Number	Modulus of Elasticity $E\,(MPa)$	Ultimate Stress $\sigma_M\,(MPa)$	Stress at Break $\sigma_B\,(MPa)$	Elongation at Break $\varepsilon_B\,(\%)$
1	3291.72	19.48	19.16	0.62
2	3097.5	18.96	18.67	0.63
3	2944.51	18.98	18.98	0.63
4	3510.67	20.08	20.08	0.63
5	3651.28	19.16	19.16	0.6
6	2714.01	19.31	19.31	0.61
7	3492.75	18.38	18.34	0.6
8	3988.59	22.03	21.92	0.66
9	3273.87	19.27	19.14	0.67
10	3272.64	21.96	21.79	0.71
Average	3323.75	19.76	19.66	0.64

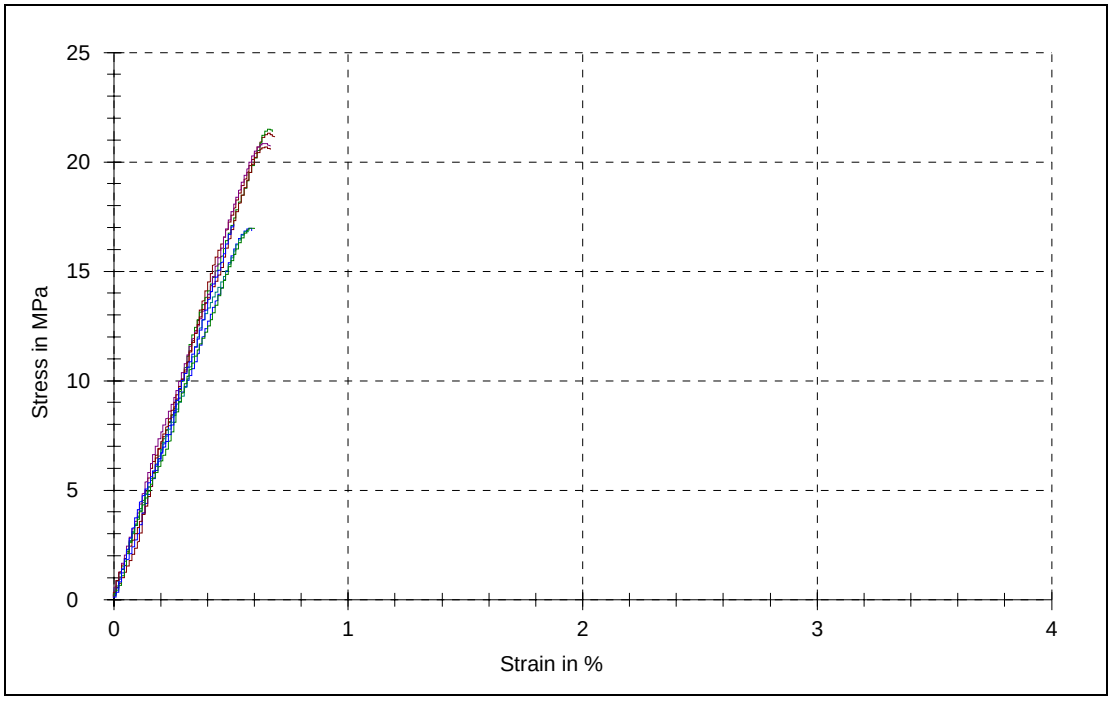

Figure B.8. The stress-strain diagram of PS for β=75 and a/w=0.1

Table B.8. The results of PS for β=75 and a/w=0.1

Specimen Number	Modulus of Elasticity $E\,(MPa)$	Ultimate Stress $\sigma_M\,(MPa)$	Stress at Break $\sigma_B\,(MPa)$	Elongation at Break $\varepsilon_B\,(\%)$
1	3999.87	21.29	21.15	0.69
2	3222.86	21.49	21.38	0.68
3	3517.77	16.98	16.85	0.59
4	3118.94	16.85	16.8	0.58
5	3565.8	20.84	20.72	0.67
6	3620.13	20.67	20.54	0.67
7	2853.39	16.97	16.93	0.6
8	2888.21	17.15	17.15	0.51
Average	3348.37	19.03	18.94	0.62

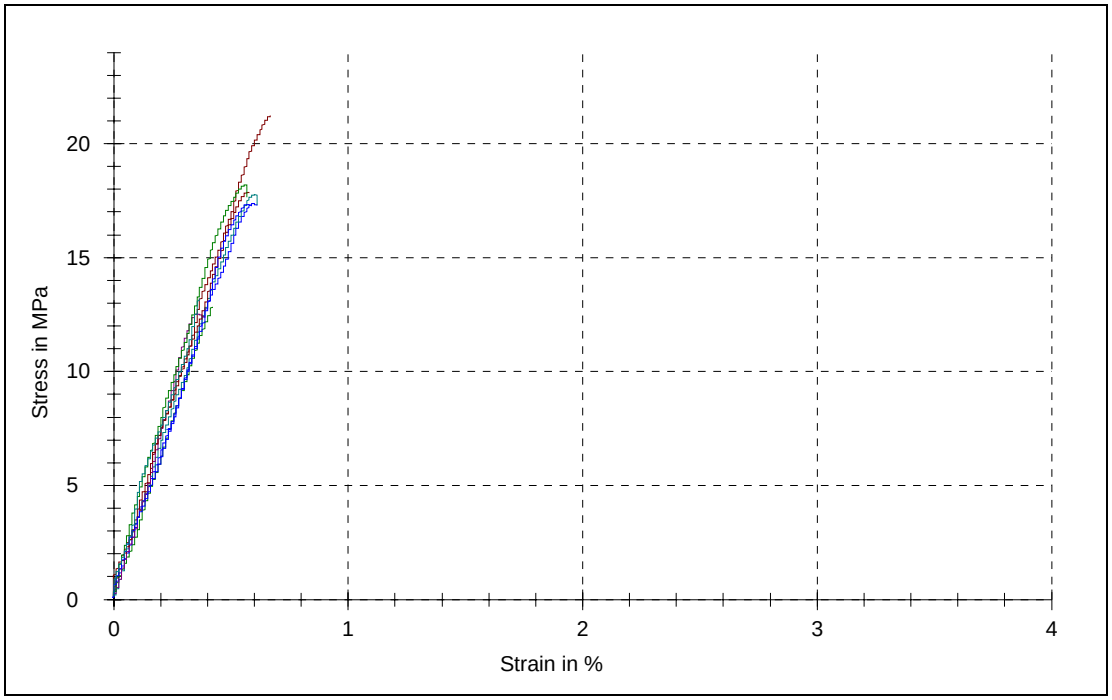

Figure B.9. The stress-strain diagram of PS for β=80 and a/w=0.1

Table B.9. The results of PS for β=80 and a/w=0.1

Specimen Number	Modulus of Elasticity $E\,(MPa)$	Ultimate Stress $\sigma_M\,(MPa)$	Stress at Break $\sigma_B\,(MPa)$	Elongation at Break $\varepsilon_B\,(\%)$
1	3560.77	21.24	21.24	0.67
2	3178.39	12.8	12.78	0.42
3	3042.84	17.36	17.29	0.61
4	3280.47	17.76	17.32	0.61
5	3802.06	12.55	12.36	0.39
6	3549.73	17.85	17.81	0.58
7	3538.4	18.2	17.64	0.57
8	2738.04	17.35	17.25	0.59
9	3434.49	13.21	13.21	0.37
Average	3347.24	16.48	16.32	0.53

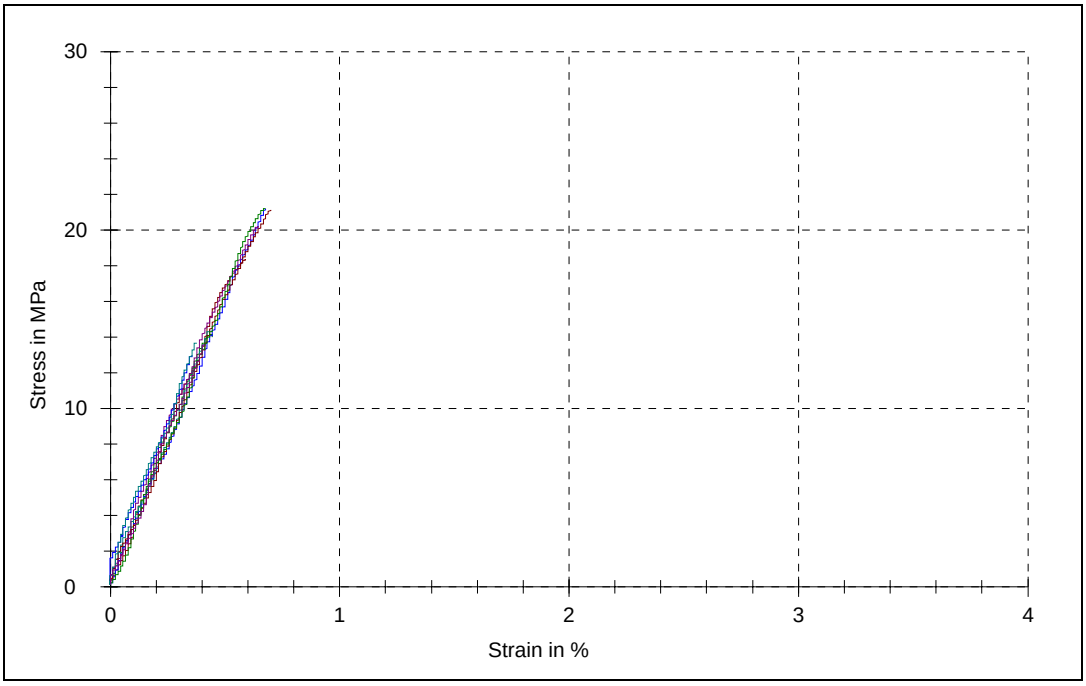

Figure B.10. The stress-strain diagram of PS for β=90 and a/w=0.1

Table B.10. The results of PS for β=90 and a/w=0.1

Specimen Number	Modulus of Elasticity $E\,(MPa)$	Ultimate Stress $\sigma_M\,(MPa)$	Stress at Break $\sigma_B\,(MPa)$	Elongation at Break $\varepsilon_B\,(\%)$
1	3670.44	18.36	18.32	0.59
2	3512.69	14.13	14	0.44
3	3010.65	21.21	21.21	0.68
4	2801.8	14.38	14.38	0.43
5	3716.93	20.21	20.17	0.64
6	2912.21	21.09	21.09	0.7
7	3709.14	21.2	21.2	0.68
8	3007.71	12.95	12.95	0.36
9	2923.83	13.66	13.66	0.38
10	3623.3	13.57	13.57	0.41
Average	3288.87	17.08	17.06	0.53

REFERENCES

1. Westergaard, H. M., "Bearing Pressure and Cracks", *Journal of Applied Mechanics,* Vol. 6, pp 49-53, 1939.

2. Williams, M. L., "On the Stress Distribution at the Base of a Stationary Crack", *J. Appl. Mech.,* Vol. 24, pp. 109-114, 1957.

3. Anderson T.L., *Fracture Mechanics: Fundamentals and Applications*, CRC Press, Florida, 1991

4. Khan, S. M. A. and M. V. Khraishes, "Analysis of Mixed Mode Crack Initiation Angle Under Various Loading Conditions", *Engnr. Fract. Mech.,* Vol. 67, pp. 397-419, 2000.

5. Broek D., *Elementary Engineering Fracture Mechanics,* Martinus Nijhoff Publishers, Lancaster, 1982.

6. Erdogan, F. and G.C. Sih, "On the crack Extension in Plates Under Plane Loading and Transverse Shear", *J. Basic Engnr.,* Vol. 85, pp. 519-527, 1963.

7. Williams, J. G. and P. D. Ewing, "Fracture Under Complex Stress the Angled Crack Problem", *Int. J. Fract. Mec.,* Vol. 8(4), pp. 441-446, 1972.

8. Ueda Y., K. Ikeda, T. Yao and M. Aoki, "Characteristics of Brittle Failure Under General Combined Modes Including Those Under Bi-axial Tensile Loading", *Engrg. Fract. Mech.,* Vol. 18-6, pp. 1131-1158, 1983.

9. Theoracis P. S., "A Higher-Order Approximation for the *T*-Criterion of Fracture in Biaxial Fields", *Engrg. Fract. Mech.,* Vol. 19, pp. 975-991, 1984.

10. Vallejo, L.E., "The brittle and Ductile Behavior of a Material Containing a Crack Under Mixed-Mode Loading", *28 th US Symposium on Rock Mechanics*, Tucson, pp. 383-390, 1987.

11. Khan, S. M. A. and M. K. Khraisheh, "A New Criterion for Mixed Mode Fracture Initiation Based on the Crack Tip Plastic Core Region", *Int. Journal of Plasticity*, Vol.20, pp. 55-84, 2004.

12. Sih. G.C. (Editor), *Methods of Analysis and Solution of Crack Problems: Recent Developments in Fracture Mechanics/Theory and Methods of Solving Crack Problems*, Leyden, Noordhoff International Pub., 1973.

13. Smith D. J., M. R. Ayatollahi and M. J. Pavier, "The Role of T-stress in Brittle Fracture for Linear Elastic Materials Under Mixed-Mode Loading, Fatigue Fracture", *Engnr. Mater. Struct.,* Vol. 24(2), pp. 137-150, 2001.

14. Kong, X. M., N. Schulter and W. Dahl, "Effect of Triaxial Stress on Mixed-Mode Fracture", *Engng. Fract. Mech.,* Vol. 52(2), pp. 379-388, 1995.

15. Çopur, H., "*Crack Initiation in Statically Loaded Functionally Graded Materials",* M.s. Thesis, Boğaziçi University, 2004.

16. Leevers P. S. and J. C. Radon, "Inherent Stress Biaxiality in Various Fracture Specimen Geometries", *Int. Journal of Fracture,* Vol. 19, pp. 311-325, 1982.

17. Swicofil Product Catalogue, http://www.swicofil.com/products/278polymethylmethacrylate.html

18. Irwin G. R., *J. Appl. Mech.,* Vol. 24, pp. 361-364, 1957.

19. Williams, M. L., "On the Stress Distribution at the Base of a Stationary Crack", *J. Appl. Mech.,* Vol. 24, pp. 109-114, 1957.

20. Maccagno T. N. and J. F. Knott, "The Fracture Behavior of PMMA in Mixed Modes I and II", *Engng. Fract. Mech.,* Vol. 34(1), pp. 65-86, 1989.

21. The University of Southern Mississippi, *Polymer Science Learning Center,* http://pslc.ws/macrog/styrene.htm

22. Williams J. G., *Fracture Mechanics of Polymers,* Halsted Press, 1987.

23. Mahajan R. V. and K. Ravi-Chandar, "an Experimental Investigation of Mixed-Mode Fracture", *Int. Journal of Fracture*, Vol. 41, pp 235-252, 1989.

24. Murakami Y., *Stress Intensity Factors Handbook, Volume 1,* Pergamon Press, Newyork, 1985.

25. Chao Y. J. and L. Shu, "On the Failure of Cracks Under Mixed-Mode Loading", *International Journal of Fracture,* Vol. 87, pp. 201-223, 1997.

26. Theocaris P.S., G. A. Kardomateas and N. P. Andrianopoulos, "Experimental Study of the T-Criterion in Ductile Material", *Engineering Fracture Mechanics,* Vol. 17, pp. 439-447, 1982.